INTEGRATED GEOLOGICAL AND GEOPHYSICAL STUDIES OF LOW PERMEABILITY CARBONATE ROCK AS AN UNCONVENTIONAL RESERVOIR: BATURAJA FORMATION, PALEMBANG BASIN, INDONESIA

A Dissertation

by

MADE SUARDANA

Submitted to the Office of Graduate and Professional Studies of
Texas A&M University
in partial fulfillment of the requirements for the degree of

DOCTOR OF PHILOSOPHY

Chair of Committee,	Mark E. Everett
Committee Members,	Juan Carlos Laya Pereira
	Robert S. Reece
	Walter B. Ayers
Head of Department,	Michael Pope

December 2018

Major Subject: Geophysics

ABSTRACT

The early Miocene carbonate Baturaja Formation in Sumatra, Indonesia, is a gas-charged tight reservoir characterized by very low permeability (mostly below 0.1 mD) and porosity (mostly below 5%). Historically, the formation has been regarded as a conventional reservoir; however, it has required acid fracturing to enable hydrocarbon production approaching an economically viable rate. Changing the exploitation strategy of the formation to that of an unconventional carbonate may improve gas recovery. The research presented herein integrates geological and geophysical methods to better characterize the Baturaja Formation, treating it as an unconventional reservoir. The first part of the dissertation defines the carbonate platform type, the influence of siliciclastic input to the different carbonate facies comprising the platform, and the porosity distribution. This is followed by the development of a scheme based on available well-log data to classify the reservoir quality using a combination of Lamé parameters and elastic moduli. In the final part of the research, the rock-quality classification is extrapolated across the field using rock parameters extracted from an amplitude variation with offset (AVO) inversion of an industry-provided seismic dataset.

The depositional setting of the early Miocene Baturaja Formation is herein suggested to be a carbonate ramp, dominated by oligopothic biota in the inner ramp and mid ramp, and by aphotic biota in the proximal outer ramp. The analysis of RMS amplitudes from the seismic dataset identified siliciclastic influences to the carbonate platform, and thereby allowed the definition of two carbonate facies (A and B) based on

the abundance of siliciclastic input. Hydrocarbons (gas and condensate) are likely to be trapped near lateral boundaries between the carbonate facies due to large contrasts in acoustic impedance and porosity.

Six carbonate reservoir-quality classes were defined within Baturaja Formation. Reservoir quality was determined based on inferred rock parameters, including brittleness, porosity, TOC and mineral content. The rock-quality class boundaries were determined using a well-based carbonate classification template. Very good to moderate reservoir quality dominates the inner ramp facies due to the high terrigenous siliciclastic content. Lower moderate to poor quality reservoirs dominate the outer ramp, due to extensive cementation. Integration of stratigraphic interpretation and carbonate rock quality was used to suggest a prospective interval for acid fracturing and to test the potential unexploited resources in the reservoir.

The inverted P-impedance explains the characteristics of the progradational, aggradational and retrogradational stratigraphic zones related to marine cementation, siliciclastic input, and the effects of carbonate drowning. The seismic-based classification scheme produces spatially-contiguous lateral and vertical distributions of reservoir quality classes across the field. The reservoir quality classification can be used to guide appropriate location of infilling wells for the purpose of increasing future gas production from Baturaja Formation.

DEDICATION

To my dearest wife “Manelia” and my kids “Lingga and Rangga”

ACKNOWLEDGEMENTS

I would like to thank my committee chair, Dr. Everett, for the discussion and comments for improving my research. I also would like thank to my committee members, Dr. Laya, Dr. Reece, and Dr. Ayers, for their guidance and support throughout the comments and suggestion for this research.

I also want to extend my gratitude to Pertamina, Indonesian national oil company, which provided financial support for my Ph.D. study at Texas A&M University, and provided the data for the research.

Thanks also go to my friends and colleagues and the department faculty and staff for making my time at Texas A&M University a great experience.

Finally, I must express my very profound gratitude to my wife for her patience and love; and to my kids for cheering me every day.

CONTRIBUTORS AND FUNDING SOURCES

This work was supervised by a dissertation committee consisting of Dr. Mark E. Everett (advisor and chair committee) and Dr. Robert S. Reece (member), Dr. Juan Carlos Laya Pereira (member) of the Department of Geology and Geophysics and Walter B. Ayers (member) of the Department of Petroleum Engineering, Texas A&M University. PT. Pertamina (Indonesian National Oil Company) provided the Ph.D. sponsorship and the data. All work for the dissertation was completed independently by the student.

NOMENCLATURE

Fm	Formation
BRF	Baturaja Formation
TAF	Talang Akar Formation
GUF	Gumai Formation
SEM	Scanning Electron Microscope
XRD	X-ray Diffraction
f	Frequency
V_P	Compressional wave velocity
V_S	Shear wave velocity
PSTM	Post Stack Time Migrated
AI	Acoustic Impedance
MFS	Marine Flooding Surface
3D	Three Dimensional
RMS	Root Mean Square
FWB	Fair Weather Base
SWB	Storm Wave Base
mD	Milli Darcy
TOC	Total Organic Carbon
AVO	Amplitude versus Offset
λ	Lambda, First lame constant

μ	Mu, Second Lame constant
ρ	Rho, Density
GR	Gamma Ray
VSH	Volumetric Concentration of Shale
PEFZ	Photoelectric Factor
PVT	Pressure Volume Temperature
k	Permeability
K	Bulk Modulus
β	Compressibility
E	Young's Modulus
υ	Poisson's Ratio (PR)
EUR	Estimated Ultimate Recovery
OGIP	Original Gas In Place
RF	Recovery Factor
Z_p	P-wave Impedance
Z_s	S-wave Impedance
PSS	Parasequence Set
DST	Drill Stem Test
R_{PP}	Reflected P-wave
R_{PS}	Reflected S-wave
T_{PP}	Transmitted P-wave
T_{PS}	Transmitted S-wave

R_{VP}	Reflectivity of P-wave
R_{VS}	Reflectivity of S-wave
$\bar{V}_P$	The average of P-wave velocity
$\bar{V}_S$	The average of P-wave velocity
$\bar{k}_{sat}$	Ratio of shear to compressional wave velocity for saturated rock
R_{AI}	Reflectivity of P-impedance
R_{SI}	Reflectivity of S-impedance
R_D	Reflectivity of Density
R_{GI}	Reflectivity of Gradient Impedance
SNR	Signal to Noise Ratio
NMO	Normal Move Out
Δt_{NMO}	NMO correction time at offset x and zero-offset time t_0
CDP	Common Depth Point
CMP	Common Mid Point
RHOB	Density log
DT	Sonic P-wave log
DTS	Sonic S-wave log
FWHM	Full Width Half Maximum
FWQM	Full Width Quarter Maximum
$\boldsymbol{m}$	Model vector
$\Delta\varphi$	Objective function
LS	Least Square

LR	Lambda-Rho
MR	Mu-Rho
MMSCFD	Million Standard Cubic Feet per Day
BCPD	Barrel Condensate Feet per Day

TABLE OF CONTENTS

Page

ABSTRACT ii

DEDICATION iv

ACKNOWLEDGEMENTS v

CONTRIBUTORS AND FUNDING SOURCES vi

NOMENCLATURE vii

TABLE OF CONTENTS xi

LIST OF FIGURES xiv

LIST OF TABLES xxiii

CHAPTER I INTRODUCTION 1

1.1 Background and Problem 2
1.2 Research Objectives 3
1.3 Dissertation Structure 4

CHAPTER II THE DEPOSITIONAL ENVIRONMENT AND POROSITY DISTRIBUTION OF AN EARLY MIOCENE CARBONATE PLATFORM 6

2.1 Summary 6
2.2 Introduction 7
2.3 Geology Background 9
2.4 Methodology 16
2.4.1 Depositional Environment Identification 16
2.4.2 Well & Seismic Analysis 18
2.4.3 Neural Network and Genetic Algorithm Inversion 26
2.5 Results 29
2.5.1 Well & Seismic Analysis 29
2.5.2 Carbonate Rock Composition and Distribution 34
2.5.3 Rock Modeling 37
2.5.4 Inverted Acoustic Impedance 38
2.6 Discussion 41

2.6.1 Depositional Environment Model of the Baturaja Carbonate Platform 41
2.6.2 Porosity Prediction....48
2.6.3 Implication of Research to Hydrocarbon Trapping....53
2.7 Conclusions....56

CHAPTER III WELL-BASED CARBONATE RESERVOIR QUALITY ASSESSMENT OF LOW-PERMEABILITY CARBONATE ROCK: BATURAJA FORMATION, PALEMBANG BASIN, INDONESIA....59

3.1 Summary....59
3.2 Introduction....60
3.3 Geological Background....61
3.4 Methodology....68
3.4.1 Stratigraphic Correlation....68
3.4.2 Lamé Parameters and Elastic Moduli....71
3.4.3 The Application of Lamé Parameters and Elastic Moduli for Rock Discrimination....73
3.5 Results....77
3.5.1 Carbonate Platform Parasequence Set....77
3.5.2 Carbonate Quality Classification....80
3.6 Discussion....86
3.7 Conclusions....99

CHAPTER IV GENERATED 3D CARBONATE QUALITY DISTRIBUTION OF BATURAJA FORMATION USING SEISMIC AVO INVERSION....101

4.1 Summary....101
4.2 Introduction....102
4.3 Geology Background....104
4.4 Methodology....111
4.4.1 Amplitude Variation with Offset (AVO)....111
4.4.2 Seismic Data Pre-Conditioning....113
4.4.3 AVO Inversion....114
4.5 Results....119
4.5.1 Pre-Conditioned Seismic Data....119
4.5.2 AVO Inversion of Lambda-Mu-Rho Analysis....121
4.6 Discussion....126
4.6.1 3D Carbonate Quality Class Distribution....126
4.6.2 Validation of Well-based and Seismic-based Carbonate Quality Classification....131
4.7 Conclusions....135

CHAPTER V CONCLUSIONS....138

REFERENCES....142

APPENDIX 154

LIST OF FIGURES

Page

Figure 2.1. (a) Location of Pagardewa Field, South Sumatra, Indonesia. (b) Major tectono-stratigraphy features of Sumatra during the Tertiary: (1) North Sumatra Basin, (2) Forearc Basin, (3) South Sumatra Basin and (4) Central Sumatra Basin (modified from Wilson, 2002 after de Smet, 1992) 10

Figure 2.2. Regional stratigraphy of South Sumatra Basin (modified from Pertamina, 2012g). Noted BRF=Baturaja Formation. 11

Figure 2.3. Petrographical descriptions from cores, sidewall cores and cutting samples. (a) Wackstone-Packstone from core sample of well C-4 at depth 1921.8 m, (b) Floatstone-Wackstone from sidewall cores sample of well C-5 at depth 1978 m and (c) Wackstone-Mudstone from cutting sample of well E-03 at depth 1480 m. 13

Figure 2.4. (a) Histogram of porosity from 12 wells. (b) Histogram of permeability from 12 wells. Based on the cumulative distributions (solid lines overlying the histograms), more than 50 % of the porosity in Baturaja Formation are below 5% and permeability are below 0.1 mD. Noted solid black line is cumulative frequencies. 14

Figure 2.5. Classification of hydrocarbon-bearing reservoirs as "conventional" or "unconventional" based on a cross-plot of viscosity μ vs permeability k, as defined by Cander (2012). The Baturaja Formation (BRF) samples (purple dots) indicate that they are associated with tight gas unconventional reservoirs. 15

Figure 2.6. The availability data for this research on the basemap of 3D seismic Pagardewa overlying with the wells location (Noted the coordinates on the basemap are not shown due to company restrictions). Three wells were used for well to seismic correlation: C-5, D-8 and L-1. 19

Figure 2.7. The estimated porosities from petrophysical calculations (blue dashed curve) closely approach the measured porosities from core of wells C-4 and E-3 (purple dot). Note BRF= Baturaja Formation, and the blue zone is the Baturaja Formation interval. 20

Figure 2.8. The higher core porosity-permeability relation on the lower part (Well E-3 and K-24) may be related with higher siliciclastic material in the carbonate rock. 22

Figure 2.9. (a) Petrography of core E-3 at depth sample 1540 m. (b) SEM of core K-22 at depth sample 1723.63 m. Those rock samples indicated the non-carbonate constituents in the form of detrital quartz and clay minerals (kaolinite) (adapted from Geoservices, 2012b; Geoservices, 2012f). 23

Figure 2.10. (a) The amplitude series and spectrum of extracted wavelet at seismic traces along wellbore of 16 wells. (b) The amplitude series and spectrum of the appropriate ricker wavelet for well seismic tie. The ricker wavelet (b) were design from the parameters of the extracted wavelet (a). 24

Figure 2.11. Well-to-seismic ties in wells L-1 (a) and C-5 (b). Synthetic seismograms (blue traces) correlate well with seismic inline traces (red traces) for the interval where the log density and sonic were available. The location of two well on the basemap can be seen in Figure 2.6. The boundaries of the carbonate interval are defined by zero crossing (+/-; top) to zero crossing (-/+; base). 25

Figure 2.12. Workflow of integrated multi-layer neural network and genetic algorithm that was used herein to generate inverted acoustic impedance from PSTM Seismic data (modified after Pavlova and Reid, 2010) 28

Figure 2.13. (a) Seismic interpretation at Pagardewa Field. (b) The carbonate interval is clearly seen in the seismic data as a large negative amplitude between zero crossings. (c) Basemap of Pagardewa Field showing depth structure map of top Baturaja Formation associated with fault interpretations, well locations and the seismic cross-section line shown (a). 30

Figure 2.14. Mesozoic layer map extracted from seismic. Note rectangular dashed line is the location of Pagardewa Field (adapted from Pertamina, 2011).....31

Figure 2.15. The thickness of Baturaja Formation map in domain time (ms) 32

Figure 2.16. (a) The flattened seismic data at MFS near top of Baturaja Formation. (b) The approximated paleotopography of top of carbonate platform at early Miocene. 33

Figure 2.17. RMS amplitude map of Baturaja Formation throughout the Pagardewa Field. Cool colors represents lower values and warm colors represents higher value of RMS amplitude.....34

Figure 2.18. The percentage distribution of grain (left) and mineral (right) occurrences in 45 samples from nine wells. 35

Figure 2.19. The thickness of Baturaja carbonate platform map in domain time overlying by the distribution of carbonate rock classification refers to

Dunham (1962) associated with carbonate composition (carbonate and non-carbonate constituents) found in each of the wells (rock sampled near the top of Baturaja Formation). Larger formanifers, smaller benthic and red algae dominated the carbonate platform. Non-carbonate minerals are dominated by quartz and pyrite with minor presence of clay and glauconite. .36

Figure 2.20. (a) Rock model for forward modeling. (b) Forward modeling of the rock model at well C-5 defined stronger amplitude, Facies "A", along the Baturaja interval. (c) Forward modeling of the rock model at well L-1 defined weaker amplitude, Facies "B", along the Baturaja interval. 38

Figure 2.21. Inverted acoustic impedance along an inline section across (a) well C-5 and (c) well D-8. The inverted acoustic impedance accurately estimates the borehole-derived acoustic impedance (blue curve). Insert figure above is depth structure map of Top Baturaja Formation (recent structure) with the inline cross-section marked with red bold line. 39

Figure 2.22. Validation analysis using blind wells C-4 and K-22. The inverted acoustic impedance trace sampled along and near well trace (background color) has a good similarity with borehole-derived acoustic impedance (black curve). 41

Figure 2.23. Genetic approach concept for identifying the type of carbonate platform based on the dominant light-dependent biota distribution (modified after Pomar, 2001). The blue curve is the suitable carbonate platform type for upper Baturaja Formation at early Miocene. 42

Figure 2.24. Facies map of upper Baturaja Formation was reconstructed from isopach map and biota distribution near top of Baturaja Formation. Larger foraminifers and red algae dominated the carbonate platform. Non-carbonate minerals are dominated by quartz and pyrite with minor presence of clay and glauconite. 43

Figure 2.25. The carbonate ramp depositional model (unscaled) of upper Baturaja carbonate platform at early Miocene along NW-SE (the cross-section is shown in Figure 2.24). The oligophotic biota are predominantly distributed across the carbonate platform. (Note Euph=Euphotic biota, Ol=Oligopohtic biota and Aph=Aphotic biota). 44

Figure 2.26. (b) The lithology model overlaid by seismic amplitude response from forward modeling process. Baturaja Formation consist of two facies: Facies A and B. The distributions of the facies are clearly seen on (a) the RMS amplitude map (see Figure 2.17 for detail figure), Facies A are represented by green-to-yellow regions and Facies B are represented by blue regions.

(c) The carbonate ramp model of Top Baturaja Formation included the interpreted of the facies along northwest to southeast. 46

Figure 2.27. Gamma ray correlation associated with volumetric concentration of shale from NW to SE (see insert picture for the line of correlation on RMS amplitude map) shows an increasing of volumetric concentration of shale/clay into southeast. This indicates higher influences of siliciclastic in inner ramp rather than in mid and outer ramp. 47

Figure 2.28. The combination of root mean square (RMS) of inverted acoustic impedance and gamma ray log of the wells from A to A' able to trace the depositional environment boundary across the field. (Note: the environment boundary is marked by brown dashed line) 49

Figure 2.29. Negative relationship of well-log porosity vs borehole-derived acoustic impedance for Baturaja Formation interval 50

Figure 2.30. RMS map of predicted porosity of the Baturaja Formation: porosity distribution range in inner ramp (10% - 12%), middle ramp (6% - 10%) and outer ramp (7% - 10%). Noted the carbonate ramp was modeled along the NW – SE red line. 52

Figure 2.31. (a) SEM of core sample of Well C-4 at depth 1921.8. (b) Photomicrograph of core sample of well C-4 at depth 1923.6 m (adopted from Geoservices (2012d)). We can see the blocky calcite and drusy mosaic of equant spar at this rock samples from outer ramp. 53

Figure 2.32. (a) RMS of inverted acoustic impedance. (b) The carbonate ramp model of Baturaja carbonate platform at Pagardewa Field. A stratigraphic hydrocarbon trap (red dotted circle line), due to facies's properties change, is inferred at the facies boundary; the boundaries are easily identified on RMS of inverted acoustic impedance map (i.e. the related boundaries shown in (b) is located inside the red dotted ellipse in (a) 56

Figure 3.1. (a) Location of Pagardewa Field, South Sumatra, Indonesia. (b) Major tectono-stratigraphy features of Sumatra during the Tertiary: (1) North Sumatra Basin, (2) Forearc Basin, (3) South Sumatra Basin and (4) Central Sumatra Basin (modified from Wilson, 2002 after de Smet, 1992) 62

Figure 3.2. Regional stratigraphy of South Sumatra Basin (modified from Pertamina, 2012g). Noted BRF=Baturaja Formation. 64

Figure 3.3. Petrographical descriptions from cores, sidewall cores and cutting samples. (a) Wackstone-Packstone from core sample of well C-4 at depth 1921.8 m, (b) Floatstone-Wackstone from sidewall cores sample of well C-

5 at depth 1978 m and (c) Wackstone-Mudstone from cutting sample of well E-03 at depth 1480 m. 65

Figure 3.4. (a) Histogram of porosity from 12 wells. (b) Histogram of permeability from 12 wells. Based on the cumulative distributions (solid lines overlying the Histograms), more than 50 % of the porosity in Baturaja Formation are below 5% and permeability are below 0.1 mD. Noted solid black line is cumulative frequencies. 67

Figure 3.5. Classification of hydrocarbon-bearing reservoirs as "conventional" or "unconventional" based on a cross-plot of viscosity μ vs permeability k, as defined by Cander (2012). The Baturaja Formation (BRF) samples (purple dots) indicate that they are associated with tight gas unconventional reservoirs. 68

Figure 3.6. Gamma ray response for different lithologies (reprinted from Rider, 2002). 70

Figure 3.7. Generalized gamma ray (GR) profiles from variations in depositional environment (After Kendall, 2003, modified from Emery and Myers, 1996) . 71

Figure 3.8. Heuristic template to interpret seismic, well log, or laboratory rock properties in terms of estimate ultimate recovery (EUR), original gas in place (OGIP), recovery factor (RF), pore pressure, and fracture density of reservoir with different quartz and clay partition (After Perez et al., 2011). ... 74

Figure 3.9. Lambda-Rho versus Mu-Rho crossplot comparing various shales and carbonates from Western Canada to the Barnett Shale with background pure mineral points and lines of constant Poisson's ratio and P-Impedance (from Goodway et al., 2010). 75

Figure 3.10. (a) Paleotopography of top Baturaja carbonate platform at early Miocene (see Chapter II). (b) Lithology correlation with stratigraphic interpretation along northwest to southeast (along line A to A' at the paleotopography map of top Baturaja Formation) showing vertical and lateral stacking patterns within the carbonate platform. (Note: Pro=Progradation, Ag=Agradation, Retro=Retrogradation). 79

Figure 3.11. Petrophysical calculations for well C-4 (see Chapter II for porosity and permeability calculation). Lame parameters and brittleness related elastic moduli (Poisson's ratio PR and Young's Modulus E) are also included in the calculation. Note: PSS=Parasequence Set; BRF=Baturaja Formation. 81

Figure 3.12. (a) Crossplot porosities of Baturaja carbonate rock on Lambda-rho versus Mu-rho. (b) Crossplot of three total organic carbon of Baturaja

carbonate rock values (data from Geoservices, 2012c, d, f) on Lambda-rho versus Mu-rho. 82

Figure 3.13. (a) Lithology classification based on minerals content resulted from crossplot of VP/VS versus ν. (b) The lithology classification in the frame of crossplot $\lambda\mu$ versus $\mu\rho$. 82

Figure 3.14. Well-based template of Baturaja carbonate rock classification. The template is built from crossplot of Lambda-rho and Mu-rho associated with Young's modulus and Poisson's ratio. 84

Figure 3.15. Six carbonate rock classes discriminated in Baturaja Formation from the well-based template. 85

Figure 3.16. Stratigraphic chart in Baturaja Formation at well C-4 87

Figure 3.17. The relationship between carbonate facies information (Geoservices, 2012b, c, d, f, 2013a) and the reservoir quality classes. 88

Figure 3.18. The combination of stratigraphic interpretation and carbonate rock quality classes-Part 1. Inset picture at right bottom is RMS acoustic impedance throughout Baturaja Formation interval with purple bold line represents well cross-section (see Chapter II). 89

Figure 3.19. The combination of stratigraphic interpretation and carbonate rock quality classes-Part 2. Inset picture at right bottom is RMS acoustic impedance throughout Baturaja Formation interval with purple bold line represents well cross-section. 91

Figure 3.20. The combination of stratigraphic interpretation and carbonate rock quality classes-Part 3. Inset picture at right bottom is RMS acoustic impedance throughout Baturaja Formation interval with purple bold line represents well cross-section. The carbonate rock are influenced by higher siliciclastic material that is reflected in the domination of higher reservoir quality and lower acoustic impedance value at the two wells in inner ramps. . 92

Figure 3.21. The distribution of carbonate rock classes in parasequences set zones 93

Figure 3.22. The prospective interval (inside red dashed line) consist of very good-good reservoir quality located between moderate to poor reservoir quality, neutron-density crossover values (yellow filled-zone), and gap between invaded formation and deep resistivity values. (a) At well K-22, upper prospective interval potentially contains gas, but lower interval probably only contains water. (b) Four prospective interval were identified at well C-5. 95

Figure 3.23. Right figure is the zoom of the left figure. Two new acid fracturing interval are suggested in Baturaja Formation in well D-6 using the technique presented in this research 98

Figure 4.1. (a) Location of Pagardewa Field, South Sumatra, Indonesia. (b) Major tectono-stratigraphy features of Sumatra during the Tertiary: (1) North Sumatra Basin, (2) Forearc Basin, (3) South Sumatra Basin and (4) Central Sumatra Basin (modified from Wilson, 2002 after de Smet, 1992) 105

Figure 4.2. Regional stratigraphy of South Sumatra Basin (modified from Pertamina, 2012g). Noted BRF=Baturaja Formation. 107

Figure 4.3. Petrographical descriptions from cores, sidewall cores and cutting samples. (a) Wackstone-Packstone from core sample of well C-4 at depth 1921.8 m, (b) Floatstone-Wackstone from sidewall cores sample of well C-5 at depth 1978 m and (c) Wackstone-Mudstone from cutting sample of well E-03 at depth 1480 m.....108

Figure 4.4. (a) Histogram of porosity from 12 wells. (b) Histogram of permeability from 12 wells. Based on the cumulative distributions (solid lines overlying the Histograms), more than 50 % of the porosity in Baturaja Formation are below 5% and permeability are below 0.1 mD. Noted solid black line is cumulative frequencies. 110

Figure 4.5. Classification of hydrocarbon-bearing reservoirs as "conventional" or "unconventional" based on a cross-plot of viscosity μ vs permeability k, as defined by Cander (2012). The Baturaja Formation (BRF) samples (purple dots) indicate that they are associated with tight gas unconventional reservoirs.....111

Figure 4.6. An incident seismic P-wave converted into reflected and transmitted P- and S-waves at the interface between two elastic layers (reprinted from Russell, 2014). 112

Figure 4.7. The AVO inversion workflow for the seismic-based carbonate quality classification. 115

Figure 4.8. Displays of (left panel) original seismic data and (right panel) pre-conditioned seismic data for vertical section passing through the location of: (a) well F-1; (b) well E-6. Note the improvement in resolution (red arrows) and continuity of reflection events (green arrows). 120

Figure 4.9. Vertical sections showing the initial model of (upper) P-Impedance and (lower) S-Impedance within a plane passing through well C-4. The Baturaja Formation has the highest P-Impedance (purple color) and S-Impedance

(blue color). Note: GUF=Gumai Formation; BRF=Baturaja Formation; TAF=Talang Akar Formation. 122

Figure 4.10. (Left) The inversion analysis for inverted P-impedance at well D-8. (Right) The inversion analysis for inverted S-impedance at well C-5. The final synthetic traces shows cross-correlation 0.96 and error 0.25 against the observed seismic trace at well D-8 and corresponding cross-correlation 0.97 and error 0.19 at well C-5. 124

Figure 4.11. The well by well correlation of inverted synthetic and observed (original) seismic traces in P-Impedance inversion analysis and S-Impedance inversion analysis shows total correlation 0.98 and 0.95 respectively. 125

Figure 4.12. Vertical slices of (left panel) inverted P-Impedance and (right panel) inverted S-Impedance passing through the location of well D-6. The insert shows the locations of the vertical slices line on the basemap. Note the different values between inverted P-Impedance and inverted S-Impedance at same location represented by white arrow is caused by variations in fluid content, but at location represented by yellow arrow is caused by variation in lithology (yellow arrow). 126

Figure 4.13. The relation of (left) inverted P-Impedance to (right) the Parasequences set zones of carbonate Baturaja Formation which were constructed in Chapter III. Lower P-Impedance value at progradational parasequences set zone, higher P-Impedance value at agradational parasequences set zones and lower P-Impedance value at retrogradational parasequences set zones... 128

Figure 4.14. The generated (a) Lambda-Rho ($\lambda\rho$) and (b) Mu-Rho ($\mu\rho$) section pass through well D-6. The insert shows the locations of the vertical slices line on the basemap. 131

Figure 4.15. Seismic-based template for carbonate quality classification in Baturaja Formation. (a) The carbonate quality classification based on cross-plot of Lambda-Rho and Mu-Rho bounded by Poisson's ratio and Modulus Young isovalue. (b) The vertical slices of 3D carbonate rock quality derived from the cross-plot pass through well D-6. The cross-section line is plotted in the basemap on Figure 4.12. 133

Figure 4.16. Well- versus seismic-based carbonate quality classification. Fewer carbonate quality classes are discriminated from seismic-based carbonate quality classification rather than well-based carbonate quality classification due to resolution of the seismic data. Note the DST tests results validated the interpreted prospective interval from the well-based and seismic-based carbonate quality classification. 134

Figure A.1. (a) Parabolic-shaped models of coherent reflection events (primary and multiple) after NMO correction; (b) an individual parabola from figure (a) is defined by its move-out in the amount of Δt at far offset (reprinted from Russel, 2011) 161

Figure A.2. Time variant trim static procedure (reprinted from Russel, 2011) 162

LIST OF TABLES

Page

Table 1. Correlation values of inverted acoustic impedance and borehole-derived acoustic impedance in each training well 40

CHAPTER I

INTRODUCTION

The continuously increasing global demand for fuel energy has not been accompanied in recent years by significant new discoveries of hydrocarbon in conventional reservoirs. To add to their hydrocarbon reserves, oil companies must either apply new concepts to existing fields or apply proven concepts to explore frontier areas. To meet the increased energy demand, industry must develop advanced technology to produce oil and gas from low-permeability reservoirs, including coal beds, tight sands, shales and carbonates. Carbonate rocks contain at least 40% of the world's hydrocarbon reserves in conventional and low-permeability (tight) reservoirs. The geoscience discipline of reservoir characterization aims to determine the physical characteristics of hydrocarbon-bearing reservoirs (Ahr, 2008). Seismic data, including images and attributes derived from them, along with other types of geophysical data such as gravity, magnetic, electromagnetic, and well logs, are very useful aids to reservoir characterization. Characterizing carbonate rock is challenging since many of the physical principles that have long worked well in siliciclastic rock cannot be applied successfully due to heterogeneous aspects of carbonate rock such as the matrix, grain size and shape, porosity and permeability. For example, unlike the case of siliciclastic rocks, compressional V_P and shear V_S seismic wave velocities of common carbonate rocks are relatively insensitive to lithology and fluid-content variations (Goodway et al., 1997). Thus, a different approach is required for reservoir characterization of the carbonate rocks of the Baturaja Formation.

1.1 Background and Problem

In United States, oil has been produced from unconventional plays since the 1970s. Holditch (2013) defined unconventional reservoirs as low quality reservoir, due to low permeability or high oil viscosity, that must be stimulated to produce hydrocarbons at commercial flow rates. Such reservoirs include tight gas sands, gas shales, heavy oil sands, coalbed methanes, oil shales, and gas hydrates. Ma et al. (2015) stated the permeability for unconventional reservoirs is mostly below 0.1 mD, but this cut-off value is not well-defined due to the heterogeneos nature of permeability for both conventional and unconventional reservoirs. Cander (2012) discriminated between an unconventional and conventional reservoir based on its location on a crossplot of viscosity versus permeability. Unconventional hydrocarbon reservoirs are defined as those that require the use of technology to alter either the rock permeability or the fluid viscosity in order to produce hydrocarbon at commercially competitive rates.

The Baturaja Formation is a gas-charged tight (0.05-0.5 mD) carbonate reservoir located in Pagardewa Field, Palembang sub-basin, Indonesia. An initial analysis of the petrography and mud-log reports from 18 wells showed that the carbonate rock interval is composed of ~75% mudstone and ~25% wackstone-packstone facies. The porosity of the Baturaja carbonates consists of open microfractures, micro-vugs, as well as intraparticle, intracrystalline, intercrystalline, interparticle and mouldic void spaces (Pertamina, 2010a, b, 2012a, b, c, d, e, g, 2013a, b). Fractures are well-developed and enhance the porosity and permeability of Baturaja Formation (Wibowo et al., 2008; Yuliandri et al., 2011), but the fractures are filled by calcite cement in several places at Pagardewa Field

(Geoservices, 2012d, e, 2013a). I found that the Baturaja carbonates are relatively tight with porosity mostly below 5% and permeability mostly below 0.1 mD. This finding is based on the histogram of porosity from 12 wells (see Chapter II). The gas viscosities are in the range of 0.016 – 0.019 cP (Pertamina, 2010b, 2012a, e, f). Due to the low permeability, the prospective interval was acid fractured to better enable hydrocarbons to flow; however, the production does not meet commercial rates for further development of the field (Pertamina, 2010b, 2012b, e, f, g, h). The reservoir has been traditionally regarded as a conventional hydrocarbon reservoir. However, the reservoir permeability, gas viscosity, and treatment history suggest that the Baturaja Formation should be re-classified as an "unconventional reservoir" based on the Cander (2012) classification scheme (see Chapter II).

1.2 **Research Objectives**

My research brings unconventional exploration tools and concepts to investigate whether any hidden economic potential of Baturaja Formation can be unlocked. The goal of the research is to better characterize the Baturaja Formation by identifying new hydrocarbon traps/plays within the carbonate platform at Pagardewa Field, suggesting new infill well locations, and selecting appropriate intervals for acid fracturing. The ultimate purpose of the research is to increase the hydrocarbon production from the Baturaja Formation at Pagardewa Field, thus raising the economic value of the field.

1.3 Dissertation Structure

This research is divided into three parts to characterize the carbonate reservoir in the study area. Part 1: "*The depositional environment and the porosity distribution of an early Miocene carbonate platform*" is discussed in Chapter II of this dissertation. That part focuses on integrating geological and geophysical methods to identify the Baturaja carbonate platform type and the spatial distribution of its various carbonate facies. Descriptions of the depositional environment and an analysis of the porosity distribution are provided. The depositional profile is reconstructed from paleotopography of the carbonate platform and the spatial distribution of light-dependent skeletal components. A combined multilayer neural network and genetic inversion algorithm was used to transform the industry-provided seismic data into an acoustic impedance profile that is consistent with well controls. The porosity distribution was then predicted from the inverted acoustic impedance. Integrating these results, a new hydrocarbon play at Baturaja Formation is inferred.

Part 2: "*Well-based carbonate reservoir quality assessment of low-permeability carbonate rock: Baturaja Formation, Palembang Basin, Indonesia*" is discussed in chapter III. The tight carbonate rock of Baturaja Formation is treated as an unconventional reservoir. A petrophysical analysis was conducted using a combination of Lamé constants and brittleness-related elastic moduli (Young's modulus and Poisson's ratio). The approach enabled a determination of reservoir quality by inferring the trends of parameters such as brittleness, porosity, TOC and minerals content such as clay, quartz and dolomite. Those parameters were derived from a combination of literature study and petrophysical

analysis of Baturaja Formation. A well-based carbonate quality classification scheme was devised, and combined with a stratigraphic interpretation to better characterize the Baturaja Formation. The results permit increased confidence in selecting previously unexploited prospective intervals for acid fracturing.

Part 3: "*3D distribution of carbonate reservoir quality of Baturaja Formation, determined from seismic AVO inversion*" is discussed in Chapter IV. The method used in this part is similar to that of Chapter III; the main difference resides in the form of the input data. The research reported in Chapter III uses only well data, whereas Chapter IV uses both well data and seismic data as input. Therefore, Chapter III describes a well-based carbonate reservoir quality classification whereas Chapter IV describes a seismic-based classification. The well-based carbonate quality classification used integrated Lamé constants and brittleness-related elastic moduli extracted from well logs; however the integrated Lamé constants in the seismic-based classification are instead derived from AVO inversion of an industry seismic dataset. The seismic data were preconditioned before being injected into the AVO inversion workflow. The result is a contiguous spatial distribution of carbonate reservoir quality classes for Baturaja Formation across Pagardewa Field. The seismic-based carbonate quality classes were compared with the well-based carbonate quality classes. The 3D carbonate quality class distribution is a useful guide to select new infilling wells location for future field development.

CHAPTER II

THE DEPOSITIONAL ENVIRONMENT AND POROSITY DISTRIBUTION OF AN EARLY MIOCENE CARBONATE PLATFORM

2.1 Summary

The Baturaja Formation is an early Miocene carbonate platform located in the Palembang sub-basin of Indonesia. It is a tight gas carbonate reservoir located within Pagardewa Field. Identifying the carbonate platform type is always of significant interest in the context of hydrocarbon exploration and development. Integrated geological and geophysical methods are used herein to identify the Baturaja carbonate platform type and its carbonate facies distribution, along with the depositional environment, and carbonate porosity distribution. The depositional profile was reconstructed from paleotopography of the carbonate platform and the spatial distribution of light-dependent skeletal components. The depositional environment was identified as a carbonate ramp. The carbonate platform comprises two carbonate facies, denoted as A and B, that are differentiated by the abundance of siliciclastic material. A combined multilayer neural network and genetic algorithm was used to invert an industry-provided seismic data into an acoustic impedance profile consistent with well controls. The porosity distribution was then predicted from the inverted acoustic impedance. The zone identified as the inner ramp has the highest porosities (10-12%) due to an increased contribution of siliciclastic material, while the middle and outer ramps have lower porosities (6-10%) due to extensive cementation in these zones. Hydrocarbons are likely to accumulate near lateral boundaries between the

carbonate facies A and B; such locations are marked by large contrasts in acoustic impedance and porosity.

2.2 Introduction

Hydrocarbon exploration efforts since 1905 have contributed to an increased understanding of the regional geology of South Sumatra. The oil company BPM between 1938-1941 drilled several wells, encountering gas in the Baturaja Formation within the Palembang sub-basin of South Sumatra Basin, Indonesia (Basuki and Pane, 1976). In Pagardewa Field, the Baturaja Formation was deposited in a carbonate platform setting. It was initially regarded as a conventional reservoir; consequently all wells were drilled in vertical trajectory. With porosities mostly below 5% and permeabilities mostly below 1 mD, the prospective intervals in the Baturaja Formation were found to require stimulation, e.g. using acid fracturing techniques, in order to produce oil and gas at significant rates (see Geology Background). Nevertheless, the hydrocarbon production rates of wells completed with conventional reservoir techniques do not meet the commercially economic rates needed to develop the field.

The term "carbonate platform" applies either to a thick sequence of shallow water carbonates that develops in any geotectonic setting (Tucker and Wright, 2009), or to depositional surfaces upon which shallow-water carbonate facies are deposited (Ahr, 2008). The distinction between different carbonate platform types is significant for hydrocarbon exploration and development. A knowledge of platform type enables geoscientists to better interpret seismic images of facies architectures and to create reservoir models that include stratigraphic traps (Loucks et al., 1998). Geoservices

(2013b) inferred a shallow marine environment for the carbonate deposition of the Baturaja Formation based on abundances and diversities of fossils preserved in rock samples. Yuliandri et al. (2011) built a depositional model of the carbonate platform based on a reefal environment. However, the Yuliandri model was conditioned only on present-day topography; thus it does not properly take into account the paleoenvironment of the early Miocene. The research presented herein results in a new carbonate platform type for the Baturaja Formation; it is based on the genetic approach developed by Pomar (2001). Integrated well and seismic data were used to support the new carbonate platform type and identify the associated carbonate facies. The depositional profile was reconstructed from the paleotopography of the carbonate platform, taking into consideration the distribution of light-dependent biota across the carbonate platform.

Porosity is an important property that helps to determine reservoir quality. The porosity distribution for the various depositional sub-environments inferred along the Baturaja carbonate platform is predicted in this research. The prediction is made on the basis of well relationships between porosity and acoustic impedance. Acoustic impedance is a rock property that depends on seismic velocity and density. The acoustic impedance of a stratum encountered in a well is readily calculated by simply multiplying the velocity and density readings from a logged interval. Yuliandri et al. (2011) inverted 3D seismic data from Pagardewa Field using a sparse-spike technique to obtain a spatial distribution of acoustic impedance. I used an integrated multilayer neural network and genetic algorithm to invert the same dataset. My algorithm requires that the obtained spatially-distributed acoustic impedance closely matches the acoustic impedance at well locations.

A major goal of this research is to obtain the spatial distribution of predicted porosity over the entire carbonate platform in Pagardewa Field.

This chapter describes a new early-Miocene carbonate platform type identified at Pagardewa Field. A new stratigraphic hydrocarbon play defined by carbonate facies boundaries is identified. The associated carbonate facies distribution and the new play within the carbonate platform can explain the performance of existing wells, i.e. whether they are proven or dry. The resulted carbonate platform model ultimately can be used to locate new, infilling wells for the further development of this oilfield.

2.3 Geology Background

Pagardewa Field is located in Prabumulih Regency, ~80 km SW of Palembang City, the capital of South Sumatra Province, Indonesia (**Figure 2.1**). The field is located within Palembang basin in the southeastern part of the larger, prolific South Sumatra basin. Palembang basin covers an area of roughly 125 by 150 km (Pulunggono, 1986). Sumatra Island comprises the southwestern margin of the stable cratonic area of Asia/Sundaland (Wilson, 2002). The basin is bounded on the southwest by faults and Mesozoic ridges that are associated with the Barisan Mountain range. On the northeast, the basin is bounded by the stable cratonic area of Asia/Sundaland and on the eastern and southeastern sides it is bounded by the Lampung High ridge (Pulunggono, 1986).

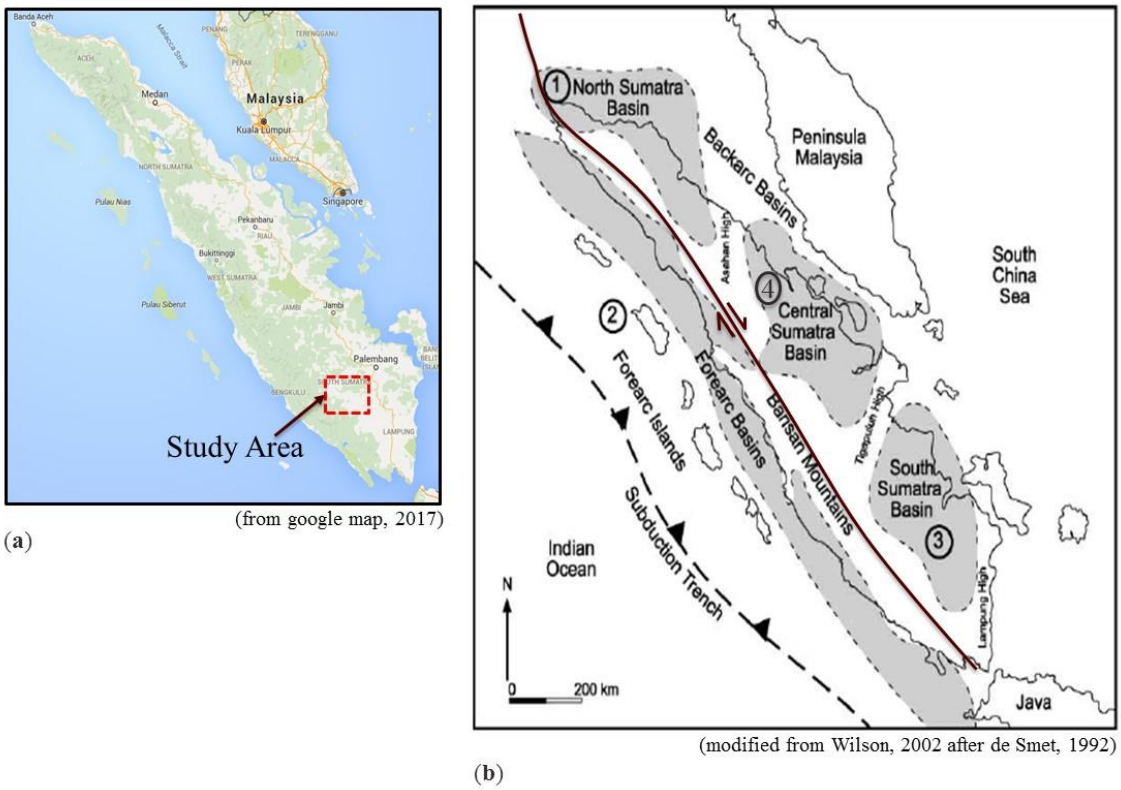

Figure 2.1. (a) Location of Pagardewa Field, South Sumatra, Indonesia. (b) Major tectono-stratigraphy features of Sumatra during the Tertiary: (1) North Sumatra Basin, (2) Forearc Basin, (3) South Sumatra Basin and (4) Central Sumatra Basin (modified from Wilson, 2002 after de Smet, 1992)

The regional tectonic history is dominated by the north-directed subduction of Indian oceanic crust. The oblique subduction has exerted a major influence on island arc and basin evolution, and contributed to an active major strike-slip system. The formation of the Barisan Mountains resulted from active Paleogene-Neogene volcanism associated with the oblique subduction. The dominant tectonic forces led to the formation of three basins in the backarc and one basin in the forearc island during the Paleogene (**Figure 2.1**). Horst and graben development during the late Eocene and Oligocene in the backarc areas was mostly infilled by lacustrine and fluvial sediment (Wilson, 2002). Consequent

Oligo-Miocene subsidence resulted in thick terrestrial deposits that are overlain by marine lithologies. During the early to middle Miocene, carbonate was extensively deposited in the South Sumatra Basin. During the middle Miocene, uplift and erosion of the Barisan Mountains increased clastic sedimentation into the surrounding areas which led to a gradual expansion of the terrestrial environment (Wilson, 2002 after de Smet, 1992).

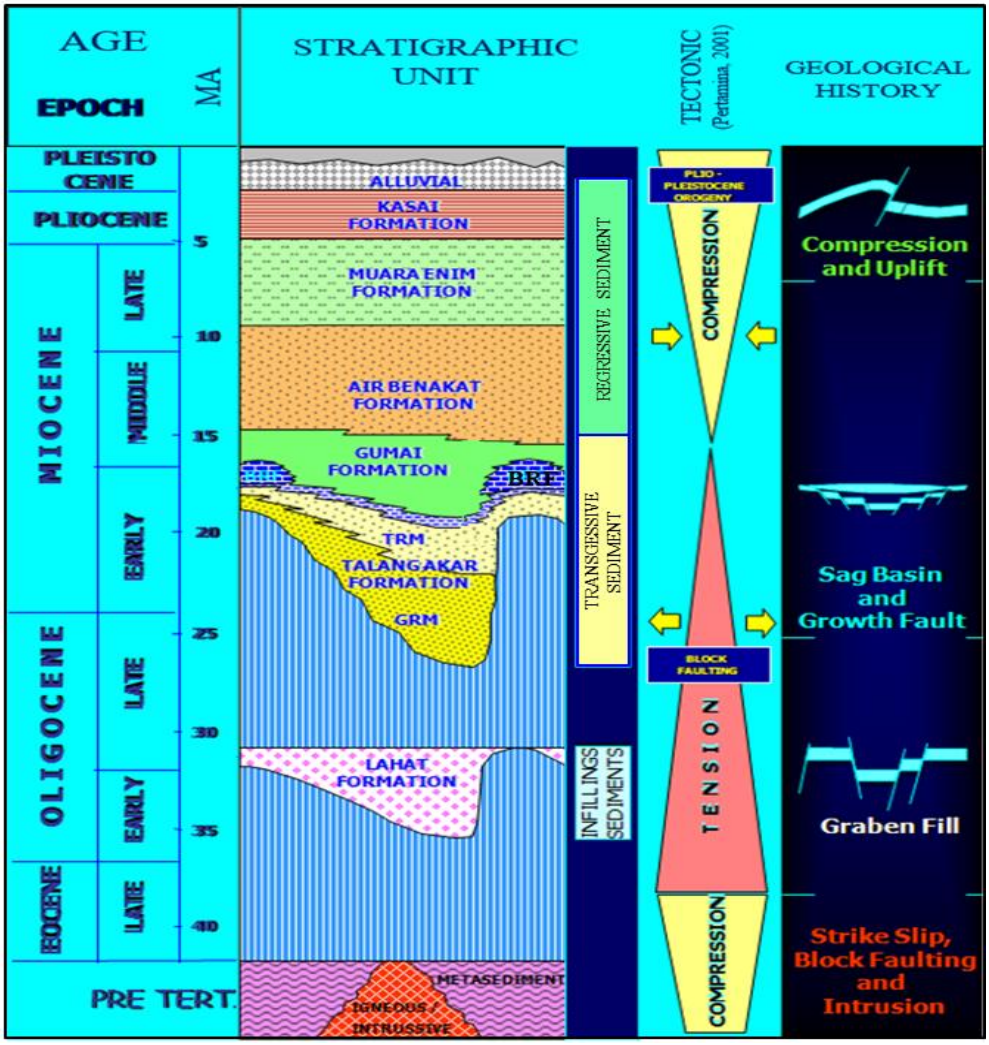

Figure 2.2. Regional stratigraphy of South Sumatra Basin (modified from Pertamina, 2012g). Noted BRF=Baturaja Formation.

The formation of the Palembang sub-basin was controlled by processes that occurred over four tectonic periods (Pertamina, 2012g) (**Figure 2.2**). Basin development started in the middle Mesozoic as older rocks were folded and fractured in association with a granitic batholith intrusion. From the late Cretaceous until the late Paleogene, dextral strike slip motion along the Semangko Fault created half grabens, controlling the sedimentation of Lahat Formation and Talang Akar Formation. Cenozoic rocks of the Palembang basin were deposited during two large-scale cycles, a lower transgressive sequence and an upper regressive sequence (**Figure 2.2**). In the Miocene, transgressive sedimentation of the lower Miocene Talang Akar Formation was followed by the deposition of Baturaja Formation. Initiation of Baturaja carbonate production was diachronous and coincided with rising sea level during the early Miocene. The carbonates were partially drowned in some places, but at the same time in other places, under relatively shallow water, carbonates continued to accumulate. The deep-water shales of the Gumai Formation were subsequently deposited over the drowning platform, and this was followed by uplift of basement rocks during the middle Miocene. The Air Benakat Formation and Muara Enim Formation were deposited during regressive stages. In a final stage during the Plio–Pleistocene, compressional tectonic processes inverted the existing structure within the basin and created several anticlines.

The Baturaja Formation was deposited in the intermediate and shelfal portions of the South Sumatra Basin on or nearby platform highs (De Coster, 1974). Basuki and Pane (1976) reported that Air Kemiling Besar, an outcrop of the Baturaja Formation located 238 km SE of Pagardewa Field, consists of two massive units (upper and lower parts) that

are separated by a finely-bedded unit of lime mudstones and lime wackstones intercalated with marls. In the finely-bedded unit, recrystallization and the presence of carbonaceous matter and glauconitic minerals are common. The massive units consist of mudstones, wackstones/packstones and boundstones with abundant large foraminifers in the upper part. Three dominant facies are interpreted from available cores, sidewall cores and cutting data (Pertamina, 2012d, g) in Pagardewa Field, respectively they are: wackstone-packstone; (ii) coral floatstone-wackstone; and (iii) wackstone-mudstone (**Figure 2.3**). However, the core intervals sampled only the top 10 m of the carbonate rock, and the sidewall cores sampled only at 5-10 m spacing. Thus, a description of the facies of the carbonate rock intervals at the wells is incomplete. However, a simplified two-facies interpretation based on grain sizes was made at the beginning of this research. This analysis shows that the carbonate rock interval is composed of ~75% mudstone and ~25% wackstone-packstone facies.

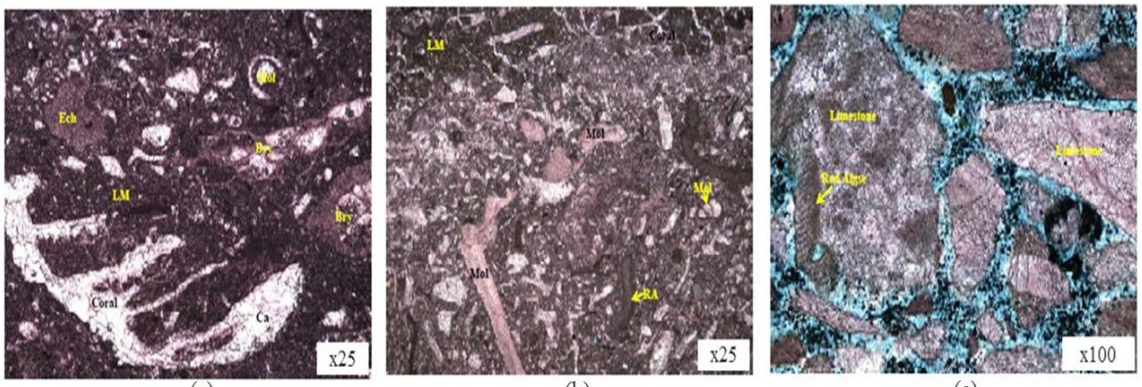

Figure 2.3. Petrographical descriptions from cores, sidewall cores and cutting samples. (a) Wackstone-Packstone from core sample of well C-4 at depth 1921.8 m, (b) Floatstone-Wackstone from sidewall cores sample of well C-5 at depth 1978 m and (c) Wackstone-Mudstone from cutting sample of well E-03 at depth 1480 m.

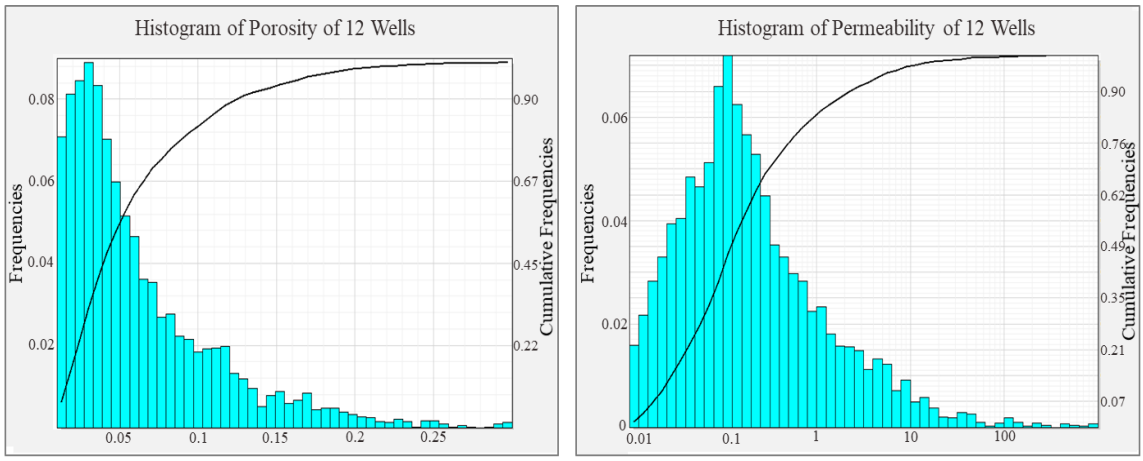

Figure 2.4. (a) Histogram of porosity from 12 wells. (b) Histogram of permeability from 12 wells. Based on the cumulative distributions (solid lines overlying the histograms), more than 50 % of the porosity in Baturaja Formation are below 5% and permeability are below 0.1 mD. Noted solid black line is cumulative frequencies.

With reference to the Choquette and Pray (1970) classification, the porosity of the Baturaja carbonates is dominated by open microfractures and micro-vugs with lesser but significant amounts of intraparticle, intracrystalline, intercrystalline, interparticle and mouldic void spaces (Geoservices, 2012a, b, c, d, e, f, 2013a, b). At Merbau Field, a gas field located 10 km west of Pagardewa Field, fractures are well developed in the Baturaja interval (Wibowo et al., 2008). Yuliandri et al. (2011) stated fractures enhanced porosity in highly faulted area of Baturaja Formation at Pagardewa Field. However, the fractures are filled by calcite cement in many places within this field (Geoservices, 2012d, e, 2013a). Petrophysical analysis of cores performed in this research shows a strong relationship between porosity and permeability at several wells (e.g well E-3 and K-24). This is unusual in carbonate rock although it is common in siliciclastic rock (see Well & Seismic Analysis in Methodology). The petrographic report shows high amounts of siliciclastic input in the form of detrital quartz and clay minerals (kaolinite) in those wells

that exhibit an unusually strong porosity–permeability relationship. Seismic attribute and acoustic impedance were used to further explore this anomaly throughout the field.

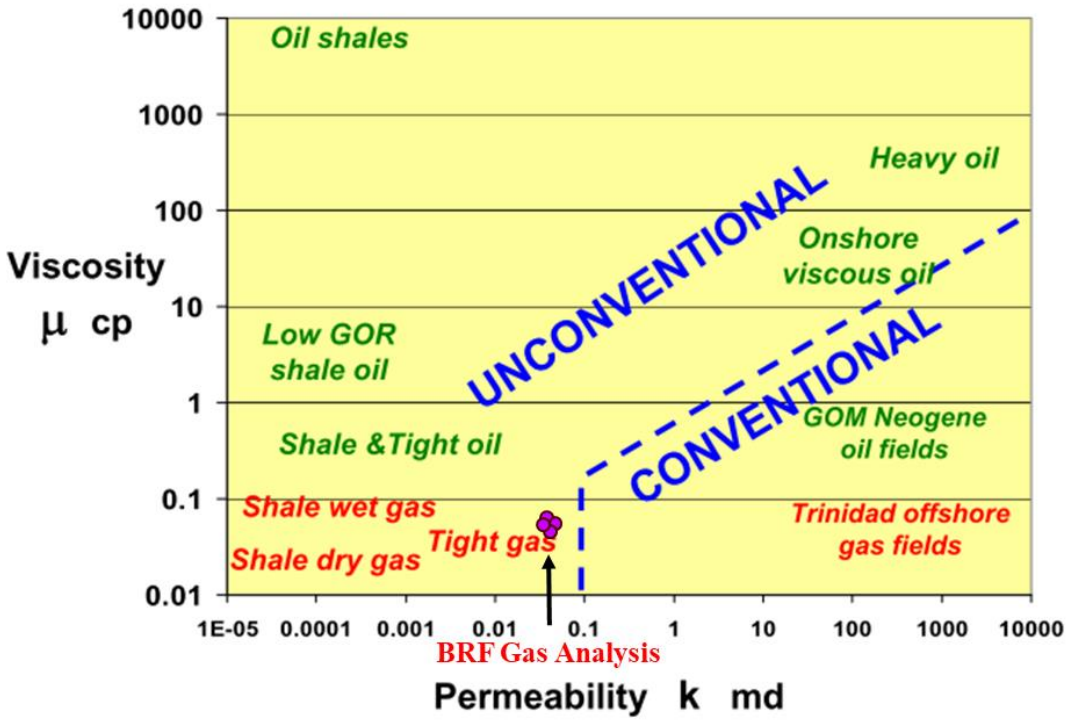

Figure 2.5. Classification of hydrocarbon-bearing reservoirs as "conventional" or "unconventional" based on a cross-plot of viscosity μ vs permeability k, as defined by Cander (2012). The Baturaja Formation (BRF) samples (purple dots) indicate that they are associated with tight gas unconventional reservoirs.

Figure 2.4 shows histograms of porosity and permeability in Baturaja Formation from 12 wells. The methods used to obtain porosity and permeability are explained in the methodology. Based on the cumulative probability distributions, shown by the solid lines in the figure, more than 50% of the porosity determinations are below 5% and a similar number of the permeability determinations are below 0.1 mD. The Baturaja carbonates are therefore relatively tight with low porosity and permeability. Since hydrocarbons in such

prospective intervals will not naturally flow at economic rates, they have been acid-fractured to raise the permeability. Cander (2012) defined unconventional and conventional reservoirs based on a crossplot of viscosity versus permeability. Pressure volume temperature (PVT) analysis of four gas samples from four wells (e.g C-4, E-6, K-22 and L-1) are plotted in Cander's graph. Their location on the crossplot suggests that Baturaja Formation is a tight gas carbonate rock and classified as an unconventional reservoir (**Figure 2.5**). In summary, the reservoir properties, such as permeability and viscosity, and treatment history suggest that the Baturaja Formation should be regarded as an "unconventional reservoir" according to the Cander (2012) classification scheme.

2.4 **Methodology**

2.4.1 Depositional Environment Identification

It is important to understand the carbonate depositional profile because it clarifies the geological evolution of the platform. Pomar (2001) stated that the variability of depositional profiles of carbonate platforms depends on the type of sediments being produced, the loci of sediment production, and the hydraulic competency. Pomar (2001) also classified the main groups of benthic biota according to their dependence on the availability of light as:

1. Euphotic biota

These biota include autotrophs and mixototrophs that require relatively strong light conditions and consequently live in shallow-water environments, such as the nearshore, wave-agitated zone. The maximum depth of this zone is 40-50 m in very clear water, but

more commonly, the depth is 20-30 m. Green algae and corals of the modern sea and stromatoporoids and rudists of ancient seas are characteristic members of this biota group.

2. Oligophotic biota

These biota comprises autotroph and mixototroph organisms that thrive in low-light environments, such as a shaded shallow-water zone or, compared to the euphotic biota, further out onto the continental shelf. The oligophotic zone is generally located below the fair weather base. Ocean currents play the primary role in transporting sediments, but the zone can also be agitated during storms. The maximum depth of this zone is ~50-100 m in clear water. Red algae and larger foraminifers are characteristic organisms present in this zone. A mesophotic zone, spanning the 40-80 m depth range, may be distinguished as intermediary between the euphotic and oligophotic zones.

3. Photo-independent biota

These biota refer to heterotrophic organisms that do not require light. Their survival depends on myriad factors such as food supply, the nature of the substrate, competitive displacements, temperature, salinity, and hydraulic energy. Bryozoans, mollusks, crinoids, brachiopods and sponges are characteristic members of this biota.

The depositional environment of the Baturaja carbonate platform is identified in this study using the method of Pomar (2001). The approach is based on an analysis of the dominant type of carbonate-producing biota distributed across the carbonate platform. The bioclast distribution and paleotopography are combined in this research to identify the depositional setting of the Baturaja Formation at Pagardewa Field.

2.4.2 Well & Seismic Analysis

Geological and geophysical data were integrated to help achieve the goals of this study. Available data from 18 wells[1] are used to delineate the boundaries of Baturaja Formation. These data include gamma ray, resistivity, photoelectric, neutron porosity, sonic and density logs. Petrographic information in the form of SEM and XRD images from cores, sidewall cores, and cuttings are combined to describe the carbonate facies of rock samples. Cores were available from four wells (C-4, E-3, K-22 and L-1), sidewall cores from six wells (C-5, D-8, E-6, E-3 and K-24) and cuttings from four wells (F-1, D-6, J-1 and E-4). **Figure 2.6** shows the location of the wells on the basemap bounded by the edges of the 3D seismic dataset coverage at Pagardewa.

Pre-conditioning procedures were applied to the well logs before performing petrophysical analysis. The well logs were first normalized and depth-corrected using the boundary of each formation obtained from mud-log reports. The core sample depths were assigned to the correct depth in the well logs. Log density and neutron logs were corrected for the limestone matrix along the Baturaja Formation interval. The porosities along the Baturaja Formation at each well were estimated using density log readings by:

$$\phi_{D,LS} = \frac{\rho_b - \rho_{LS}}{\rho_f - \rho_{LS}} \tag{2-1}$$

where $\phi_{D,LS}$ is density porosity in the fluid-filled limestone units (%), ρ_b is the measured density log, ρ_{LS} is the density of calcite limestone matrix 2.71 (g/cm^3) and ρ_f is the density of the fluid filling the rock. The latter was defined by assessing the cross-over of neutron

[1] Well names were changed due to company confidentiality

and density values, with water density (1 g/cm^3) used where there is no cross-over indication, while gas density (0.2 g/cm^3) is used where there are cross-overs. The estimated porosities are plotted alongside the measured porosities from the cores at similar depths to investigate the validity of the estimated porosities. **Figure 2.7** shows the estimated porosities from the logs closely match the porosities from laboratory analysis of the core data.

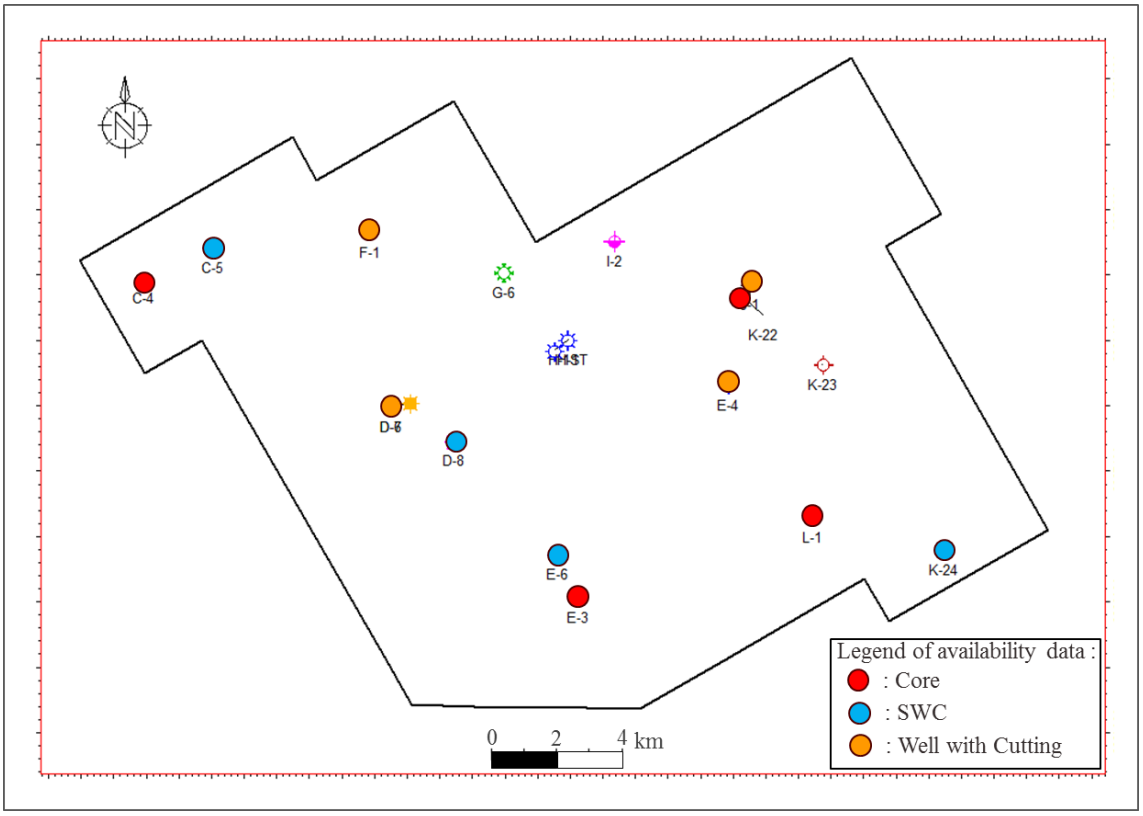

Figure 2.6. The availability data for this research on the basemap of 3D seismic Pagardewa overlying with the wells location (Noted the coordinates on the basemap are not shown due to company restrictions). Three wells were used for well to seismic correlation: C-5, D-8 and L-1.

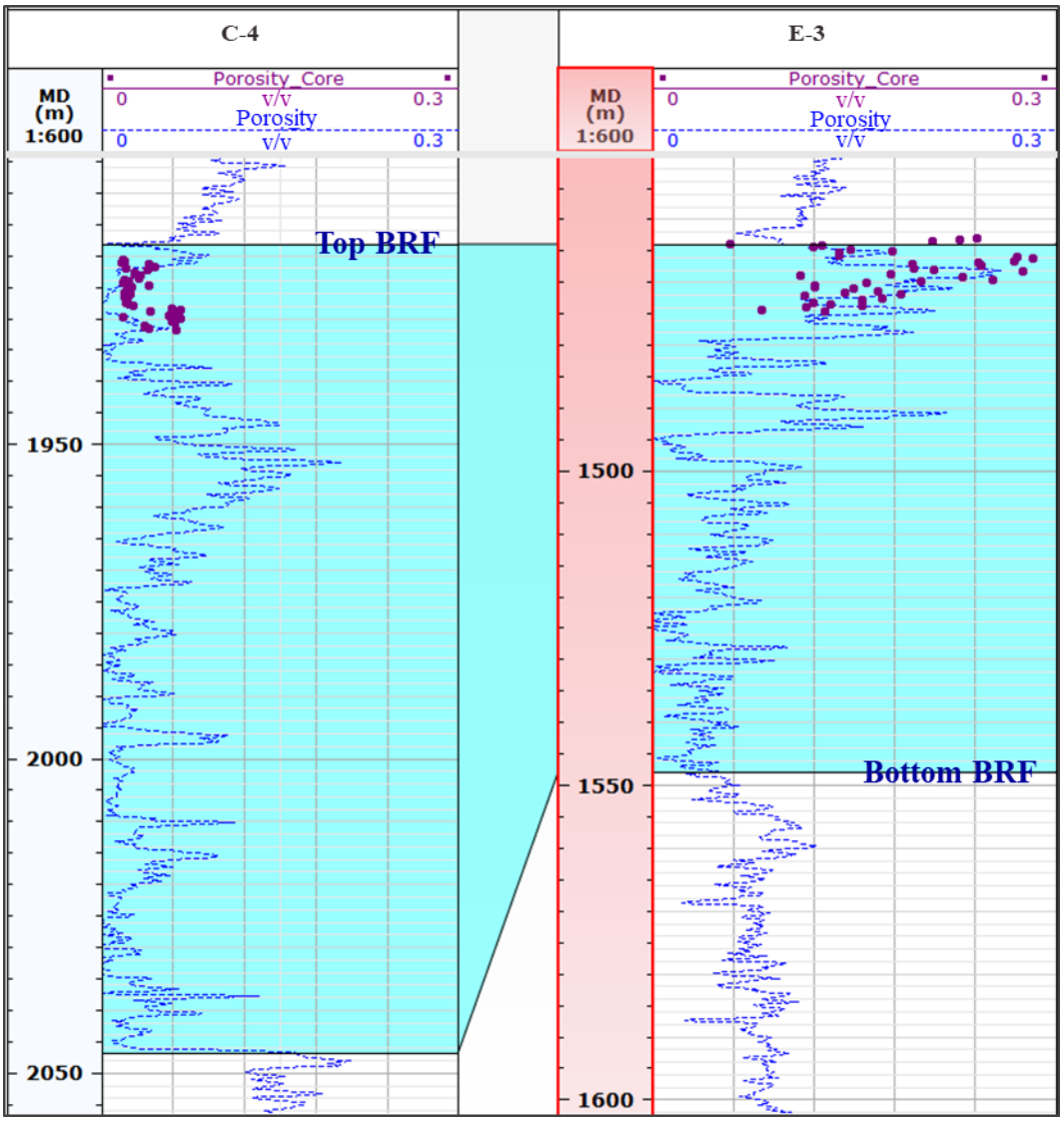

Figure 2.7. The estimated porosities from petrophysical calculations (blue dashed curve) closely approach the measured porosities from core of wells C-4 and E-3 (purple dot). Note BRF= Baturaja Formation, and the blue zone is the Baturaja Formation interval.

The permeability of Baturaja Formation was estimated from porosity using the core porosity-permeability relationship:

$$k = a\phi^b \tag{2-2}$$

where k is permeability in mD, a and b are constants, and ϕ is porosity. Since the core data sampled only 10 m below the top of Baturaja Formation, except side-wall cores which sampled every 10 m, the correlation (2-2) was applied to the entire Baturaja interval to estimate permeability values. For example, **Figure 2.8** shows the core porosity-permeability correlation for four wells. The linear relationship of core porosity and permeability at well C-4 and D-8 shows a small correlation coefficient, which is considered to be a "normal" value due the heterogeneity of the carbonate rock. However, the cross-plots of porosity and permeability core at wells E-3 and K-24 show higher correlation coefficients. Such high values are unusual in carbonate rock although common in siliciclastic rock. The petrography reports (Geoservices, 2012b, f) show high amounts of siliciclastic material in the form of detrital quartz and clay minerals (kaolinite) (**Figure 2.9**). Clay minerals such as kaolinite may reflect proximity to the sediment sources and deposition in relatively nearshore settings, but post-depositional diagenetic alteration of clays related to burial and pore-water geochemistry must also be considered (Flügel, 2013).

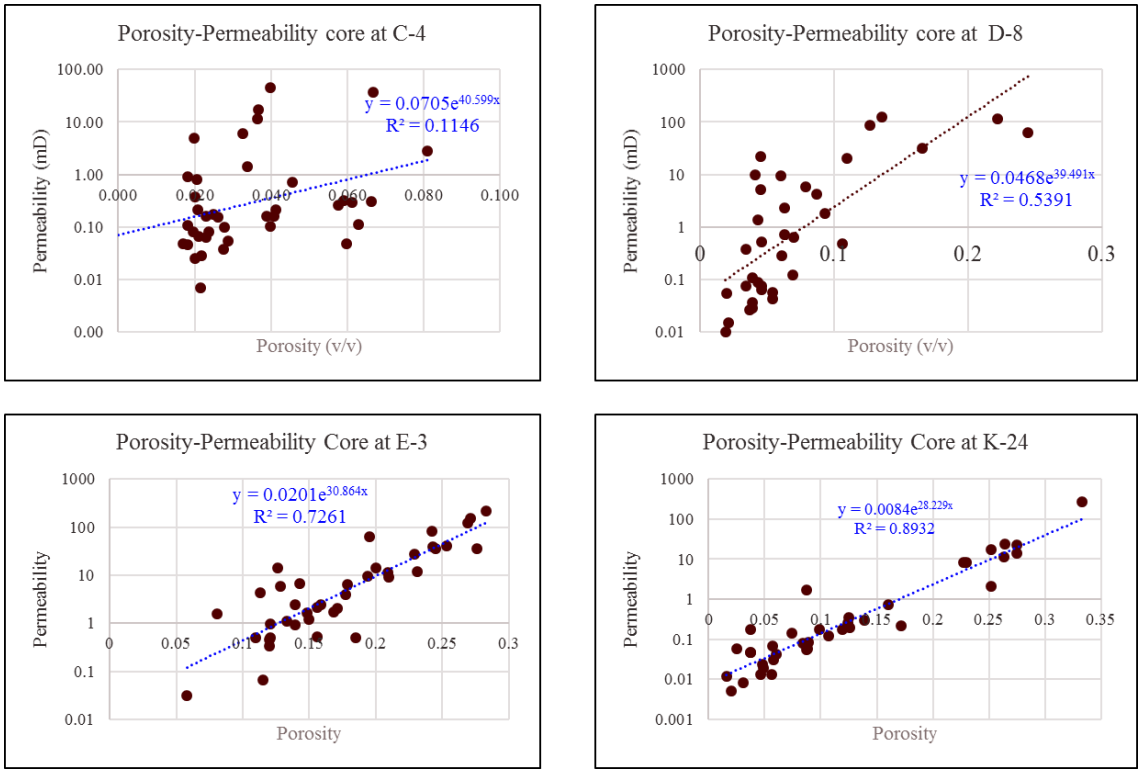

Figure 2.8. The higher core porosity-permeability relation on the lower part (Well E-3 and K-24) may be related with higher siliciclastic material in the carbonate rock.

The geophysical information was extracted from the seismic "3D Pagardewa" dataset, acquired in 2004, which covers an area ~350 km^2. The boundary of the seismic data coverage is shown on the basemap in **Figure 2.6**. Both post-stack and pre-stack migrated seismic data are available, however only the post-stack data were used here. The dominant seismic frequency is $f = 20$ Hz which determines the spatial seismic resolution of subsurface layers. With the average P-wave velocity V_P~5,414 m/s of the carbonate interval extracted from several wells, the vertical seismic resolution $h = \lambda/4$~68 m, where λ is the seismic wavelength in m.

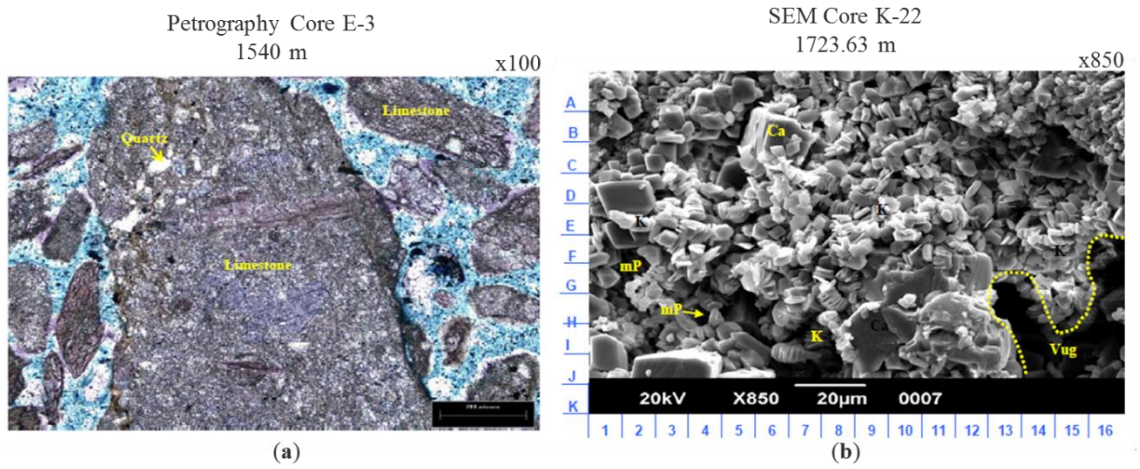

Figure 2.9. (a) Petrography of core E-3 at depth sample 1540 m. (b) SEM of core K-22 at depth sample 1723.63 m. Those rock samples indicated the non-carbonate constituents in the form of detrital quartz and clay minerals (kaolinite) (adapted from Geoservices, 2012b; Geoservices, 2012f).

A well-seismic tie procedure was used to locate rock formation boundaries. The well-to-seismic tie is a process that matches, at well locations, synthetic seismograms to actual seismic data. The former was created by a convolution of reflection coefficients with an appropriate wavelet. The reflection coefficients were calculated by computing the acoustic impedance contrast between lithological layers. The borehole-derived acoustic impedance at a well location was calculated simply by multiplying the density log and sonic (P-wave) log readings. A standard check-shot correction was used to ensure that the sonic log was placed at the correct time sample within the seismic section (Hampson-Russell, 2011). The wavelet used to create the synthetic seismograms should resemble that of the actual seismic wavelet used during original seismic processing. However, due to the absence of this information, a Ricker wavelet was used. A wavelet extracted from the seismic trace along the wellbore was used to design the Ricker wavelet. The Ricker

wavelength had dominant frequency 20 Hz, length 100 ms and its phase was rotated -90^0 from maximum phase (**Figure 2.10**).

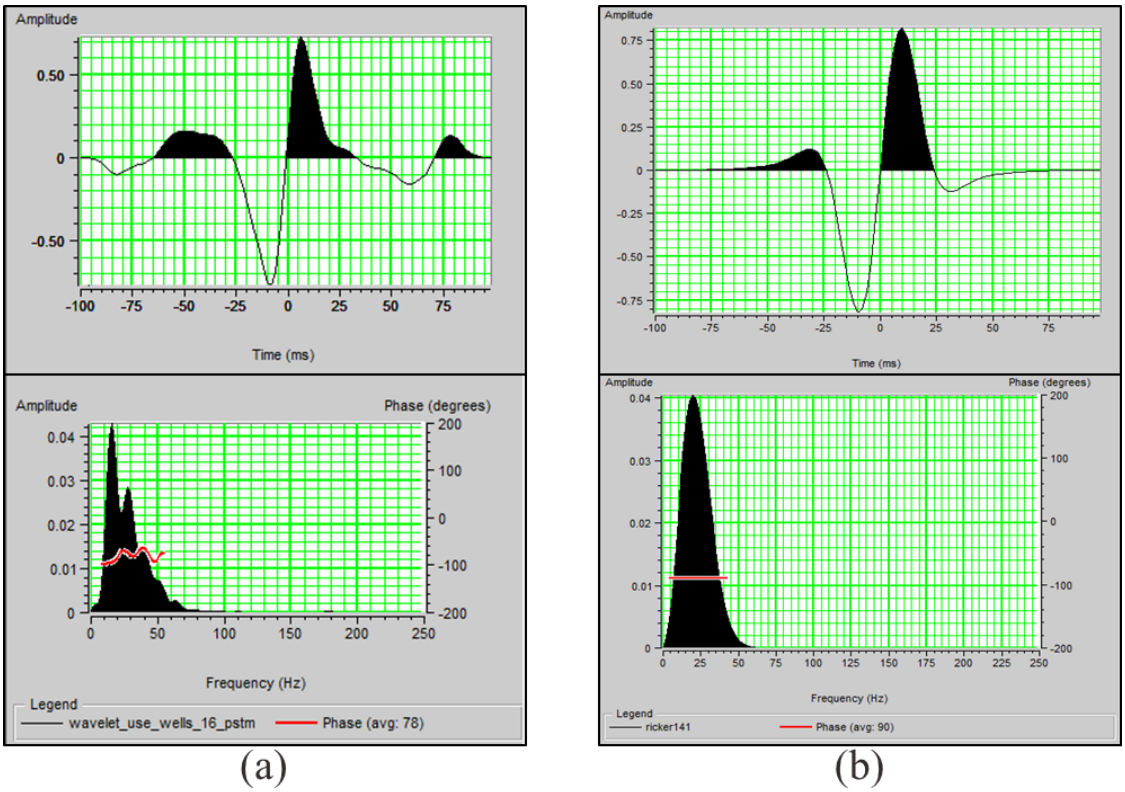

Figure 2.10. (a) The amplitude series and spectrum of extracted wavelet at seismic traces along wellbore of 16 wells. (b) The amplitude series and spectrum of the appropriate ricker wavelet for well seismic tie. The ricker wavelet (b) were design from the parameters of the extracted wavelet (a).

The post-stack migrated (PSTM) seismic data was processed using the convention that increasing acoustic impedance is represented by a negative amplitude (or trough) and decreasing acoustic impedance is represented by a positive amplitude (or peak). This convention is also applied to the synthetic seismograms in the well-to-seismic tie process. For example, in the ties to wells L-1 and C-5, (**Figure 2.11**) the synthetic seismograms of both wells correlate to the PSTM seismic data. While the top of Baturaja Formation is

represented by the zero-crossing from peak to trough, the bottom is represented by a reversed zero-crossing from trough to peak. The upper zero- crossing indicates the acoustic impedance change from the overlying, deeper-water shale of Gumai Formation to the carbonate rock of Baturaja Formation. The lower zero- crossing indicates the acoustic impedance change from carbonate rock to the deltaic siliciclastic deposits of the underlying Talang Akar Formation.

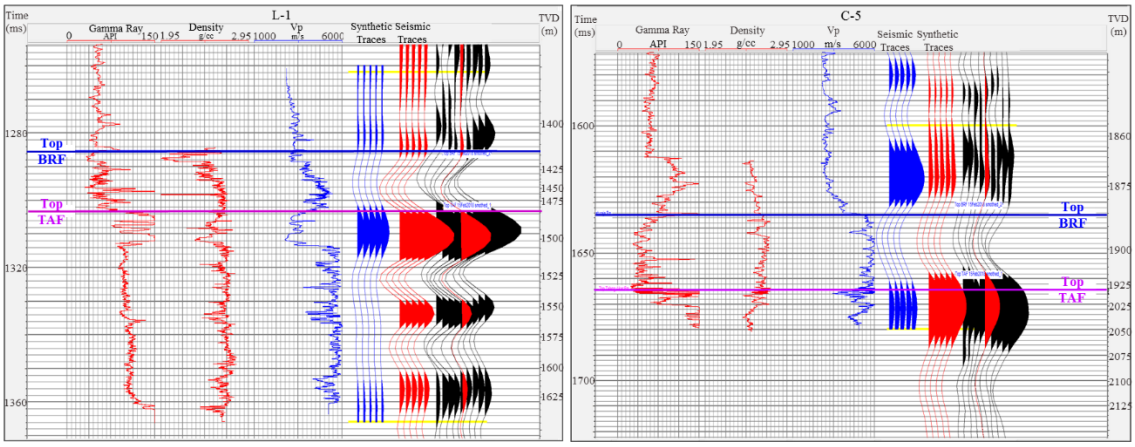

Figure 2.11. Well-to-seismic ties in wells L-1 (a) and C-5 (b). Synthetic seismograms (blue traces) correlate well with seismic inline traces (red traces) for the interval where the log density and sonic were available. The location of two well on the basemap can be seen in **Figure 2.6**. The boundaries of the carbonate interval are defined by zero crossing (+/-; top) to zero crossing (-/+; base).

Top and bottom of Baturaja Formation were interpreted through the field resulted a time-structure map of the top and bottom of Baturaja Formation. The time-structure map has been converted into a depth-structure map by applying a velocity-depth function. The velocity model is assumed to be linear: $V(Z) = V_0 + K * Z$, where V is velocity (m/s) at depth Z, V_0 is the velocity at the surface, and K is the slope of the velocity function. A different linear velocity model was calculated for each rock formation interval based on

time-depth relationships found in the wells, and then interpolated laterally using a convergent gridding algorithm (see Haecker (1992) for more details about the algorithm).

2.4.3 Neural Network and Genetic Algorithm Inversion

Seismic inversion is widely applied in the petroleum industry to extract subsurface parameters from seismic traces. Geophysical inversion of seismic data is generally formulated as a non-linear optimization problem. There are two main approaches to non-linear optimization. The first uses the local gradient of an objective function to iteratively improve a starting model. Least squares, steepest descent and conjugate gradient methods belong to this group. Such local methods depend strongly on the starting model, but are prone to entrapment in local minima, often become unstable, and the calculation of derivative information is often difficult and costly (Sambridge and Drijkoningen, 1992). The second approach does not require derivative information, instead using a quasi-random search through model space to find an optimal subsurface model. Global methods including Monte Carlo, simulated annealing and genetic algorithms belong to this group.

Genetic algorithm (Holland, 1992) is a quasi-random search method that requires no derivative information. The method is significantly more efficient than a pure random walk through model space. The algorithm is based on an analogy with biological evolution in that models with lower misfits tend to survive and reproduce at the expense of poorer-fitting models, in a manner akin to "survival of the fittest." The method was introduced into geophysics by Gallagher et al. (1991) and Sambridge and Drijkoningen (1992) who compared it to Monte Carlo and simulated annealing methods. As described in many places (e.g. Everett, 2013), the three stages that comprise a single iteration of a genetic

algorithm are reproduction, crossover and mutation. The reproduction step ensures the survival of "fit" models, while crossover allows models to exchange "genetic" information between themselves, and mutation adds randomness to the population to help ensure that the search does not converge on a local minimum of the objective function.

Recently, genetic algorithms have been applied in petroleum geoscience to invert seismic data. At a geothermal field in South Australia, Pavlova and Reid (2010) used a genetic inversion (a patented Schlumberger product integrated into the commercial Petrel^{TM} software package) to generate a porosity cube from 3D seismic data. Al-Rahim and Abdulateef (2017) used the acoustic impedance found by genetic inversion to generate effective porosity for the purpose of reservoir characterization and prospect identification at Al-Kumait oil field, South Iraq. The genetic inversion module in Petrel is based on a combination of a neural network and a genetic algorithm. A neural network (e.g. Rumelhart et al., 1986) resembles a human brain that acquires knowledge from the environment and stores it via inter-neuron connection strengths known as synaptic weights. A multilayer neural network consists of an input signal (stimulus), a hidden layer (where information processing is performed), and an output signal (response).

A workflow based on a hybrid neural network/genetic algorithm was used in this research to generate acoustic impedance from the PSTM seismic data (**Figure 2.12**). The main inputs are seismic amplitudes and borehole-derived acoustic impedance at the wells. During the learning phase, instead of back-propagating the error (as in a standard neural network algorithm), the genetic algorithm was used to update the network weights. This allowed the neural network to discover the global minimum error of the objective function,

whereas standard neural network algorithms generally converge only to a local minimum (Pavlova and Reid, 2010). The iterations stop when an optimal solution is reached; the result is termed an "inverted acoustic impedance cube".

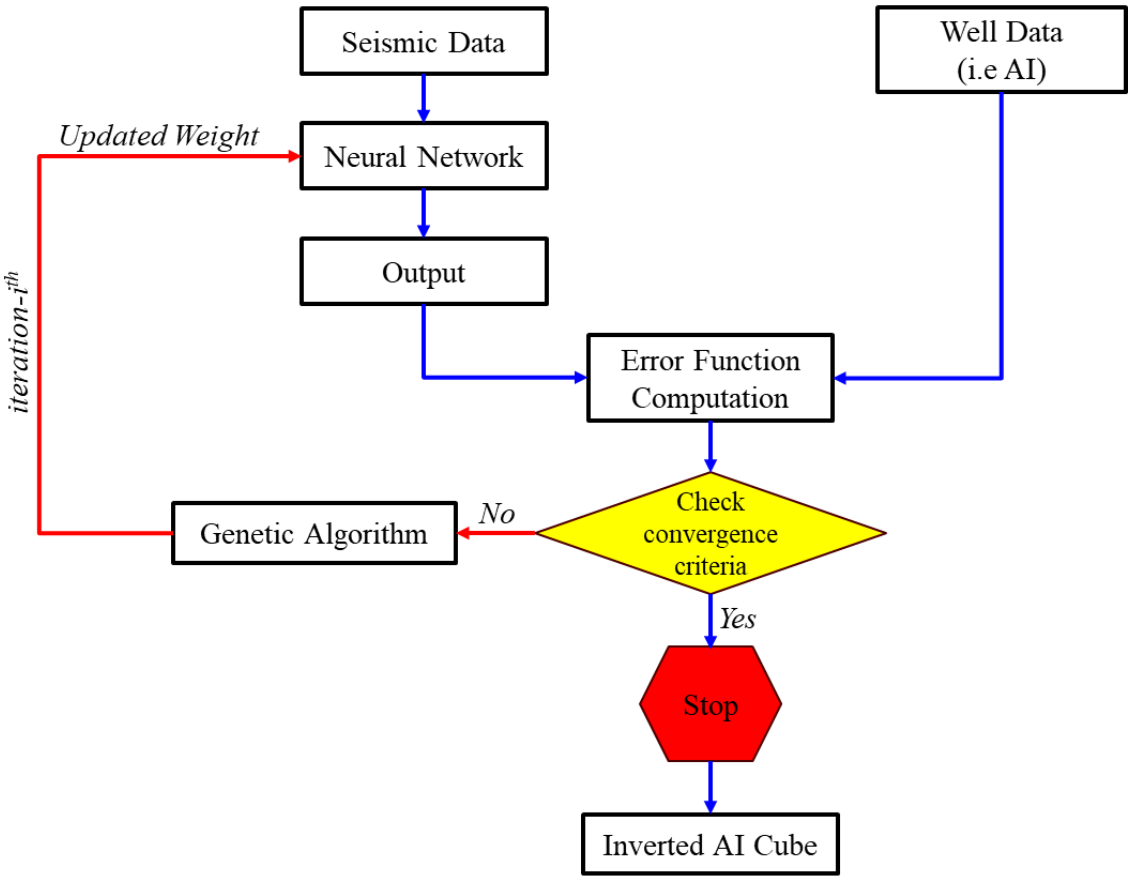

Figure 2.12. Workflow of integrated multi-layer neural network and genetic algorithm that was used herein to generate inverted acoustic impedance from PSTM Seismic data (modified after Pavlova and Reid, 2010)

The quality of the inversion result was measured using the following tests. The borehole-derived acoustic impedance data at a given training well were regressed on inverted acoustic impedance traces near a well location. Such a regression was made at

each well location. A global regression line was then constructed using the same process at all well locations. A number of "blind" wells, excluded from the set of training wells, were selected to validate the robustness of the inverted acoustic impedance.

2.5 Results

2.5.1 Well & Seismic Analysis

The Baturaja carbonate interval, identified based on the well-seismic tie process, is represented by large negative seismic amplitudes across the survey area (**Figure 2.13**). The top and bottom of Baturaja Formation were distributed laterally through Pagardewa Field. This resulted in a time-structure map that was then converted into depth-structure map. The depth-structure map of the top of Baturaja Formation shows deepening to the NW direction, whereas landward is to the SSE direction. These directions are aligned with the position of Pagardewa Field at the SW of South Palembang Basin according to the Mesozoic layering sediment map extracted from seismic (Pertamina, 2011) (**Figure 2.14**). This map indicates that the depositional strike of the sediment at this location is NE-SW, with layers dipping to the NW. The interpreted faults shown on the seismic basemap have a dominant NE-SW direction, although one fault in the east has a N orientation. The N- and WNW-trending major faults are basement-rooted faults in Palembang Basin. They are important structural elements and are associated with Tertiary sedimentary infill of rugged paleotopography.

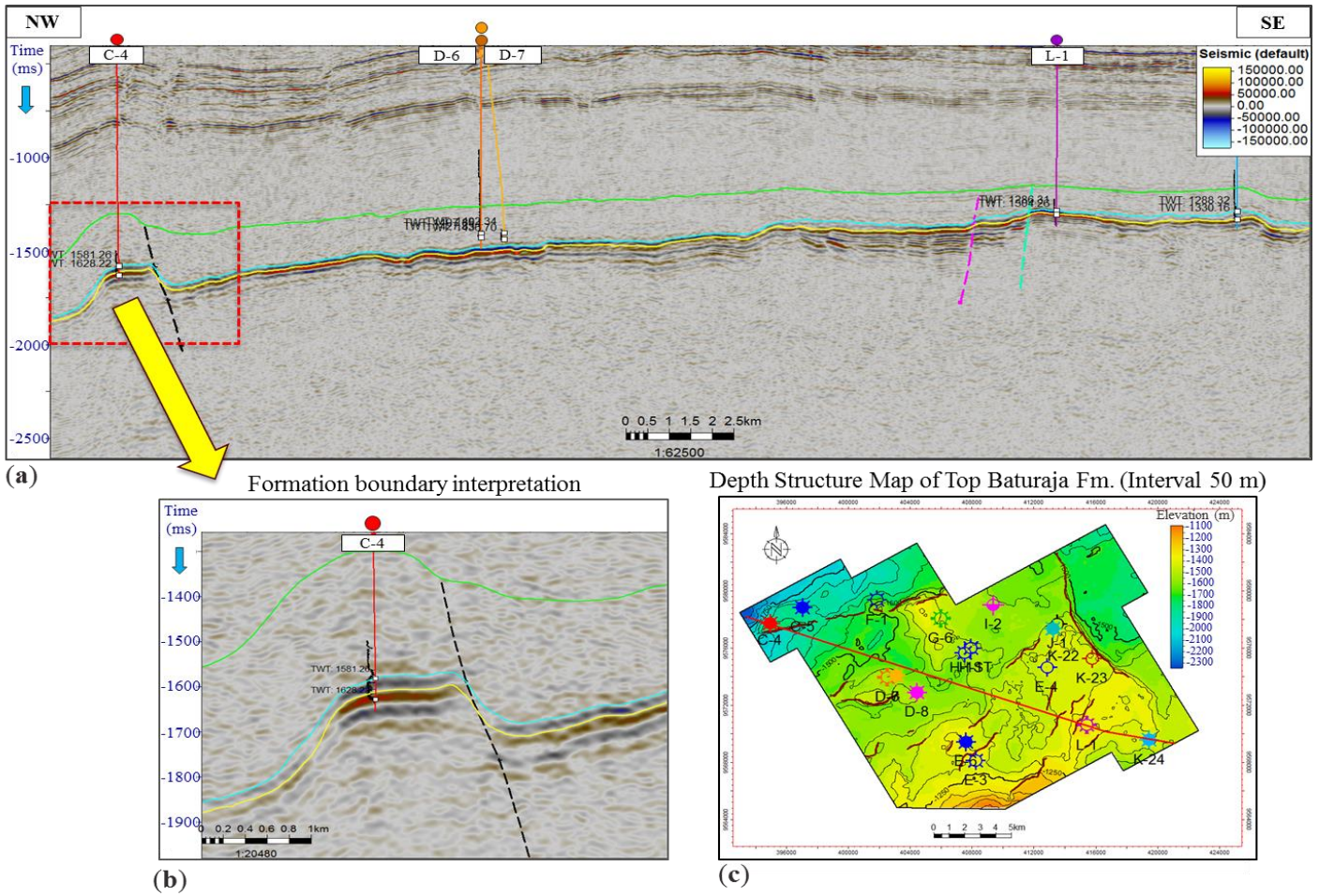

Figure 2.13. (a) Seismic interpretation at Pagardewa Field. (b) The carbonate interval is clearly seen in the seismic data as a large negative amplitude between zero crossings. (c) Basemap of Pagardewa Field showing depth structure map of top Baturaja Formation associated with fault interpretations, well locations and the seismic cross-section line shown (a).

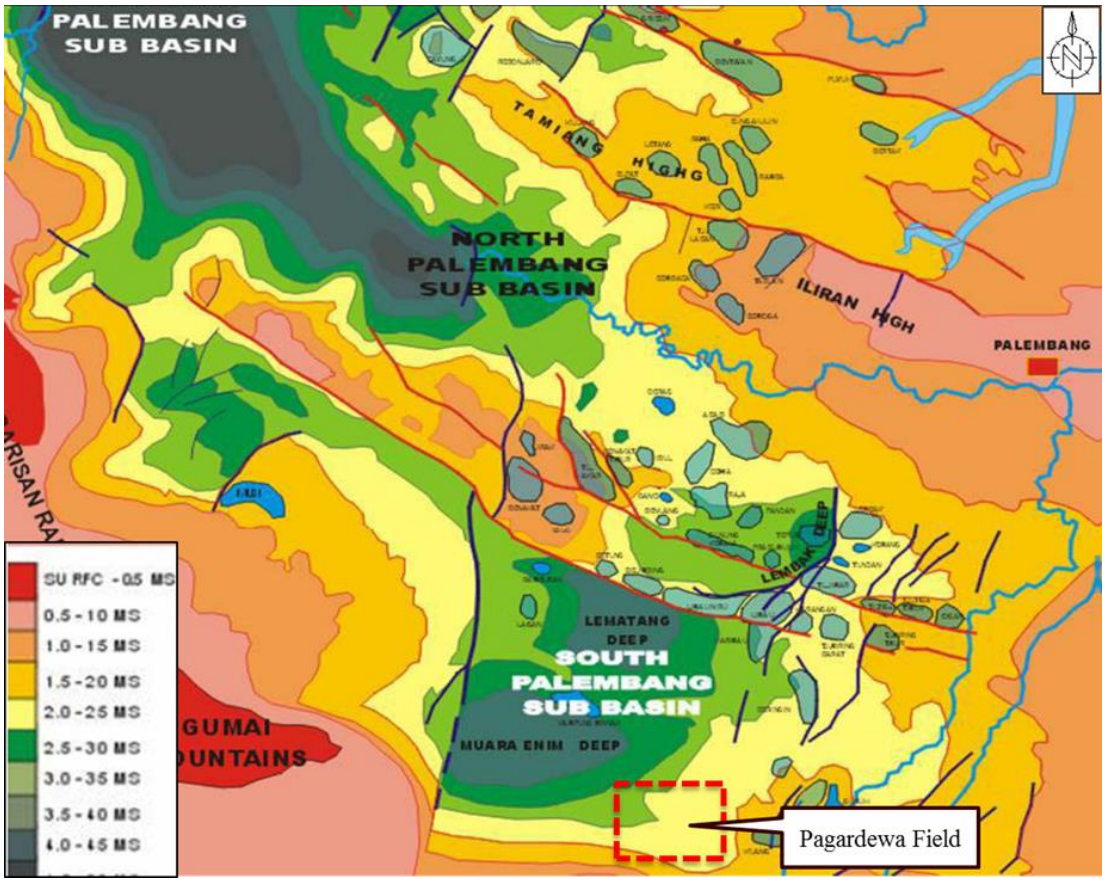

Figure 2.14. Mesozoic layer map extracted from seismic. Note rectangular dashed line is the location of Pagardewa Field (adapted from Pertamina, 2011)

The thickness of Baturaja Formation (isochron) indicates that the carbonate platform thickens to the SE and thins to W and NW (**Figure 2.15**). The isopach map indicates the depositional strike of the formation is NE-SW. The migrated seismic data was flattened at the maximum flooding surface (MFS) near the top of Baturaja Formation (**Figure 2.16**). This surface represents the approximate paleotopography associated with carbonate deposition at early Miocene. The maximum flooding surface near the top of Baturaja Formation was selected as a datum because: 1) the MFS is distributed widely

across the area, and 2) the paleo-topography at the of top of Baturaja Formation is not significantly affected by the overburden layer.

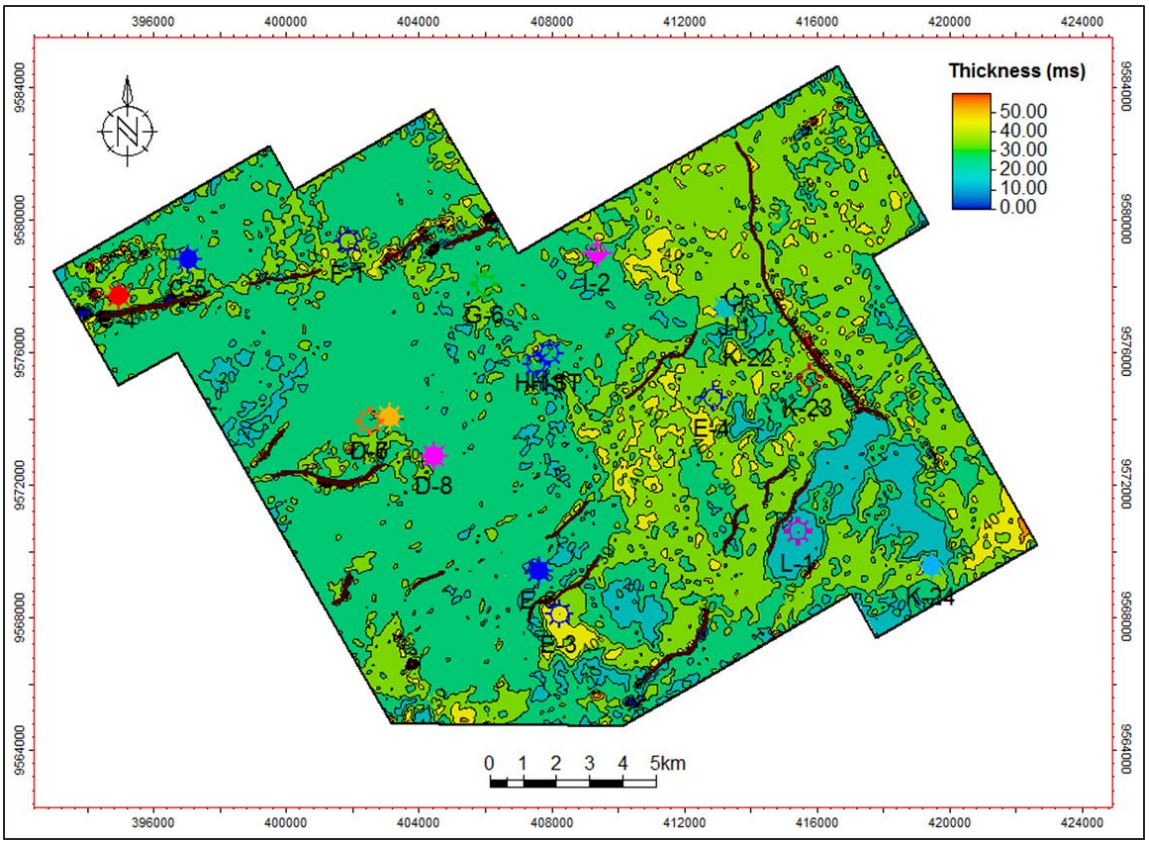

Figure 2.15. The thickness of Baturaja Formation map in domain time (ms)

An RMS-amplitude seismic attribute is defined as the root mean square of the amplitudes of instantaneous trace samples over a specific time or depth interval. The attribute reveals anomalous amplitudes that may be related to facies or lithological changes along the interval. The RMS amplitude extracted along the Baturaja Formation interval shows lower RMS amplitude values to the east and southeast and higher RMS amplitudes toward the west (**Figure 2.17**).

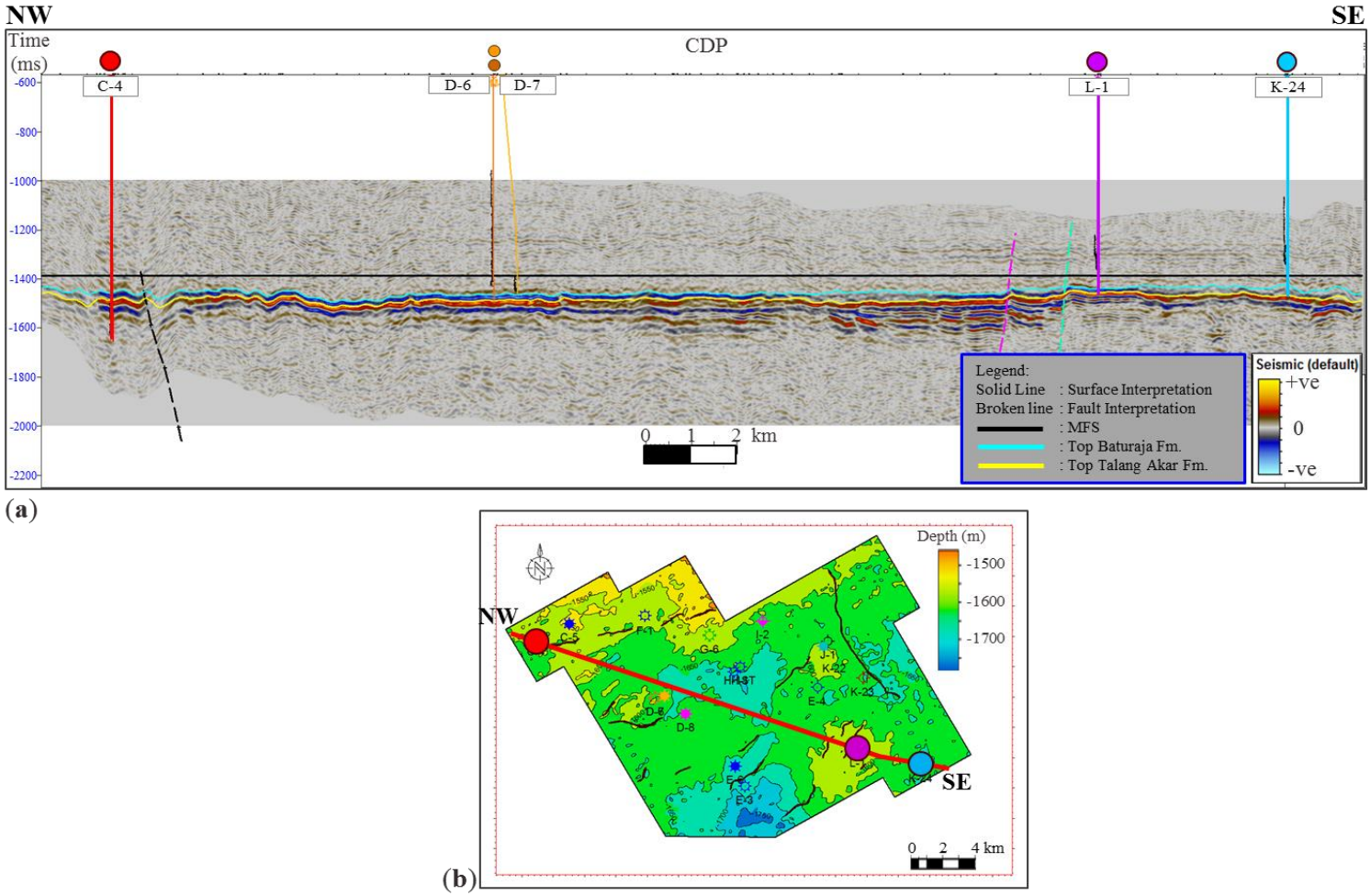

Figure 2.16. (a) The flattened seismic data at MFS near top of Baturaja Formation. (b) The approximated paleotopography of top of carbonate platform at early Miocene.

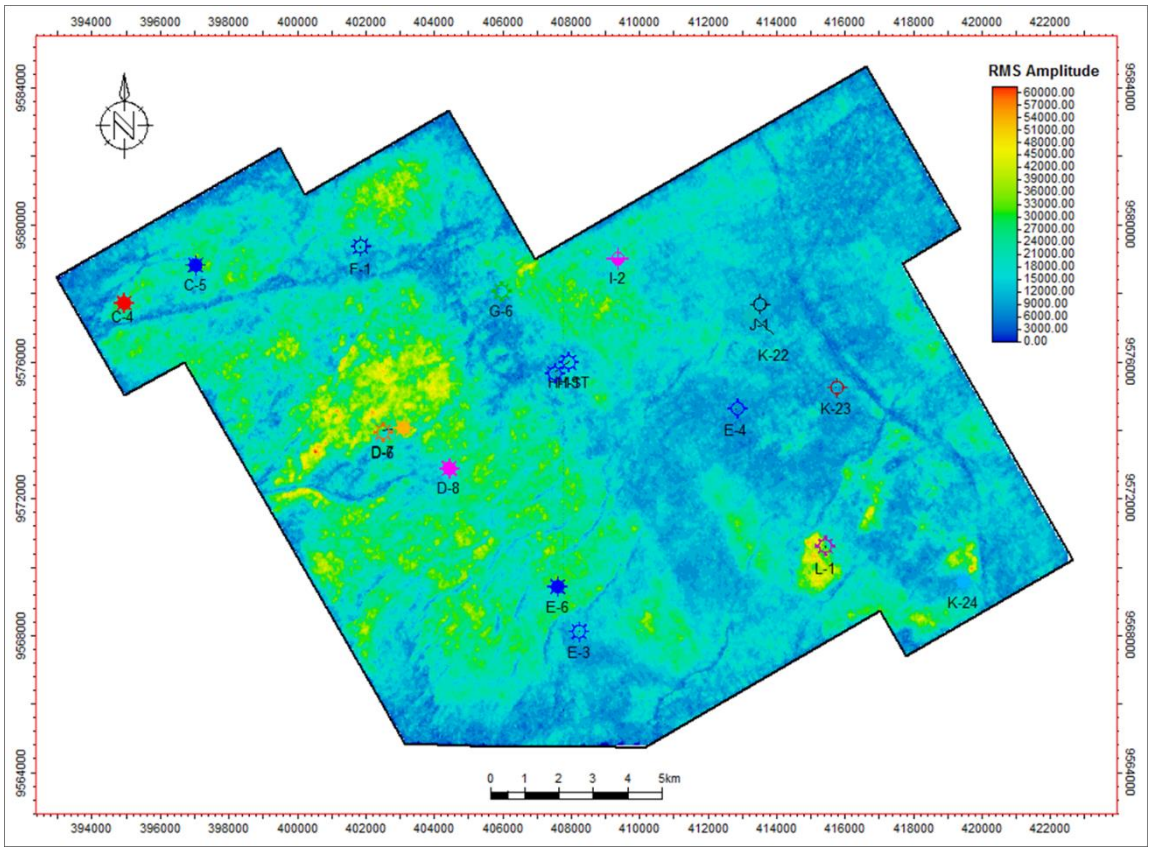

Figure 2.17. RMS amplitude map of Baturaja Formation throughout the Pagardewa Field. Cool colors represents lower values and warm colors represents higher value of RMS amplitude.

2.5.2 Carbonate Rock Composition and Distribution

A carbonate rock description was determined from the available petrographic and XRD information. There are 45 samples from cores (although sampled only 10 m from the top of Baturaja Formation), sidewall cores (sampled at several points along the Baturaja Formation interval), and cuttings from nine wells (K-22, K-24, F-1, D-7, D-8, E-3, L-1, C-4 and C-5). The histograms in **Figure 2.18** show rock compositions in percentages. Carbonate constituents include bioclast and carbonate minerals. Non-carbonate constituents include insoluble residues: clay minerals and detrital quartz; and

authigenic minerals: pyrites and feldspar (the carbonate composition term refer to Flügel (2013)). Benthic foraminifers comprise the highest occurrences of bioclasts, followed by planktonic foraminifers and red algae. Aphotic biota such as mollusks is abundant, while coral are also common.

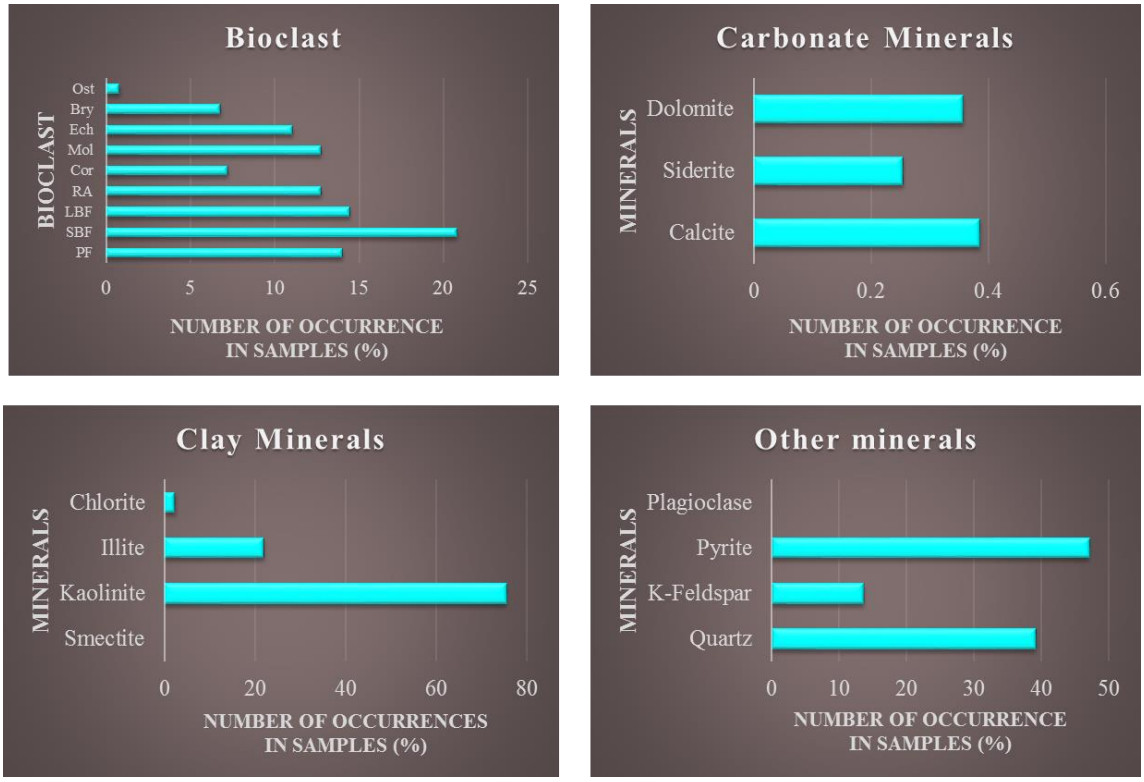

Figure 2.18. The percentage distribution of grain (left) and mineral (right) occurrences in 45 samples from nine wells.

The "other minerals" are dominated by authigenic pyrite and detrital quartz with minor K-feldspar. The carbonate minerals consist mainly of calcite and dolomite with moderate siderite abundance. Clay minerals are present in some wells, dominated by kaolinite with subordinate illite and chlorite. Another authigenic mineral, glauconite, is sparsely present in a few of the samples. **Figure 2.19** shows the distribution of carbonate

facies that were sampled mostly at the top of Baturaja Formation. The facies are based on the Dunham (1962) classification scheme. The carbonate rock composition is reported from dominant to subordinate at each well. The underlying map is the isopach map of Baturaja Formation.

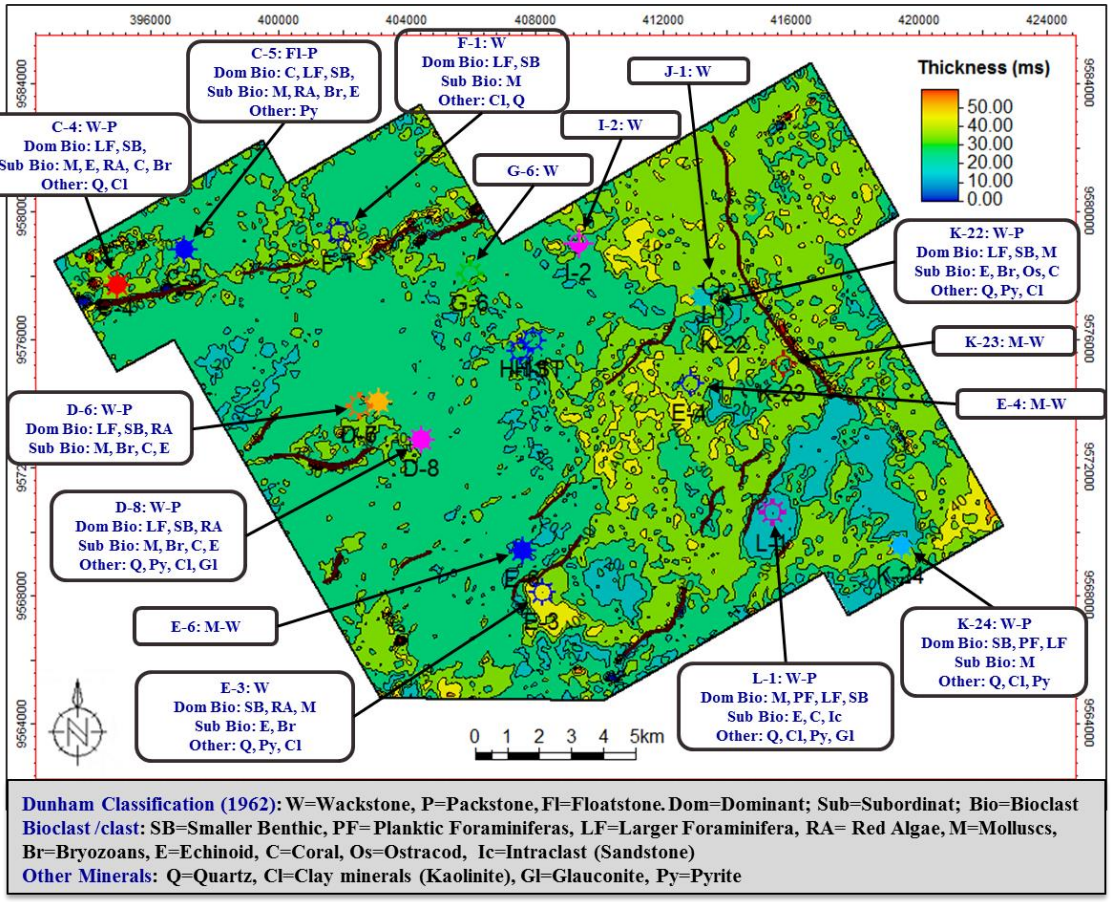

Figure 2.19. The thickness of Baturaja carbonate platform map in domain time overlying by the distribution of carbonate rock classification refers to Dunham (1962) associated with carbonate composition (carbonate and non-carbonate constituents) found in each of the wells (rock sampled near the top of Baturaja Formation). Larger formanifers, smaller benthic and red algae dominated the carbonate platform. Non-carbonate minerals are dominated by quartz and pyrite with minor presence of clay and glauconite.

2.5.3 Rock Modeling

Seismic amplitudes were simulated using forward modeling of the facies model. This was done to infer the siliciclastic input influences in the carbonate platform. The amplitude modeling determines the effect on acoustic impedance contrast as an incident seismic wave traverses different lithologies. The rock model was built from properties observed at the wells. The rock model consists of two layers; the deep-water shale of Gumai Formation overlying two different carbonate rock facies: facies "A" and facies "B" (**Figure 2.20**a). Facies A is composed of carbonate constituents with low siliciclastic input, whereas facies B is similar but has higher siliciclastic input. The following are examples of representative P-wave velocity, S-wave velocity and density values of the three lithologies in the model, as extracted from wells:

- Gumai Fm shale: $V_P = 2900$ m/s; $V_S = 1773$ m/s; $\rho = 2.52$ g/cm^3
- Facies A: $V_P = 4700$ m/s; $V_S = 1350$ m/s; $\rho = 2.6$ g/cm^3
- Facies B: $V_P = 4200$ m/s; $V_S = 2000$ m/s; $\rho = 2.54$ g/cm^3
- Talang Akar Fm. sandstone: $V_P = 3500$ m/s; $V_S = 1700$ m/s; $\rho = 2.45$ g/cm^3

The synthetic seismic traces were generated from the model by convolution of the Ricker wavelet and the reflection coefficients. The latter were calculated by computing the acoustic impedance contrast between lithological layers. The acoustic impedance within a layer is calculated by multiplication of the borehole log density and the logged P-wave velocity. The same convention is used as per the seismic data analysis: increasing acoustic impedance is represented by a negative amplitude, or trough. **Figure 2.20**b and

Figure 2.20c shows the result of forward modeling. The amplitude of a seismic wave traveling from shale to carbonate facies A is stronger (in terms of negative amplitude) than that of the same wave traveling from shale to carbonate facies B.

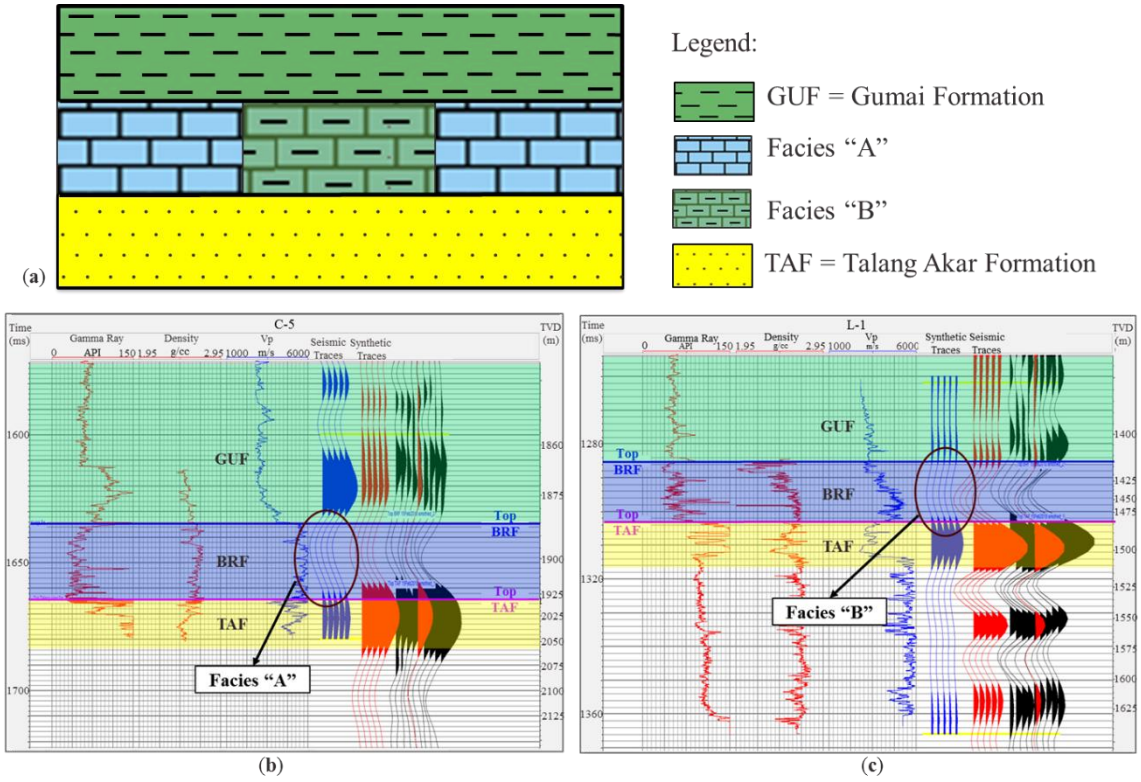

Figure 2.20. (a) Rock model for forward modeling. (b) Forward modeling of the rock model at well C-5 defined stronger amplitude, Facies "A", along the Baturaja interval. (c) Forward modeling of the rock model at well L-1 defined weaker amplitude, Facies "B", along the Baturaja interval.

2.5.4 Inverted Acoustic Impedance

The neural network/genetic algorithm was used to transform the seismic data into an acoustic impedance cube. The inversion used seismic traces and borehole-derived acoustic impedance at 13 wells as the training dataset. The result is an inverted acoustic impedance cube spanning the seismic coverage area. The inverted acoustic impedance

accurately estimates the borehole-derived acoustic impedance at wells C-5 and D-8 (**Figure 2.21**). The correlations are 0.93 and 0.88, respectively. **Table 1** shows the well-by-well correlations, with the global value of 0.79. Note also that the inverted acoustic impedance accurately defines the top and bottom of the Baturaja carbonate interval boundary.

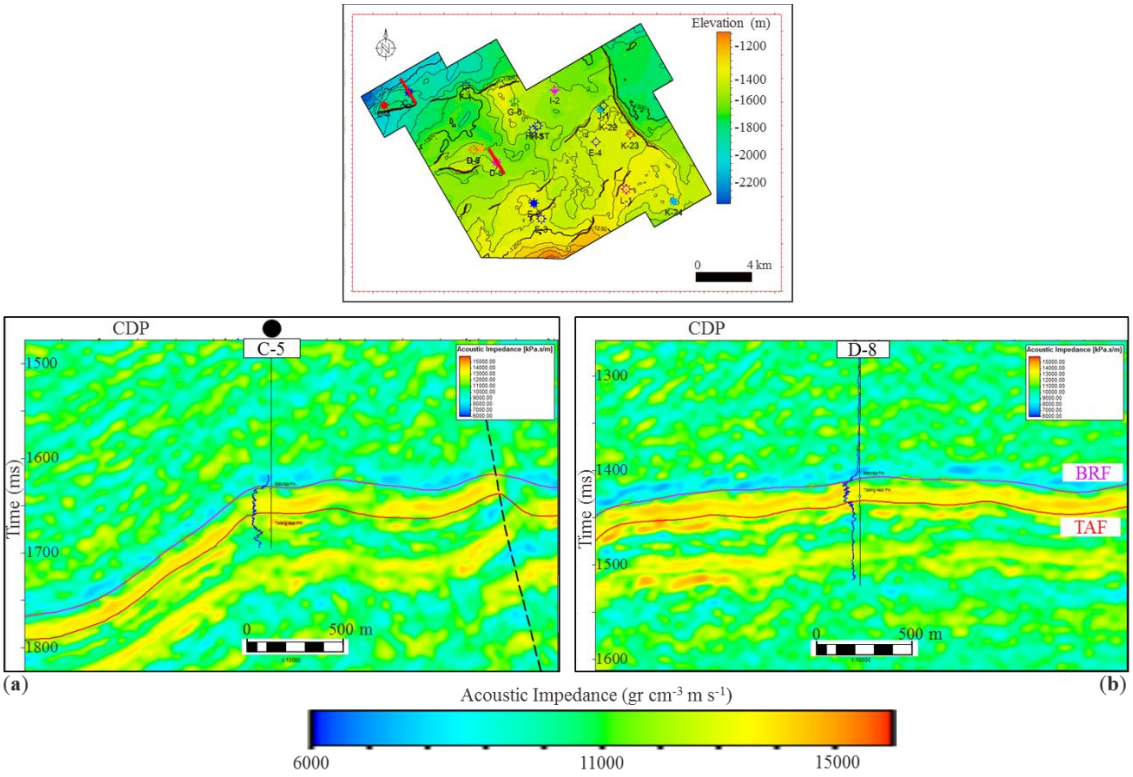

Figure 2.21. Inverted acoustic impedance along an inline section across (a) well C-5 and (c) well D-8. The inverted acoustic impedance accurately estimates the borehole-derived acoustic impedance (blue curve). Insert figure above is depth structure map of Top Baturaja Formation (recent structure) with the inline cross-section marked with red bold line.

Table 1. Correlation values of inverted acoustic impedance and borehole-derived acoustic impedance in each training well

Training wells	C-5	F-1	G-6	D-8	E-4	K-22	K-23	I-2	D-6	J-1	E-6	E-3	L-1
Correlation	0.93	0.92	0.90	0.88	0.87	0.84	0.83	0.82	0.80	0.78	0.72	0.69	0.37
Samples	38	46	35	44	24	53	36	48	44	41	43	54	34

The acoustic impedance logged in the two blind wells C-4 and K-22 show a good match with the seismic-inverted acoustic impedance (**Figure 2.22**). A minor uncorrelated zone at the upper part of the C-4 log is present. This results from the difficulty of sampling the inverted acoustic impedance along a deviated well trajectory. It proved easier to sample only a vertical trace (inline or crossline) near the deviated well trajectory for correlation purposes. The inclination of the well at the top of the carbonate interval (depth 1918.2 m) is ~5^0, decreasing to <2^0 at depth 1992 m, from there becoming almost vertical to the bottom of the carbonate interval. The well trajectory that straightens with depth explains why the reduced correlation appears only at the upper part while the remainder of the carbonate interval shows a higher correlation.

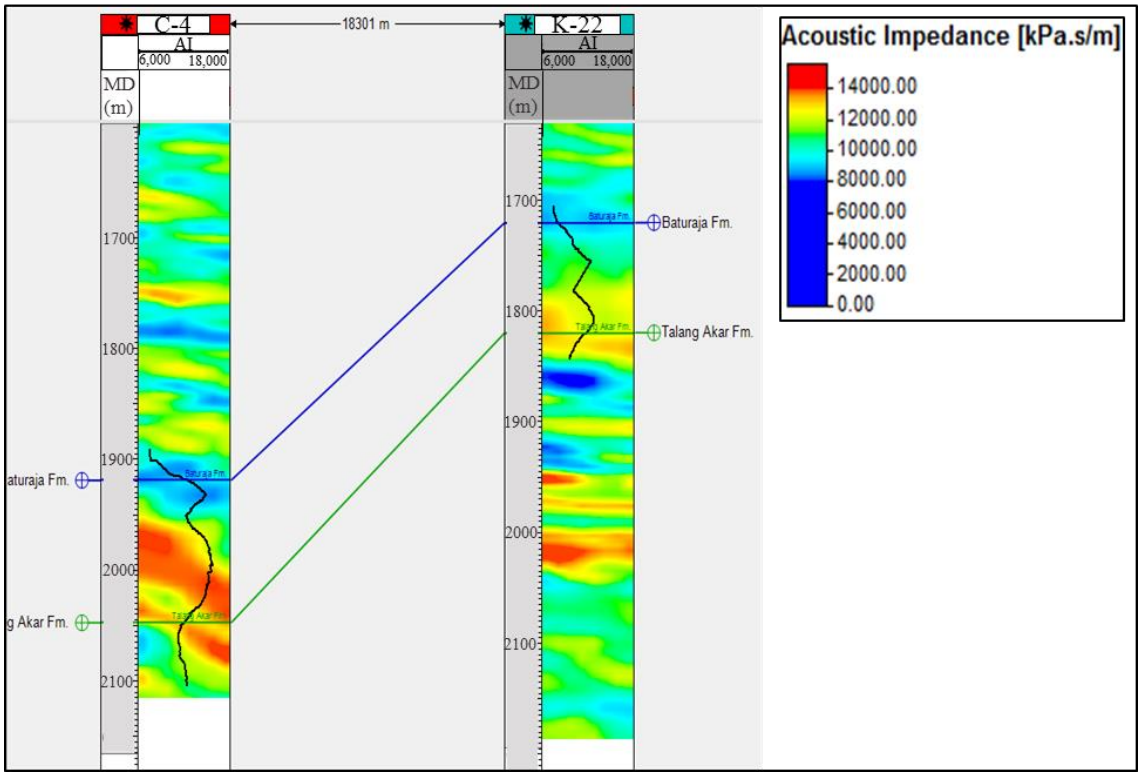

Figure 2.22. Validation analysis using blind wells C-4 and K-22. The inverted acoustic impedance trace sampled along and near well trace (background color) has a good similarity with borehole-derived acoustic impedance (black curve).

2.6 Discussion

2.6.1 Depositional Environment Model of the Baturaja Carbonate Platform

The carbonate platform type of the Baturaja Formation was identified using the genetic approach developed by Pomar (2001) (**Figure 2.23**). The depositional profile was reconstructed from the paleotopography of the platform and the light-dependent biota distribution across the carbonate platform. The bioclast distribution near the top of carbonate platform (see **Figure 2.18** and **2.19**) shows that the dominant biota are larger foramanifers and red algae. These organisms commonly live in the oligophotic zone. The subordinate biota are aphotic biota that can survive in any water depth.

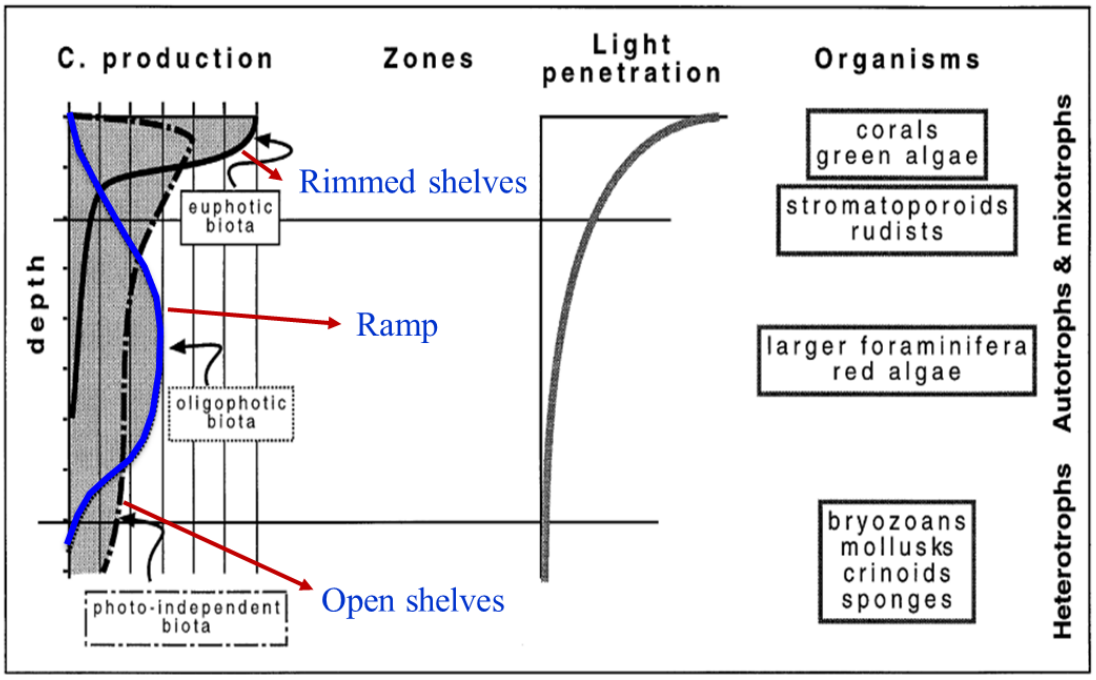

Figure 2.23. Genetic approach concept for identifying the type of carbonate platform based on the dominant light-dependent biota distribution (modified after Pomar, 2001). The blue curve is the suitable carbonate platform type for upper Baturaja Formation at early Miocene.

The slope of the top surface of the carbonate platform (the top of the Baturaja Formation) is gentle, ~1^0 (**Figure 2.16**). The facies map was reconstructed from the isopach map and the biota distribution across the carbonate platform (**Figure 2.24**). The oligophotic biota are predominantly distributed across the carbonate platform. Based on the Pomar (2001) guidelines, considering the abundance of biota associated with the paleotopography of the top of the carbonate platform, the suitable depositional environment of the early Miocene carbonate platform is carbonate ramp. A carbonate ramp depositional model of upper carbonate platform was built, and it is shown in **Figure 2.25**.

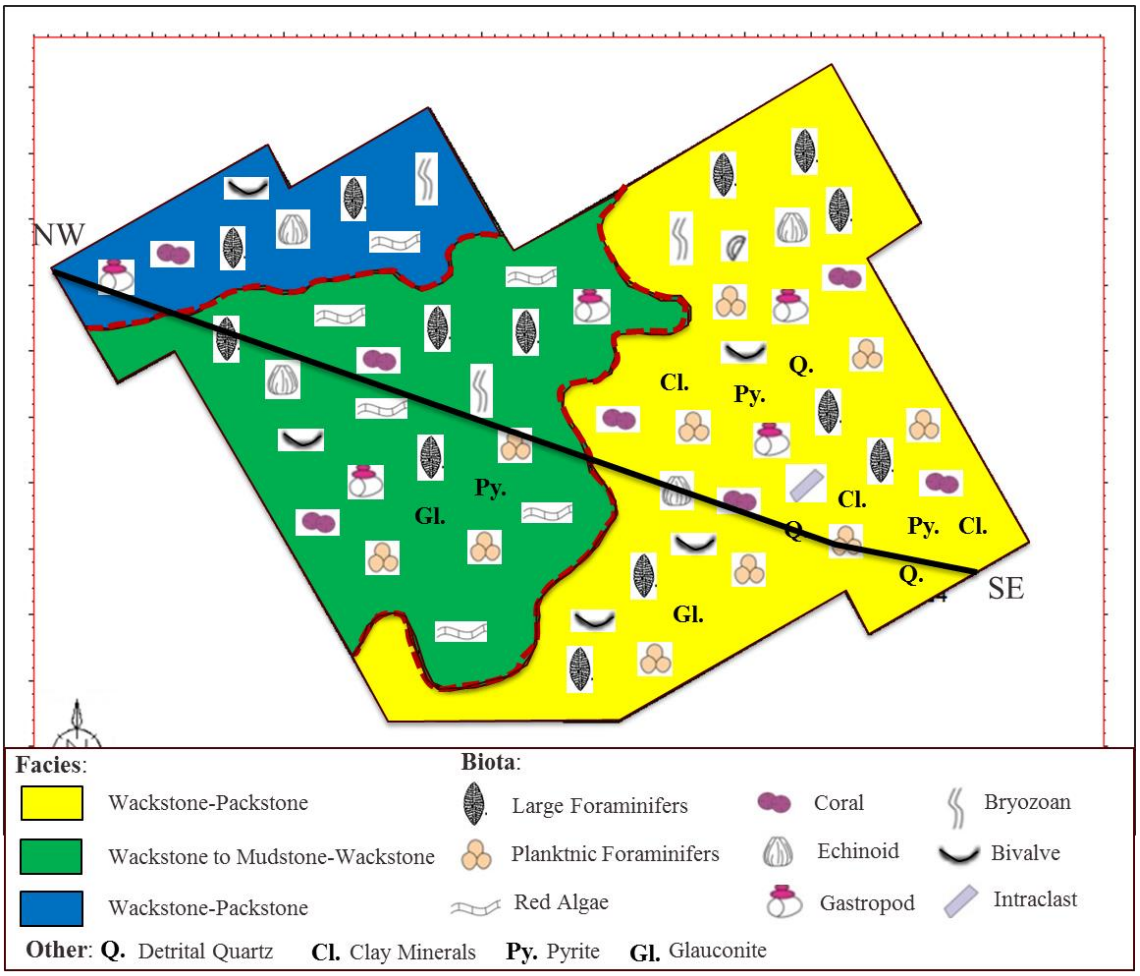

Figure 2.24. Facies map of upper Baturaja Formation was reconstructed from isopach map and biota distribution near top of Baturaja Formation. Larger foraminifers and red algae dominated the carbonate platform. Non-carbonate minerals are dominated by quartz and pyrite with minor presence of clay and glauconite.

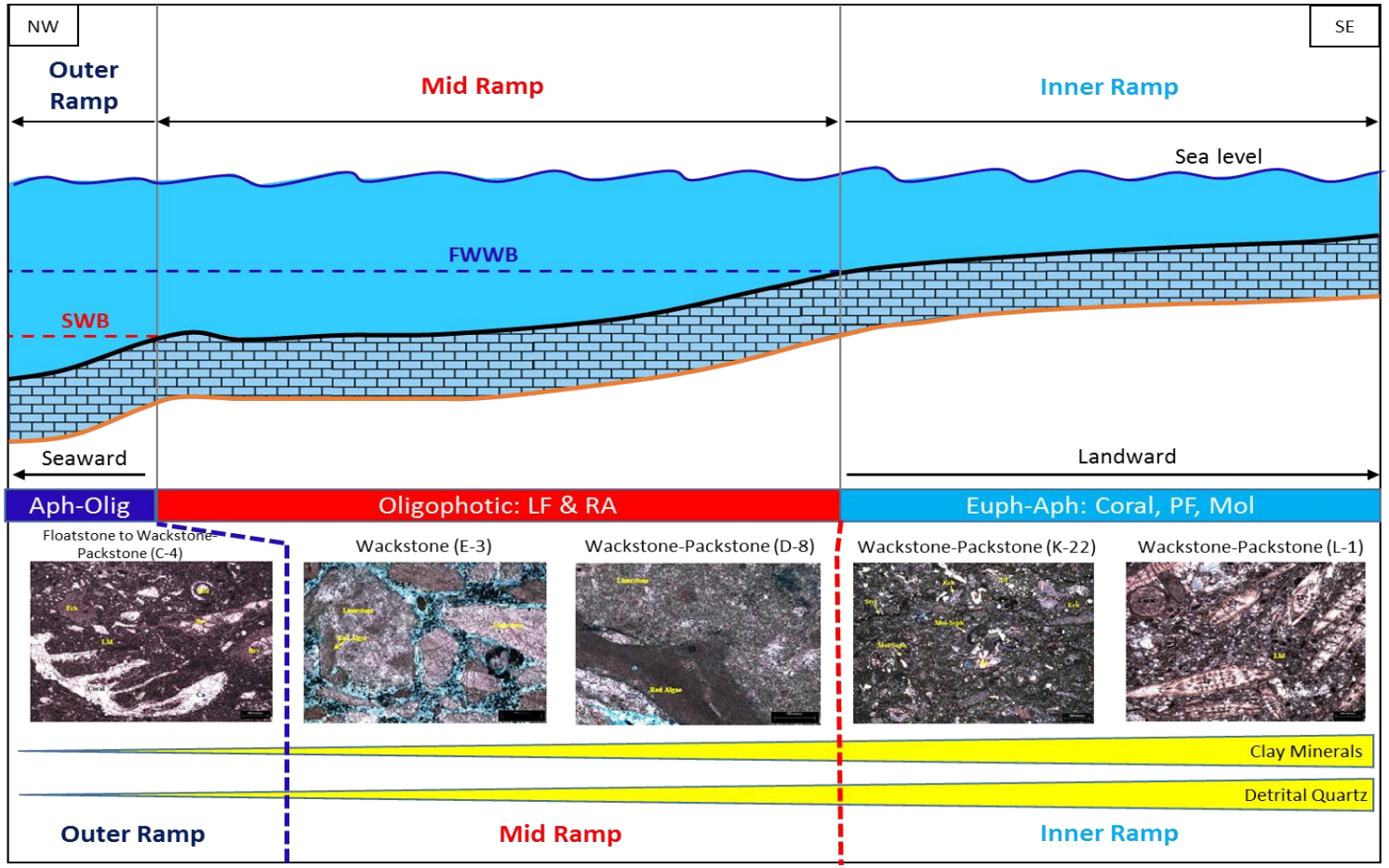

Figure 2.25. The carbonate ramp depositional model (unscaled) of upper Baturaja carbonate platform at early Miocene along NW-SE (the cross-section is shown in **Figure 2.24**). The oligophotic biota are predominantly distributed across the carbonate platform. (Note Euph=Euphotic biota, Ol=Oligopohtic biota and Aph=Aphotic biota).

Larger foraminifers and red algae commonly live in non-wave-agitated areas or below the fair weather base. Such locations are situated in mid-ramp, although this area may still be influenced by storms. The outer ramp is not influenced by storm waves but dominantly by gravity flow and turbidity. The proximal outer ramp, or upper part of ramp slope, where well C-4 is located, was populated largely by mollusks, echinoids, bryozoans, and ostracods, together with small amounts of larger foraminifers. This distribution of biota suggests a depositional environment that is intermediate between oligophotic and aphotic. The inner ramp is in the euphotic zone, dominated by smaller benthic foraminifers and mollusks. Analogous carbonate platform types are the lower Tortonian Migjorn ramp, in Menorca, Spain and the Serravalian and lower Tortonian Ragusa ramps, in SE Siciliy, Italy (Pomar et al., 2012).

Two wells, L-1 and K-24 located in the inner ramp, show a significant amount of detrital quartz and a clay trace. This indicates that the environment was influenced by siliciclastic input from the coast (**Figure 2.25**). How far is the siliciclastic input transported into the basin? To answer this question, the RMS amplitude in **Figure 2.17** is studied. To interpret the map, forward modeling of the lithology model from the wells was conducted. The result is shown in **Figure 2.20**. The amplitude of a seismic wave traveling from shale to carbonate rock facies A is stronger (in negative amplitude) than that of the same wave traveling from shale to carbonate rock facies B. This is because the acoustic impedance ($V_P * \rho$) contrast is higher between shale and facies A. The latter consists of mainly pure carbonate mineral constituents such as calcite and dolomite and therefore generates higher acoustic impedances. In addition to carbonate constituents, higher non-

carbonate constituents in the form of detrital quartz and clay minerals in facies B serve to generate lower acoustic impedances. I suppose that an anomalous dimming of seismic amplitude at the top of the carbonate interval occurs where carbonate rock B is present (**Figure 2.26**). Such anomalies are clearly seen on the RMS amplitude extraction map.

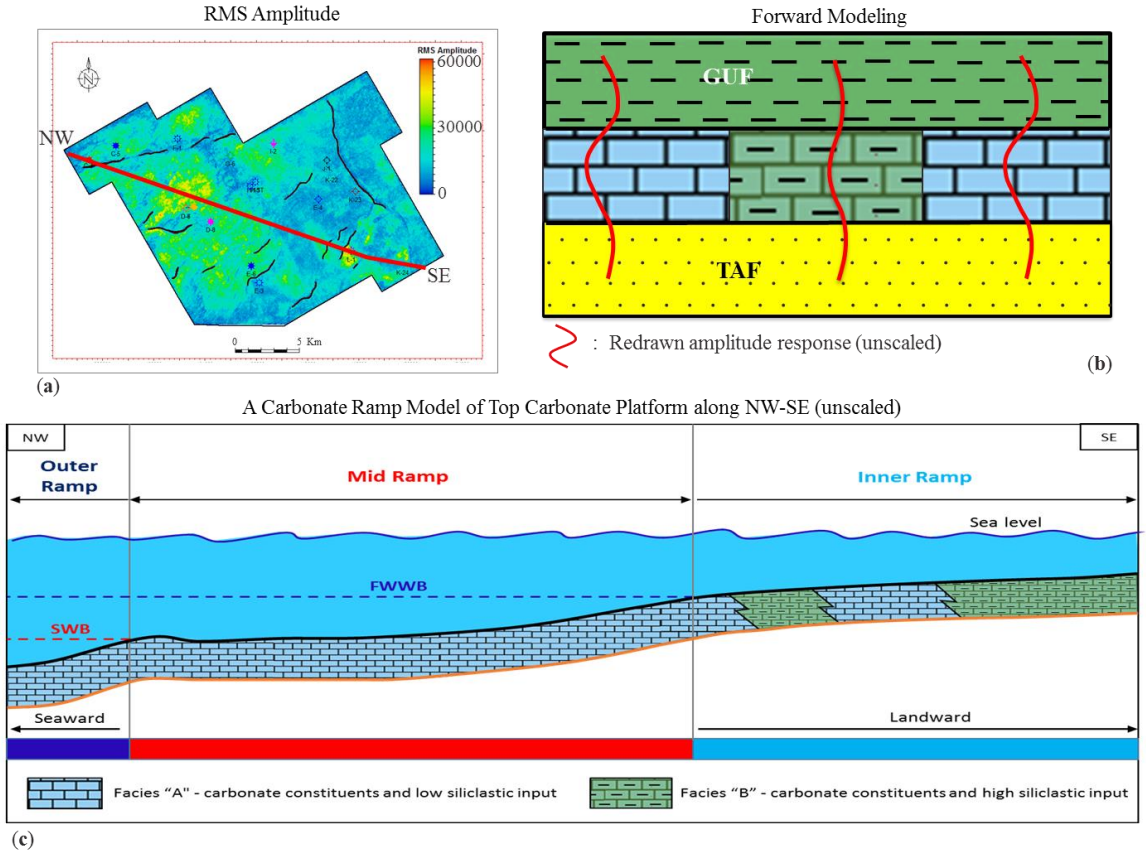

Figure 2.26. (b) The lithology model overlaid by seismic amplitude response from forward modeling process. Baturaja Formation consist of two facies: Facies A and B. The distributions of the facies are clearly seen on (a) the RMS amplitude map (see **Figure 2.17** for detail figure), Facies A are represented by green-to-yellow regions and Facies B are represented by blue regions. (c) The carbonate ramp model of Top Baturaja Formation included the interpreted of the facies along northwest to southeast.

The siliciclastic influences on the carbonate platform should be higher within the inner ramp since it is closest to the coast. This was confirmed by the volumetric concentration of shale that was generated from gamma ray values at the two wells: L-1 and K-24 (**Figure 2.27**). The higher volumetric concentration of shales/clay at wells located in inner ramp compared to those located in the mid-ramp and outer ramp indicate a stronger influence of siliciclastic input into the inner ramp. The gamma ray log readings, along with root mean square (RMS) of inverted acoustic impedance, were used to identify depositional boundaries across the field (**Figure 2.28**).

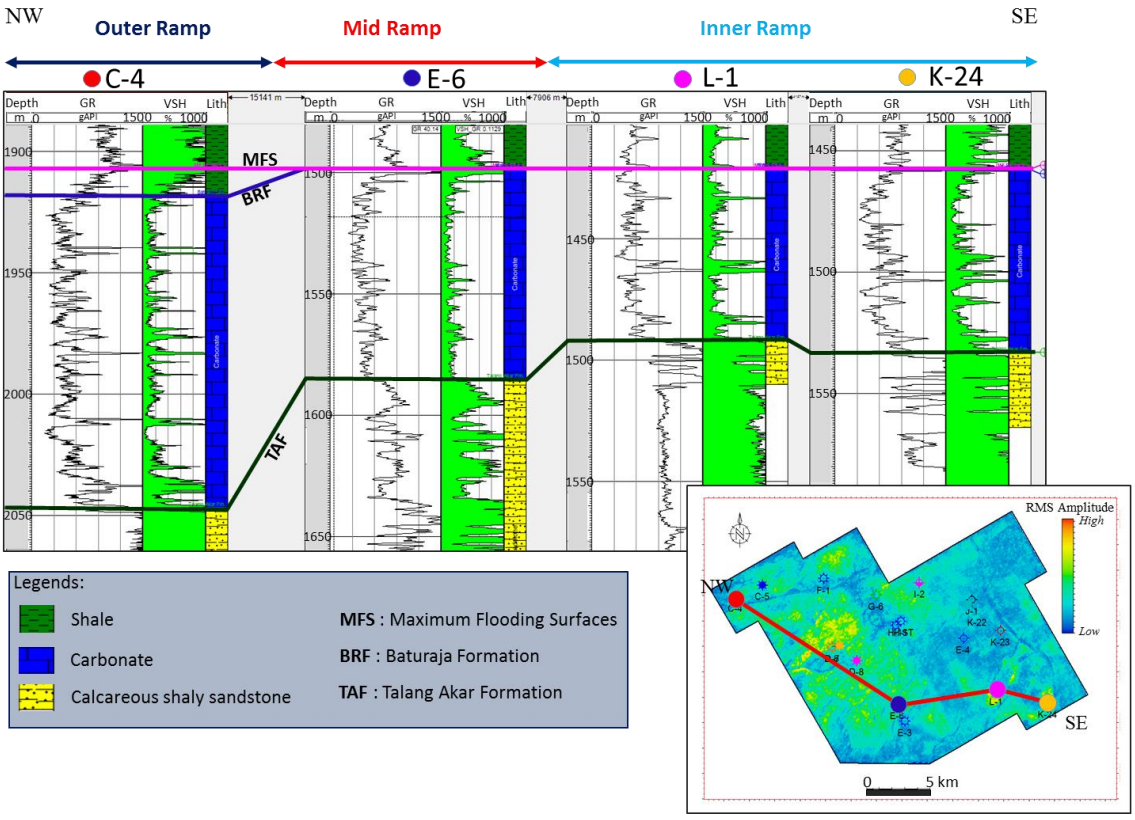

Figure 2.27. Gamma ray correlation associated with volumetric concentration of shale from NW to SE (see insert picture for the line of correlation on RMS amplitude map) shows an increasing of volumetric concentration of shale/clay into southeast. This indicates higher influences of siliciclastic in inner ramp rather than in mid and outer ramp.

The outer and mid-ramp zones exhibit moderate to high values of acoustic impedance due to high concentrations of calcite and dolomite, as well as abundant cementation. Siliciclastic influences in the inner ramp zone contribute to its lower acoustic impedance. The type and degree of cementation in this environment is uncertain, but an increase in the degree of cementation generally leads to porosity reduction (Wangen, 2000). Laboratory measurements of velocity, as a function of porosity, for typical limestones is reported by Anselmetti and Eberli (1997), and shows a negative linear trend. Thus, the higher the degree of cementation, the higher the velocity of the carbonate rock, and concomitantly the higher the acoustic impedance.

2.6.2 Porosity Prediction

Laboratory data on water-saturated sandstones and carbonates show negative linear trends of velocity versus porosity (Anselmetti and Eberli, 1997; Han, 1987; Vernik and Nur, 1992). Popular relations, such as those of Han (1987), Wyllie et al. (1956) and Raymer et al. (1980), describe a steep velocity-porosity relationship. These are appropriate if porosity is controlled by diagenesis (Avseth et al., 2010). Acoustic impedance, the product of velocity and density, is mainly influenced by velocity rather than density. Variations in velocity are generally much larger than variations in density. Thus, acoustic impedance shows a linear relationship when plotted against velocity. Numerous seismic studies have inferred porosities from inverted acoustic impedance values (e.g. Alamsyah et al. (2015); Avseth et al. (2010); Dolberg et al. (2000); Huuse and Feary (2005); Jalalalhosseini et al. (2015); Yuliandri et al. (2011)).

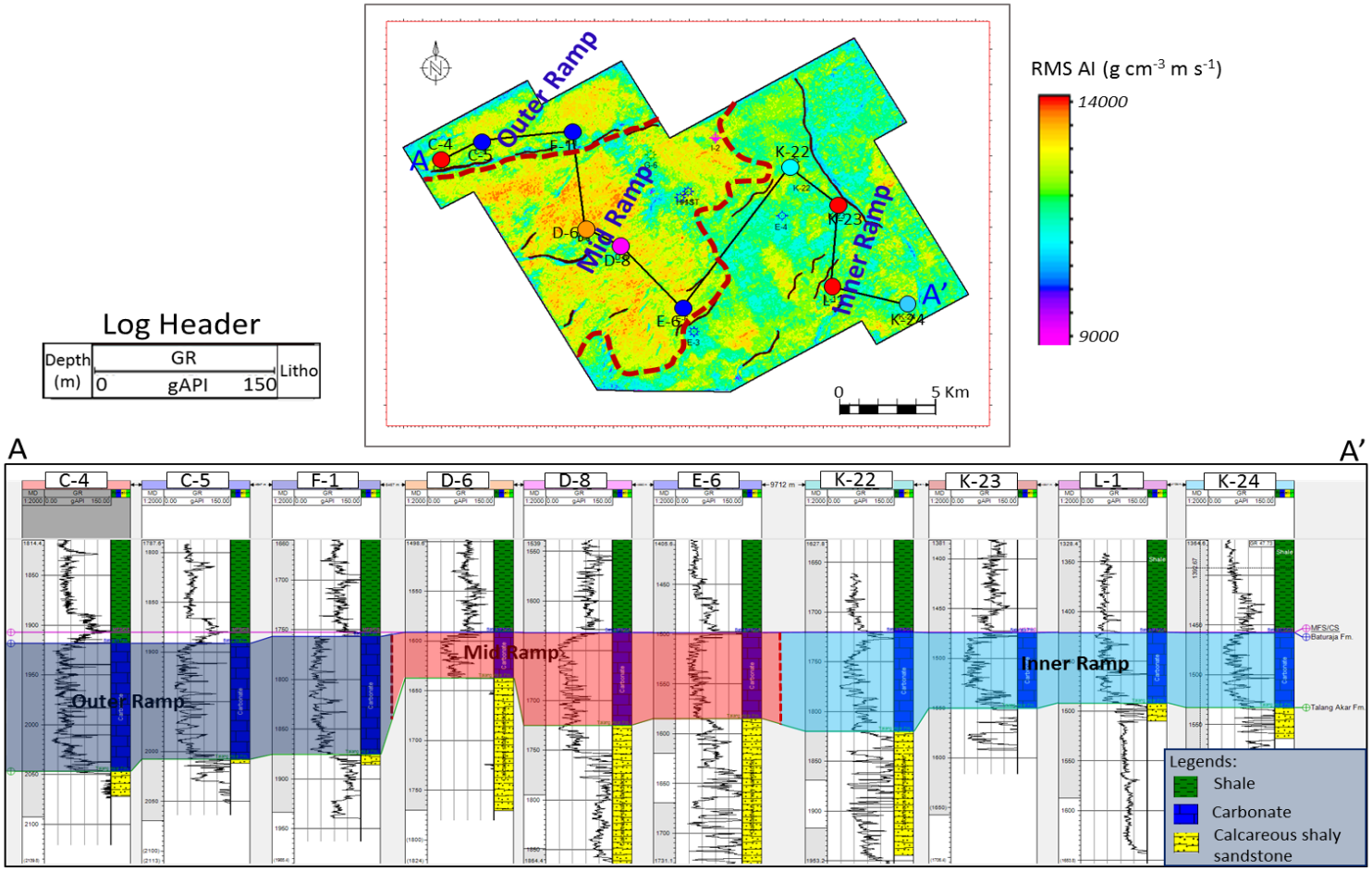

Figure 2.28. The combination of root mean square (RMS) of inverted acoustic impedance and gamma ray log of the wells from A to A' able to trace the depositional environment boundary across the field. (Note: the environment boundary is marked by brown dashed line)

The borehole-derived acoustic impedance throughout Baturaja Formation shows a negative linear trend with respect to well-log-derived porosities (**Figure 2.29**). The relationship is approximated by $Porosity = -2 \times 10^{-5} * Acoustic\ Impedance + 0.3304$. With coefficient of correlation 0.6, the porosity of carbonate rock of Baturaja Formation can be predicted from the inverted acoustic impedance using the above equation. This was done to obtain a "porosity cube" spanning the Baturaja carbonate interval within Pagardewa Field.

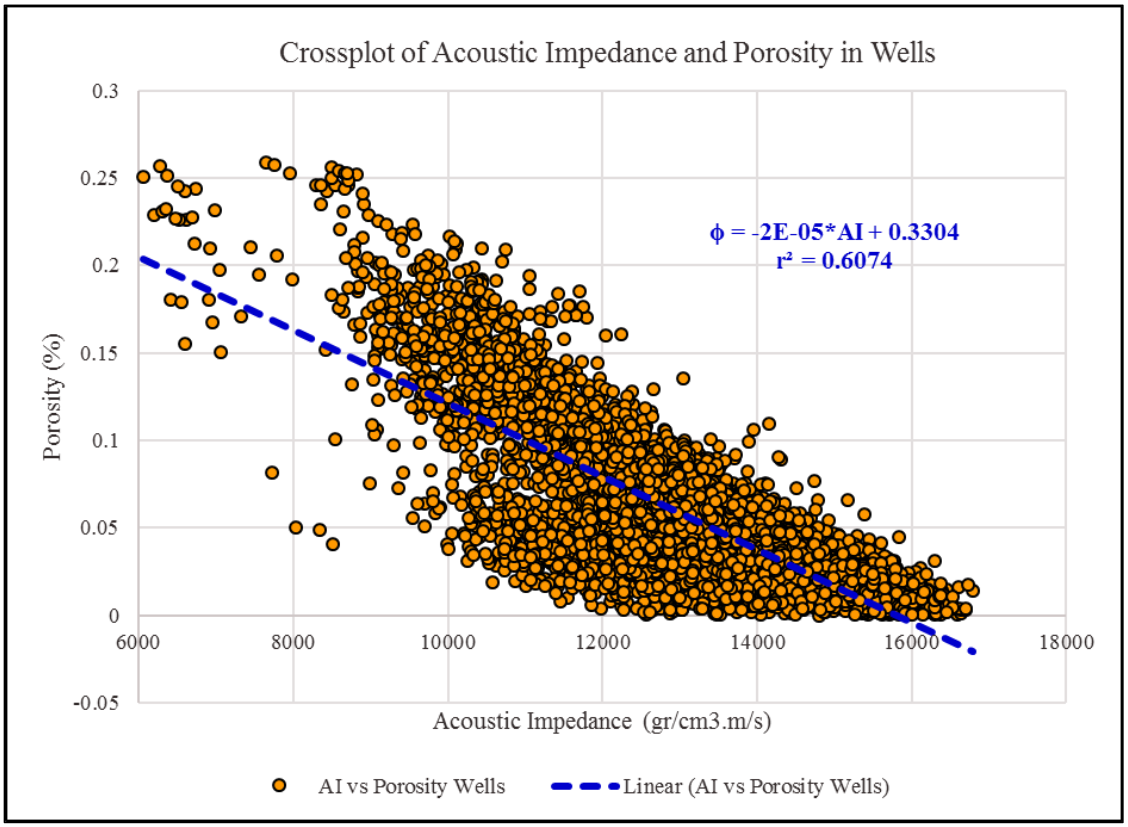

Figure 2.29. Negative relationship of well-log porosity vs borehole-derived acoustic impedance for Baturaja Formation interval

The RMS value of predicted porosity throughout the Baturaja Formation is shown in **Figure 2.30**. The inner ramp is characterized by the highest porosities (10–12%). The

porosities in the inner ramp are influenced by the carbonate constituents and siliciclastic input. Higher porosity values are due to the increased contribution of siliciclastic input (i.e clay minerals and detrital quartz) due to good sorting of siliciclastic grains, rather than the heterogeneity of the carbonate grains. Higher siliciclastic material input in specific areas can prevent calcite precipitation, and thereby decrease the intensity of cementation in areas affected by siliciclastic influences. Maliva and Dickson (1992) found a good correlation between the non-carbonate fraction and porosity in Eldfisk Field. In Pagardewa Field likewise, the siliciclastic input plays an important factor in determining the total porosity. The inner ramp is vulnerable to 4^{th} or 5^{th} order sea level cycles which can cause carbonate rock to become occasionally exposed at the surface and subject to diagenesis by meteoric water. The diagenetic processes of leaching, dissolution, and recrystallization create secondary porosity. Dolomitization may also contribute to higher porosity of the carbonate rock in the inner ramp.

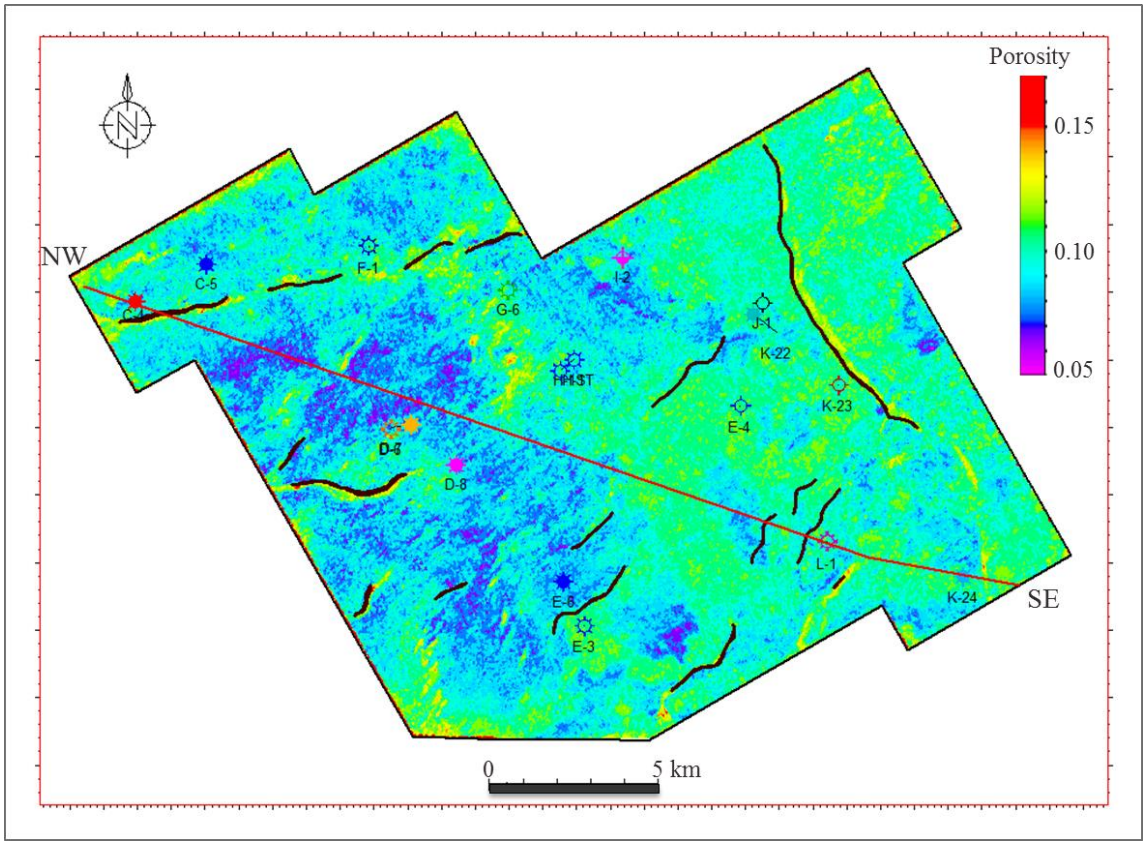

Figure 2.30. RMS map of predicted porosity of the Baturaja Formation: porosity distribution range in inner ramp (10% - 12%), middle ramp (6% - 10%) and outer ramp (7% - 10%). Noted the carbonate ramp was modeled along the NW – SE red line.

The predicted porosity values in both the middle and outer ramps are 6–10% (**Figure 2.30**). These low values of porosity are most likely due to a high degree of cementation. Blocky and drusy mosaic of equant spar cement from core sample at well C-4 shows different cementation type (**Figure 2.31**). The first is of meteoric type while the latter is of burial type. Additional analysis is required to explain the development of the cement in Baturaja Formation from early to late stages. Considering the evidence at well C-4 located at outer ramp, I infer that the early cement type was marine cementation that later was replaced by meteoric and burial diagenesis cementation. Various diagenetic

processes such as cementation, recrystallization or neomorphism, mechanical fracturing and pressure dissolution in the form of stylolitisation (Geoservices, 2012a, b, c, d, e, f, 2013a, b) have significantly reduced the primary/depositional porosity.

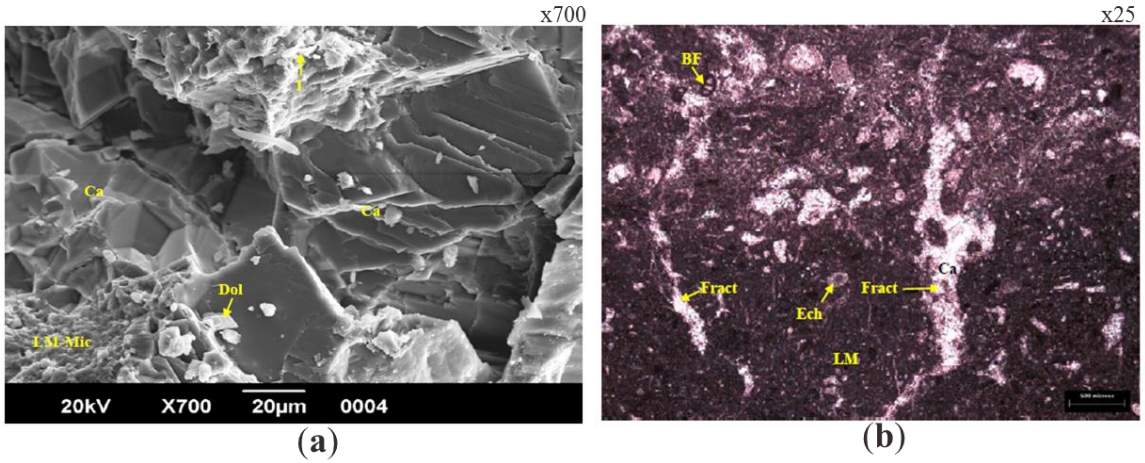

Figure 2.31. (a) SEM of core sample of Well C-4 at depth 1921.8. (b) Photomicrograph of core sample of well C-4 at depth 1923.6 m (adopted from Geoservices (2012d)). We can see the blocky calcite and drusy mosaic of equant spar at this rock samples from outer ramp.

2.6.3 Implication of Research to Hydrocarbon Trapping

The carbonate platform type of Baturaja Formation in Pagardewa Field was not clearly defined in previous studies. Geoservices (2013b) used the general term "shallow marine environment" based on the abundance and diversities of fossils recorded in samples. Yuliandri et al. (2011) built a reefal depositional model of the carbonate platform based on present-day topography. That model, which does not take into account the paleoenvironment at early Miocene, indicated that the main hydrocarbon plays in this field are composed of reefal build-up facies. Subsequent tectonism and uplift during the Miocene and Plio-Pleistocene caused inversion of the Cenozoic basins, with folding and

fault reactivation creating structural inversion traps. Since the Yuliandri et al. (2011) model is not corrected at early Miocene, it is uncertain if the interpreted reefal build-up is a depositional carbonate structure or a structural inversion due to the compressive tectonics of the late Miocene and Plio-Pleistocene. Geoservices (2012b, 2012c, 2012d, 2012f, 2013a, 2013b) reported the presence of stylolites and fractures in the carbonate samples. Stylolites can trap light hydrocarbons, especially gas. Fractures are well developed in Baturaja Formation due to the intensification of faults in this area (Wibowo et al., 2008; Yuliandri et al., 2011). The fractures are filled by calcite at several places at Pagardewa Field, as shown by several rock samples from the Baturaja Formation (Geoservices, 2012d, e, 2013a), so they might comprise an important hydrocarbon play at several places in the field. Therefore, explorationists have generally searched for structural traps near fault structures and reefal plays in Pagardewa Field.

The new carbonate platform type model proposed herein suggests a new type of hydrocarbon trap is present in Pagardewa Field. The trap is located at the boundaries between facies A and facies B. Such hydrocarbon traps are proposed to be a new stratigraphic play in the Baturaja Formation reservoir (**Figure 2.32**). Facies A has higher acoustic impedance than facies B, which indicates a porosity contrast. The contrast obstructs hydrocarbon flow at the boundary during its migration through the carbonate platform. The boundary thus inhibits and traps hydrocarbons preferentially here compared to other parts of the platform, although sealing faults may also obstruct hydrocarbons elsewhere. Several wells drilled close to the facies boundary have shown significant amounts of flowing hydrocarbon. These wells include C-4 (gas), D-6 (gas & condensate),

G-6 (gas & condensate), K-22 (gas & condensate) and L-1 (gas) (Pertamina, 2010a, b, 2012a, e, g). However, poor flow rates occured in wells drilled far from the facies boundary or in the middle of facies B. The wells are either dry (E-4 and F-1) or show only a minor oil trace (J-1 and K-24) (Pertamina, 2012b, c, d, 2013b). A similar situation occurs for well E-6 result drilled in the middle of facies A, producing only a dry hole with no oil trace (Pertamina, 2013a). An oil trace is due to hydrocarbon migration along the carbonate platform, but little hydrocarbon is expected to be found within the middle of siliciclastic-carbonate facies. However, substantially more hydrocarbon should be trapped near the lateral boundaries between facies A and B, due to the large contrasts in acoustic impedance and porosity. The lateral facies boundaries are easily defined in the inverted acoustic impedance map as an area between high and low acoustic impedance value (between yellow and light blue color). In this way, the map can be used as 2D dimensional hydrocarbon trap for suggesting locations of new infilling wells in Pagardewa Field.

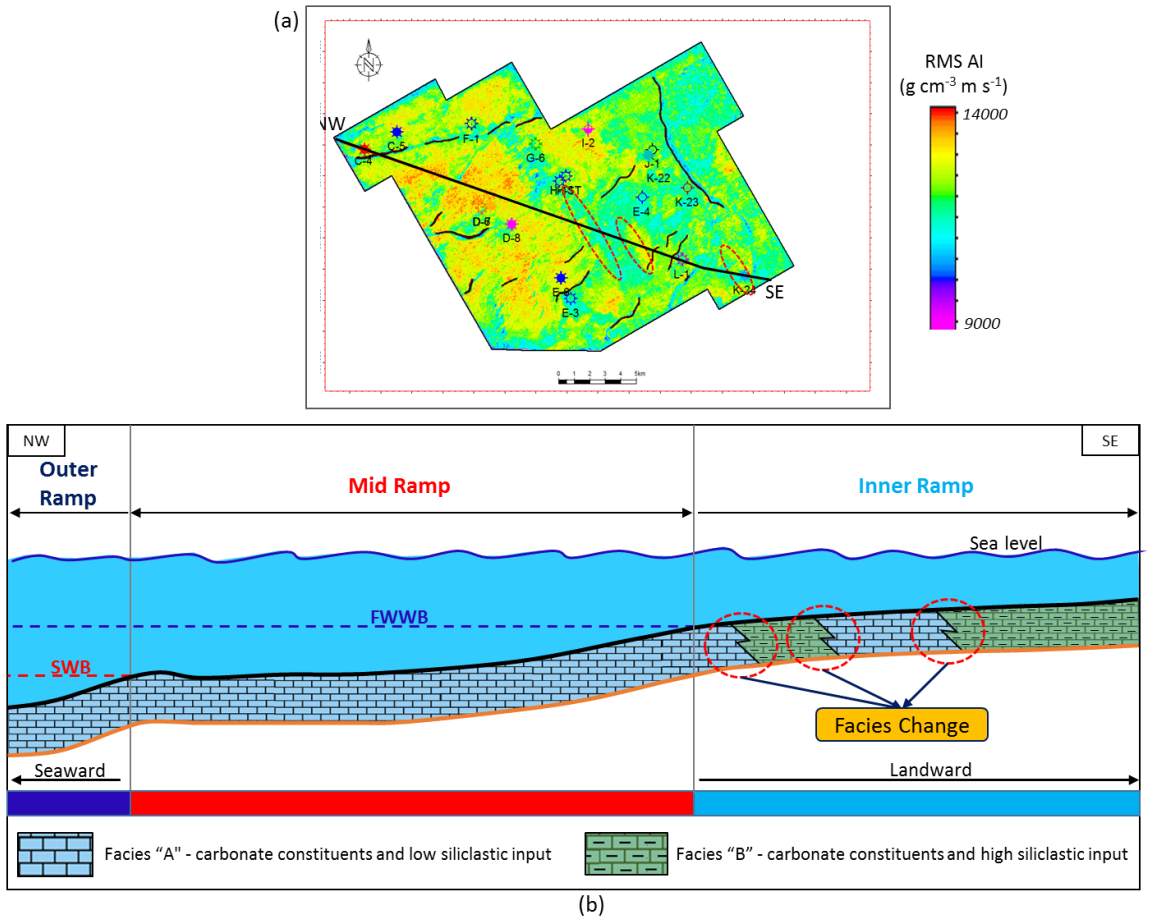

Figure 2.32. (a) RMS of inverted acoustic impedance. (b) The carbonate ramp model of Baturaja carbonate platform at Pagardewa Field. A stratigraphic hydrocarbon trap (red dotted circle line), due to facies's properties change, is inferred at the facies boundary; the boundaries are easily identified on RMS of inverted acoustic impedance map (i.e. the related boundaries shown in (b) is located inside the red dotted ellipse in (a)

2.7 **Conclusions**

Carbonate production at upper Baturaja carbonate platform is dominated by oligophotic gravel-producing biota such as larger foraminifers and red algae with subordinate aphotic biota such as mollusks, bryozoans and echinoids. Based on the dominant light-dependent biota distribution and the paleotopography of the carbonate

platform at early Miocene, the suitable depositional environment of top Baturaja Formation at Pagardewa Field is proposed herein to have been a carbonate ramp.

The carbonate platform is defined by two facies, A and B, that are based on seismic amplitude simulation and rock descriptions from core samples. Facies A produces higher seismic amplitudes due to its mainly carbonate constituents: calcite and dolomite. Higher amounts of non-carbonate constituents such as siliciclastic material in facies B generate lower seismic amplitudes. The degree of siliciclastic influence can be inferred from a combination of gamma ray log readings and seismic-inverted acoustic impedance values. The siliciclastic input is significant in core samples taken from the inner ramp. The siliciclastic influence is found to be higher in the inner ramp than in the mid- and outer-ramps, as indicated by the higher gamma-ray values. The outer and mid ramp zones have moderate to highest acoustic impedance values due to the abundant calcite and dolomite. Moreover, a higher degree of cementation occurs in this environment. To the contrary, the higher siliciclastic influence in the inner ramp contributes to its lower acoustic impedance value. Therefore, facies B dominates the inner ramp while facies A dominates the mid and outer ramps.

The porosity distribution throughout the field was predicted from the inverted acoustic impedance using the negative linear relationship between the borehole-derived acoustic impedance and porosities extracted from the well logs. The rock deposited in the inner ramp setting has the highest porosities (10%–12%), owing to the enhanced contribution of siliciclastic input (i.e clay and detrital quartz). Furthermore, the inner ramp was frequently exposed to sea level variations and thus subjected to diagenetic processes

including leaching, dissolution, recrystallization and dolomitization; all of which tend to increase total porosity. Lower porosities (6 – 10%) are present in the mid and outer ramp due to the higher degree of cementation.

A stratigraphic hydrocarbon trap is suggested from the carbonate platform analysis of Baturaja Formation in Pagardewa Field. Potential stratigraphic plays are suggested at lateral contrasts in rock properties between the two facies. The facies A has higher acoustic impedance than does the facies B. Hydrocarbons are suggested to accumulate near the lateral boundaries between the two carbonate facies.

CHAPTER III

WELL-BASED CARBONATE RESERVOIR QUALITY ASSESSMENT OF LOW-PERMEABILITY CARBONATE ROCK: BATURAJA FORMATION, PALEMBANG BASIN, INDONESIA

3.1 Summary

Baturaja Formation is a Miocene tight carbonate gas-charged reservoir in Pagardewa Field, Indonesia. The classification of Baturaja Formation is herein suggested to be changed from a conventional reservoir to an unconventional reservoir. Progradational, aggradational and retrogradational parasequence sets mark the geological evolution of a carbonate ramp of Baturaja Formation. Six carbonate classes are defined from reservoir quality information derived from wells; specifically, the information includes brittleness behavior, porosity, TOC, clay, quartz, and dolomite content. The carbonate quality classes were determined from a combination of the Lamé parameters and brittleness-related elastic moduli. Very good to moderate rock quality appears to dominate the inner ramp due to high terrigeneous siliciclastic input. Less moderate to poor quality dominates the outer ramp due to pervasive cementation. An integration of stratigraphic interpretation and carbonate rock quality was used herein to suggest a prospective interval for acid fracturing and to reveal potential unexploited resources in the reservoir.

3.2 **Introduction**

Unconventional, low-permeability reservoirs have become important exploration targets due to the ongoing depletion of conventional reservoirs at most of the major hydrocarbon fields of the world. Unconventional reservoirs may require multiple fracture-stimulated intervals in horizontal wells to produce hydrocarbon at commercial rates. Baturaja Formation comprises tight gas-charged carbonate rock at Pagardewa Field, Palembang Sub-basin, Indonesia. Petrophysical analysis performed in prelude to this research shows that porosity of the carbonate are mostly below 8% and the permeability are mostly below 0.1 mD. Prospective intervals previously have been acid fractured to enable hydrocarbon production (Pertamina, 2010a, b, 2012b, e, f, g, h). The reservoir properties and treatment history combine to indicate that the Baturaja Formation should be classified as an "unconventional reservoir" based on Cander (2012) classification scheme. The motivation for the research described herein arose while considering such a change in the paradigm characterizing the Baturaja Formation. To improve the reservoir characterization, I integrate rock physics and seismic-derived properties from available data, to generate a carbonate rock-quality classification scheme based on reservoir quality criteria.

Rock physics can identify quantitative connections amongst seismic, well-logging, and reservoir engineering analyses. While compressional V_P and shear V_S seismic wave velocities are relatively insensitive to lithology and fluid-content variations in common carbonate rocks, amplitude versus offset (AVO) inversion for the Lamé parameters (more specifically, their products with density, $\lambda\rho \; and \; \mu\rho$) has been shown to enable improved

lithology discrimination and fluid detection (Goodway et al., 1997). In related work, Takahashi and Tanaka (2010) showed that static and dynamic Young's moduli exhibit inverse relationships to porosity in soft sedimentary rocks. Kumar et al. (2012) reported an inverse relationship between Young's modulus and porosity, in addition to TOC and clay content in some shale plays. In general, exploring the relationship between elastic moduli and reservoir quality indicators provides an avenue for identification of hydrocarbon prospective intervals. I further hypothesize that Poisson's ratio can help to discriminate between brittle and ductile zones in Baturaja Formation.

The successful application of acid fracturing depends on the properties of the carbonate interval that is fractured. In this study, the tight carbonate rock of Baturaja Formation is analyzed using a combination of Lamé parameters and brittleness-related elastic moduli. The quality classification of the rock is based on petrophysical parameters such as brittleness behavior, porosity, TOC and mineral content such as clay, quartz and dolomite. In this chapter, the carbonate reservoir quality classes derived from available well information are combined with stratigraphic interpretation. This procedure results in decreased uncertainty in suggesting a prospective interval for acid fracturing and may help to reveal unexploited hydrocarbon potential. The paramount objective is to increase the production of hydrocarbon from Baturaja Formation.

3.3 **Geological Background**

Pagardewa Field is an oil and gas field located in Prabumulih Regency, ~80 km SW of Palembang City, the capital of South Sumatra Province, Indonesia (**Figure 3.1**). The field is located within Palembang basin in the southeastern part of the larger, prolific

South Sumatra basin. Palembang basin covers an area of roughly 125 by 150 km^2 (Pulunggono, 1986). Sumatra Island comprises the southwestern margin of the stable cratonic area of Asia/Sundaland (Wilson, 2002). The basin is bounded on the southwest by faults and Mesozoic ridges that are associated with the Barisan Mountain range. On the northeast, the basin is bounded by the stable cratonic area of Asia/Sundaland and on the eastern and southeastern sides it is bounded by the Lampung High ridge (Pulunggono, 1986).

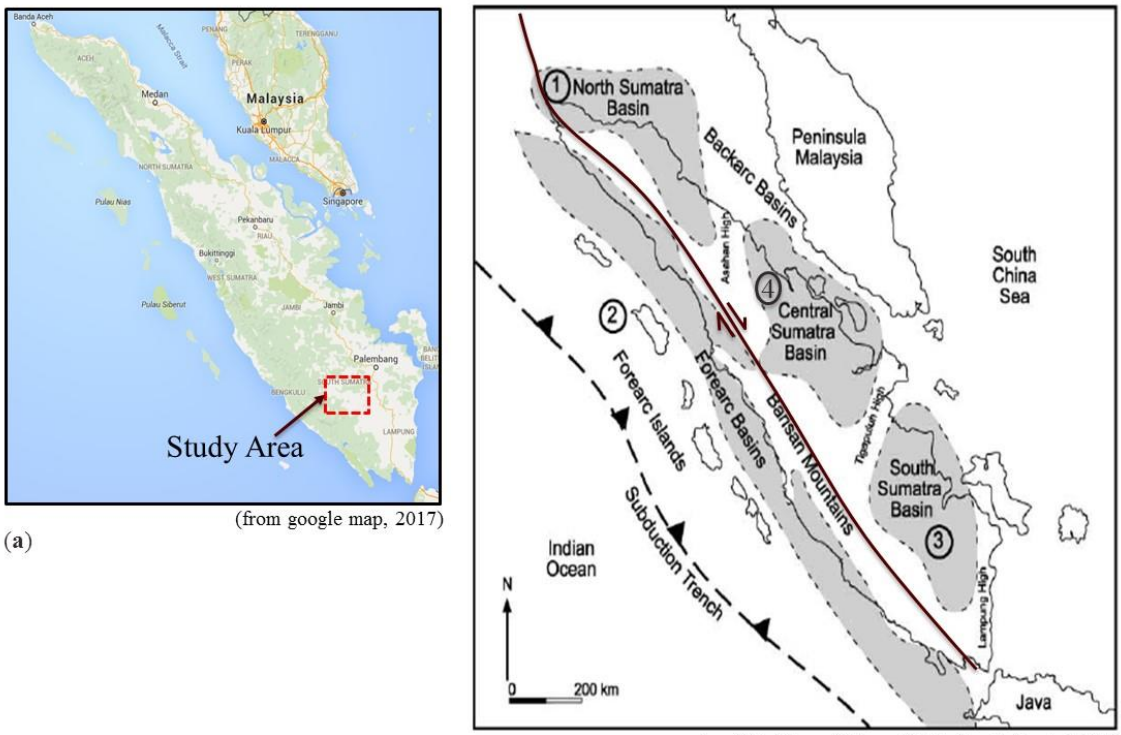

Figure 3.1. (a) Location of Pagardewa Field, South Sumatra, Indonesia. (b) Major tectono-stratigraphy features of Sumatra during the Tertiary: (1) North Sumatra Basin, (2) Forearc Basin, (3) South Sumatra Basin and (4) Central Sumatra Basin (modified from Wilson, 2002 after de Smet, 1992)

Tectonically, north-directed subduction of Indian oceanic crust has exerted a major influence on island arc and basin evolution, and contributed to an active major strike-slip system. The formation of the Barisan Mountains resulted from Paleogene-Neogene volcanism associated with the oblique subduction. The dominant tectonic forces led to the formation of three basins in the backarc and one basin in the forearc island during the Paleogene (**Figure 3.1**). Horst and graben development during the late Eocene and Oligocene in backarc areas has been mostly infilled by lacustrine and fluvial sediment (Wilson, 2002). Consequent Oligo-Miocene subsidence resulted in thick terrestrial deposits that are overlain by marine lithologies. During the early to middle Miocene, carbonate was extensively deposited in the South Sumatra Basin. During the middle Miocene, uplift and erosion of the Barisan Mountains increased clastic sedimentation into the surrounding areas and led to a gradual expansion of the terrestrial environment (Wilson, 2002 after de Smet, 1992).

The formation of the Palembang sub-basin was controlled by geological processes that occurred over four tectonic periods (Pertamina, 2012g) (**Figure 3.2**). Basin development started in the middle Mesozoic when older rocks were folded and fractured in association with a granitic batholith intrusion. From the late Cretaceous until the late Paleogene, dextral strike slip motion along the Semangko fault created half grabens, controlling the sedimentation of Lahat Formation and Talang Akar Formation. Cenozoic rocks of the Palembang basin were deposited during two large-scale cycles, a lower transgressive sequence and an upper regressive sequence (**Figure 3.2**). In the Miocene, transgressive sedimentation of the lower Miocene Talang Akar Formation was followed

by the deposition of Baturaja Formation. Initiation of Baturaja carbonate production was diachronous and coincided with rising sea level in the early Miocene. The carbonates were partially drowned in some places, but at the same time in other places, under relatively shallow water, carbonates continued to accumulate. The deep-water shales of the Gumai Formation were subsequently deposited over the drowning platform, and this was followed by uplift of basement rocks during the Middle Miocene. The Air Benakat Formation and Muara Enim Formation were deposited during regressive stages. In a final stage during the Plio–Pleistocene, compressional tectonic processes inverted the existing structure within the basin and led to the formation of several anticlines.

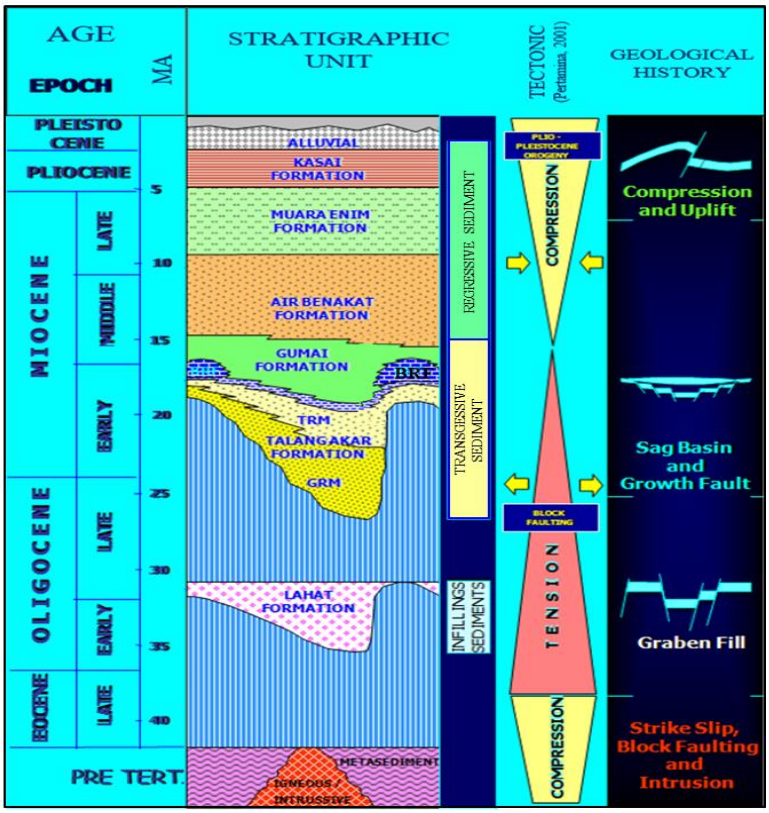

Figure 3.2. Regional stratigraphy of South Sumatra Basin (modified from Pertamina, 2012g). Noted BRF=Baturaja Formation.

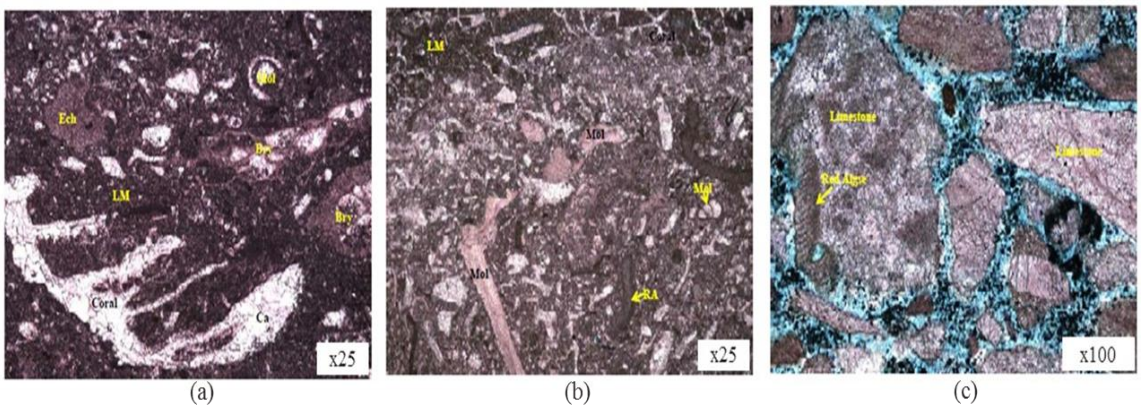

(a) (b) (c)

Figure 3.3. Petrographical descriptions from cores, sidewall cores and cutting samples. (a) Wackstone-Packstone from core sample of well C-4 at depth 1921.8 m, (b) Floatstone-Wackstone from sidewall cores sample of well C-5 at depth 1978 m and (c) Wackstone-Mudstone from cutting sample of well E-03 at depth 1480 m.

The Baturaja Fm. was deposited in the intermediate and shelfal portions of the South Sumatra Basin on or nearby platform highs (De Coster, 1974). Basuki and Pane (1976) reported that Air Kemiling Besar, an outcrop of the Baturaja Formation located 238 km SE of Pagardewa Field, consists of two massive units (upper and lower parts) that are separated by a finely-bedded unit of lime mudstones and lime wackstones intercalated with marls. In the finely-bedded unit, recrystallization and the presence of carbonaceous matter and glauconitic minerals are common. The massive units consist of mudstones, wackstones/packstones and boundstones with abundant large foraminifers in the upper part. Three dominant facies are interpreted from available cores, sidewall cores and cutting data (Pertamina, 2012d, g) in Pagardewa Field, respectively they are: wackstone-packstone; (ii) coral floatstone-wackstone; and (iii) wackstone-mudstone (**Figure 3.3**). However, the core intervals sampled only the top 10 m of the carbonate rock, and the sidewall cores sampled only at every 5-10 m spacing while the average thickness of

Baturaja Formation is 90 m. Thus, a description of the facies comprising the carbonate rock intervals at the wells is incomplete. However, a simplified two-facies interpretation based on grain sizes from cutting descriptions was made at the beginning of this research. This analysis shows that the carbonate rock interval is composed of ~75% mudstone and ~25% wackstone-packstone facies.

With reference to the Choquette and Pray (1970) classification scheme, the porosity of the Baturaja carbonates are dominated by open microfractures and micro-vugs with minor intraparticle, intracrystalline, intercrystalline, interparticle and mouldic void spaces (Geoservices, 2012a, b, c, d, e, f, 2013a, b). At Merbau Field, a gas field located 10 km west of Pagardewa Field, fractures are well developed in the Baturaja Formation (Wibowo et al., 2008). Yuliandri et al. (2011) stated fractures enhanced porosity in highly faulted area of Baturaja Formation at Pagardewa Field. However, the fractures are filled by calcite cement in many places at this field (Geoservices, 2012d, e, 2013a). Petrophysical analysis performed in this research show a strong relationship between porosity and permeability in the core data of several wells (e.g well E-3 and K-24). This is unusual in carbonate rock although it is common in siliciclastic rock (see Chapter II). The available petrographic reports show higher amount of siliciclastic input in the form of detrital quartz and clay minerals (mainly kaolinite) in those wells that exhibit the unusual porosity–permeability core relationship.

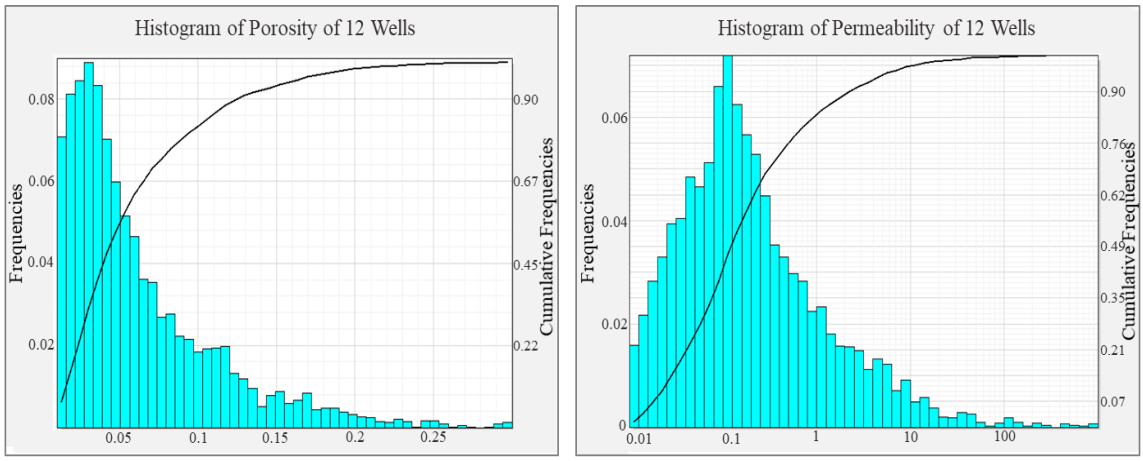

Figure 3.4. (a) Histogram of porosity from 12 wells. (b) Histogram of permeability from 12 wells. Based on the cumulative distributions (solid lines overlying the Histograms), more than 50 % of the porosity in Baturaja Formation are below 5% and permeability are below 0.1 mD. Noted solid black line is cumulative frequencies.

Figure 3.4 shows histograms of porosity and permeability in Baturaja Formation from 12 wells. The porosity and permeability estimates were discussed in Chapter II. Based on the cumulative probability distributions, as shown by the solid lines in the figure, more than 50% of the porosity estimates are below 5% and a similar number of the permeability estimates are below 0.1 mD. The Baturaja carbonates are therefore relatively tight with low porosity and permeability. Since hydrocarbons in the prospective intervals of these types of formations do not naturally flow at economic rates, the intervals have been acid-fractured to raise the permeability. Cander (2012) discriminated between unconventional and conventional reservoirs based on a crossplot of viscosity versus permeability. Pressure volume temperature (PVT) analysis of four gas samples from four wells (e.g C-4, E-6, K-22 and L-1) are plotted in Cander's graph. Their location on the crossplot suggests that Baturaja Formation is a tight gas carbonate rock and classified as an unconventional reservoir (**Figure 3.5**). Overall, the reservoir properties, such as

permeability and viscosity, and the treatment history involving acid fracturing suggest that the Baturaja Formation should be regarded as an "unconventional reservoir".

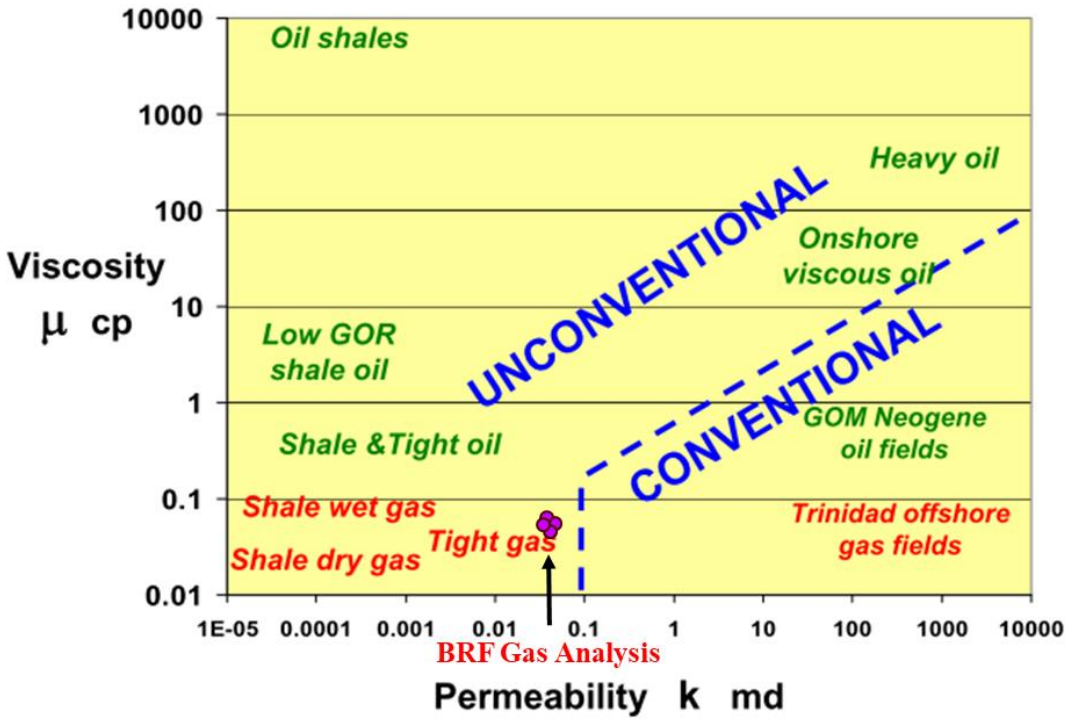

Figure 3.5. Classification of hydrocarbon-bearing reservoirs as "conventional" or "unconventional" based on a cross-plot of viscosity μ vs permeability k, as defined by Cander (2012). The Baturaja Formation (BRF) samples (purple dots) indicate that they are associated with tight gas unconventional reservoirs.

3.4 **Methodology**

3.4.1 Stratigraphic Correlation

This study was initiated with a stratigraphic correlation based on the available well data. I used sequence stratigraphy concepts to analyze the geologic evolution of the carbonate platform of the Baturaja Formation. Sequence stratigraphy is an interpretive, largely qualitative study of rock relationships within a chronostratigraphic framework of

repetitive, genetically related strata bounded by surfaces of erosion or non-deposition, or their correlative conformities (Van Wagoner et al., 1988). The important surfaces in sequence stratigraphy, such as sequence boundaries, parasequence boundaries and parasequence set boundaries, provide the necessary chronostratigraphic framework for correlation and mapping of sedimentary formations. A parasequence is a relatively conformable succession of genetically related beds or bedsets bounded by marine flooding surfaces (Van Wagoner, 1985). The latter is a surface that separates younger from older strata, across which there is evidence of an abrupt increase in water depth (Van Wagoner et al., 1988). A parasequence set is a succession of genetically related parasequences which form a distinctive stacking pattern that is bounded, in many cases, by major marine flooding surfaces and their correlative surfaces (Van Wagoner, 1985). In other words, a parasequence set consists of a stacked pattern of parasequences.

A major tool used for performing stratigraphic correlation is the gamma ray log, which measures natural gamma radiation emitted from rock units (Sam Boggs, 2006). The source of gamma ray emission is decay of radioactive potassium ^{40}K, thorium ^{232}Th and uranium ^{238}U (Nichols, 2009). Minerals containing those isotopes are common in clays, therefore the gamma ray log is used to distinguish shale beds from other lithologies and to estimate the volumetric concentration of shale. Mudrock or shale generally has a high natural radioactivity, whereas both sandstone and limestone normally have lower natural radioactivity (**Figure 3.6**).

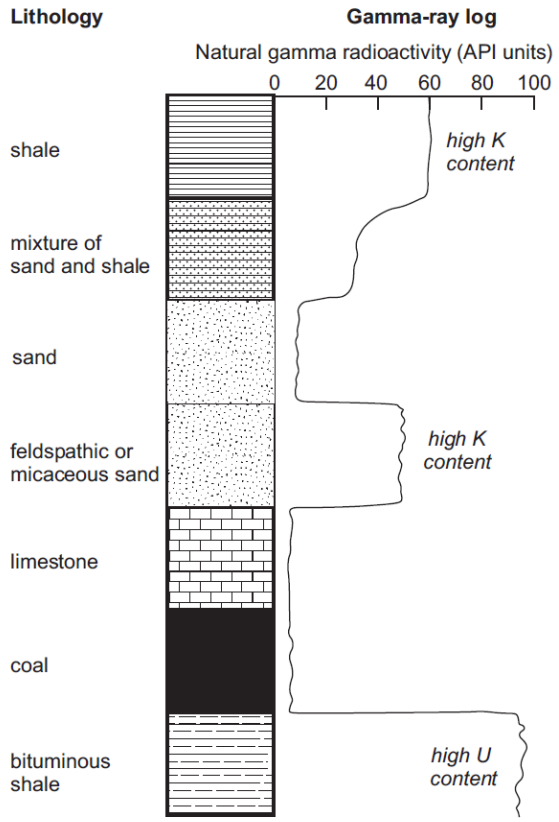

Figure 3.6. Gamma ray response for different lithologies (reprinted from Rider, 2002).

The important boundaries in stratigraphic correlation, such as parasequence sets, parasequences, and marine flooding surfaces, are generally recognized by changes in the shape of the gamma ray log. The overall shape of a gamma ray log through a clastic interval depends on the variation in grain size in the rock. Depending on the specific depositional environment, the shape of a gamma ray log may be blocky, funnel-shaped, bell-shaped, symmetrical or serrated (**Figure 3.7**). The depositional stacking patterns, in the form of aggradation, progradation, or retrogradation or some combination of them, characterize the depositional environments.

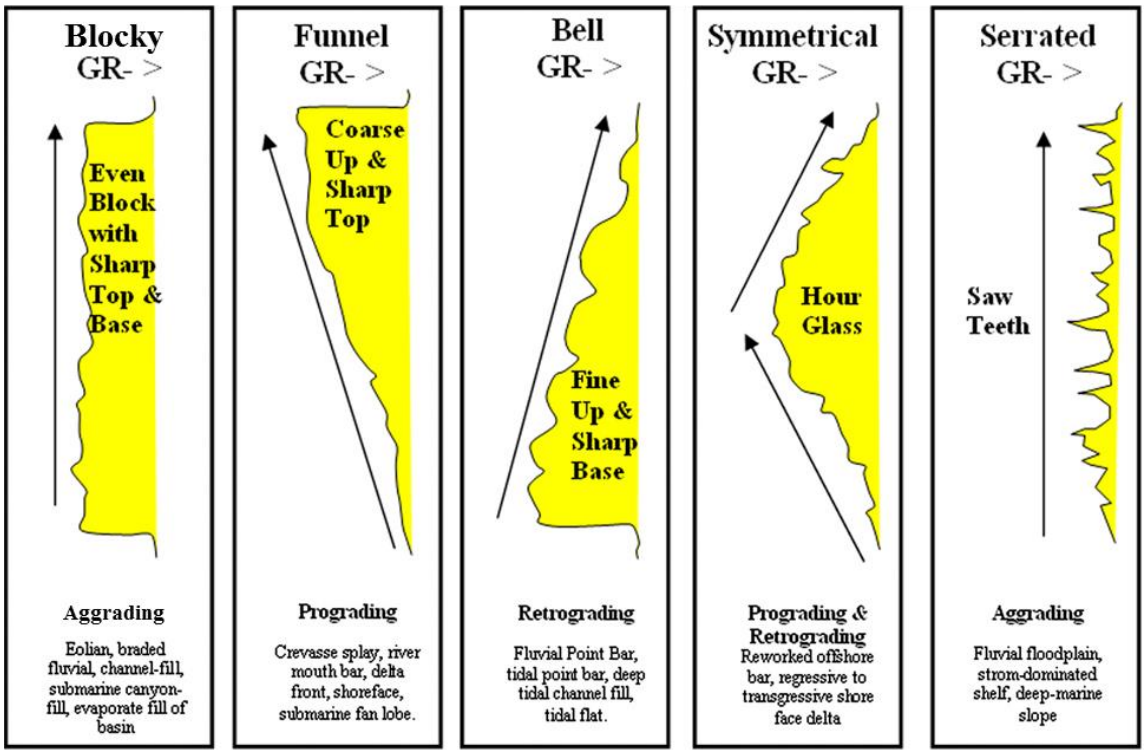

Figure 3.7. Generalized gamma ray (GR) profiles from variations in depositional environment (After Kendall, 2003, modified from Emery and Myers, 1996)

3.4.2 Lamé Parameters and Elastic Moduli

The physical properties of an isotropic material are independent of direction. At the microscopic scale, a rock composed of randomly oriented crystals or grains can be treated as isotropic (Ikelle and Amundsen, 2005). In an isotropic linear elastic material, stress and strain are related by Hooke's law. Only two independent constants, namely the "Lamé parameters" μ and λ, are needed to characterize the elastic behavior of such a material. The constant μ, or shear modulus, measures the ratio of shear stress to shear strain. The constant λ has no simple physical meaning. However, the bulk modulus K is related to the two Lamé parameters by

$$K = \frac{3\lambda + 2\mu}{3} \tag{3-1}$$

and measures the ratio of hydrostatic stress to volumetric strain. The bulk modulus is the reciprocal of the compressibility, $\beta = 1/K$, a parameter that is widely used to describe the volumetric compliance of a liquid, solid, or gas (Mavko et al., 2009). Young's modulus E is expressed by

$$E = \frac{\mu(3\lambda + 2\mu)}{\lambda + \mu} \tag{3-2}$$

and gives the ratio of axial stress to axial strain under the application of a uniaxial stress. In other words, Young's modulus measures the resistance of a material to elastic (recoverable) deformation when subjected to a load. A stiff material has a high Young's modulus while a flexible material has a low Young's modulus.

Finally, Poisson's dimensionless ratio of lateral strain to axial strain is expressed by:

$$\upsilon = -\frac{\lambda}{2(\lambda + \mu)} \tag{3-3}$$

The maximum value ($\upsilon = 0.5$) applies to a nonviscous fluid but most consolidated sedimentary rocks exhibit a Poisson's ratio between 0.2 and 0.35, with unconsolidated rocks exhibiting $0.4 < \upsilon < 0.45$.

3.4.3 The Application of Lamé Parameters and Elastic Moduli for Rock Discrimination

In tight sandstones and carbonates, seismic compressional and shear wave velocities are relatively insensitive to changes in pore fluid content and lithology (Goodway et al., 1997; Goodway et al., 2010; Russell, 2014). According to Goodway et al. (1997), converting velocity measurements to the Lamé parameters can improve identification of reservoir zones since the (μ, λ) parameters exhibit a higher sensitivity to pore fluids and lithology. Moreover, Rickman et al. (2008) show that the brittleness of a rock can be estimated from borehole-derived Poisson's ratio υ and Young's modulus E. A brittle zone is characterized by a high value of E along with a low value of υ, while a ductile zone is characterized by a low value of E along with a high value of υ (Chopra et al., 2013).

There exist inverse relationships between Young's modulus and parameters such as porosity, TOC and clay content in some unconventional shale plays, as shown by Takahashi and Tanaka (2010) and Kumar et al. (2012). I anticipate that a similar relationship could apply to the rocks of the Baturaja Formation. Other authors have further analyzed relations between reservoir rock properties and elastic moduli. Importantly, Perez et al. (2011) created a heuristic template to interpret seismic, well log, or laboratory properties of rocks with different quartz and clay contents in terms of parameters such as estimated ultimate recovery (EUR), original gas in place (OGIP), recovery factor (RF), pore pressure, and fracture density (**Figure 3.8**). Goodway et al. (2010) developed "Lambda-Rho versus Mu-Rho" $(\lambda\rho - \mu\rho)$ crossplots to faciliatate a comparison of shales

and carbonates from Western Canada to those of the Barnett Shale (**Figure 3.9**). Knapp et al. (1995) developed crossplots of V_P/V_S and Poisson's ratio to discriminate sedimentary rocks.

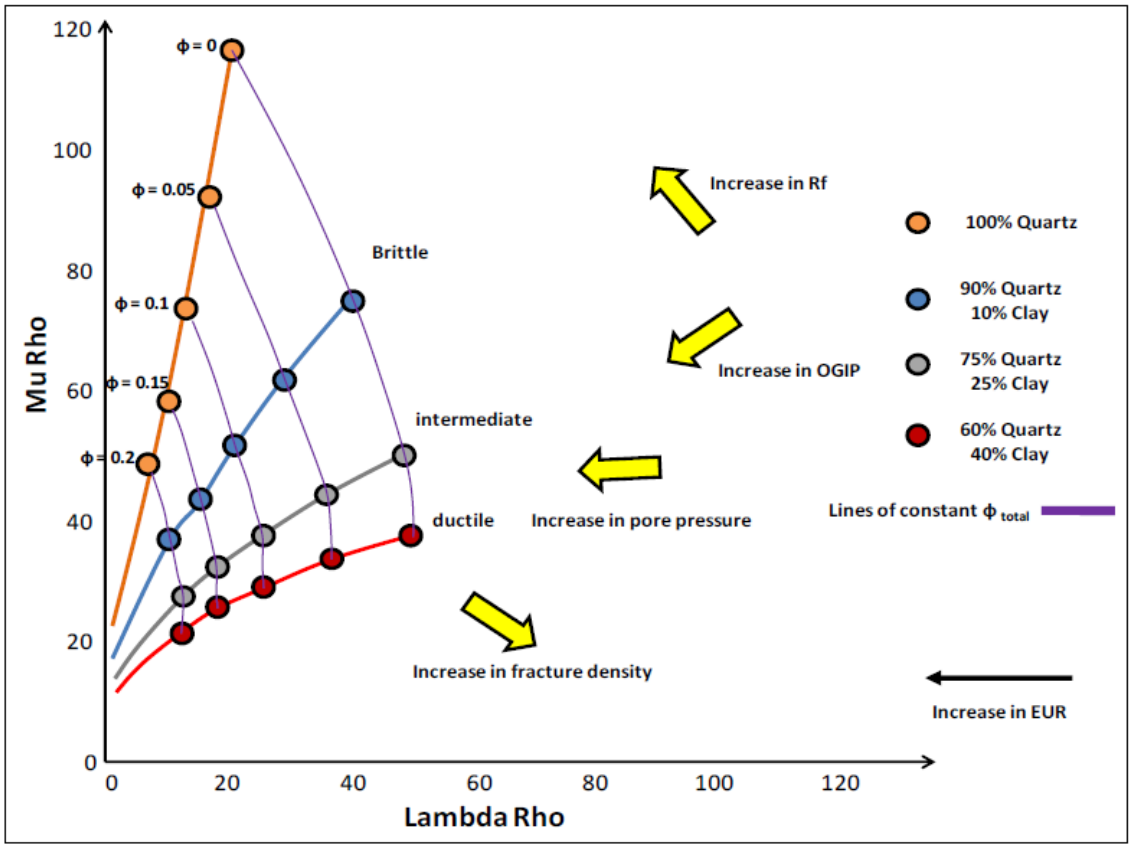

Figure 3.8. Heuristic template to interpret seismic, well log, or laboratory rock properties in terms of estimate ultimate recovery (EUR), original gas in place (OGIP), recovery factor (RF), pore pressure, and fracture density of reservoir with different quartz and clay partition (After Perez et al., 2011).

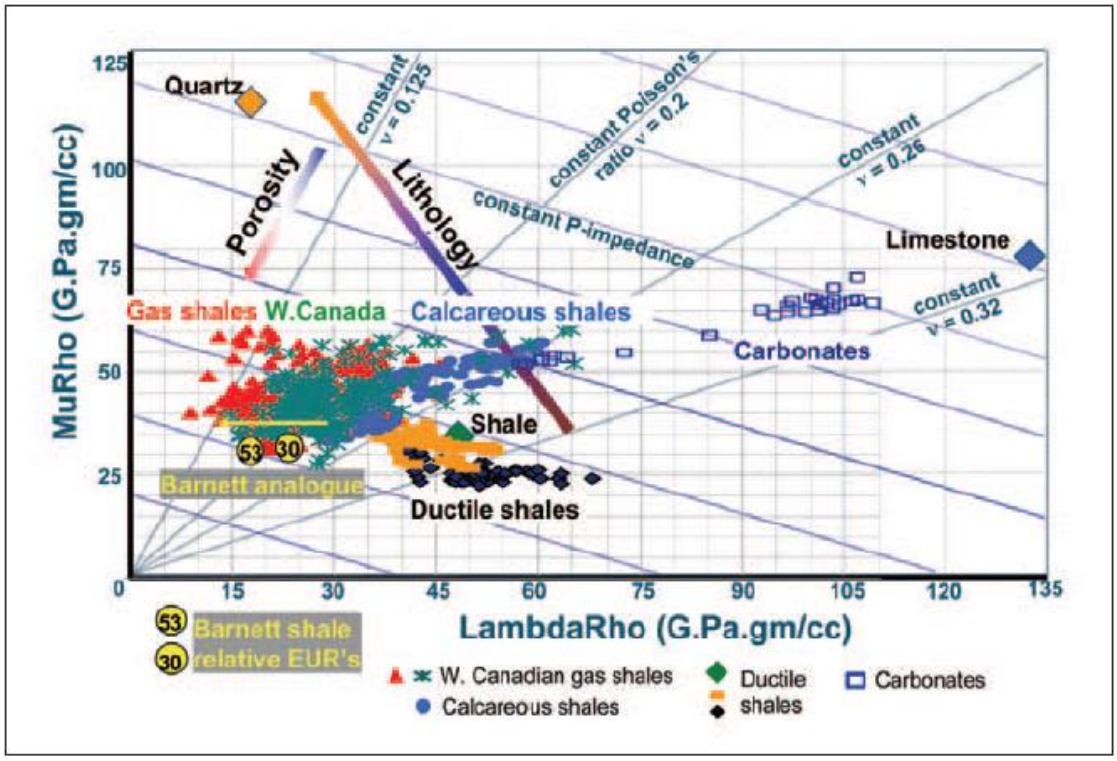

Figure 3.9. Lambda-Rho versus Mu-Rho crossplot comparing various shales and carbonates from Western Canada to the Barnett Shale with background pure mineral points and lines of constant Poisson's ratio and P-Impedance (from Goodway et al., 2010).

Building upon these previous works, I defined a new well-based classification of the Baturaja Formation using a combination of Lamé parameters ($\lambda\rho, \mu\rho$) and elastic moduli, namely Poisson's ratio and Young's modulus. The methodology estimates the reservoir quality of carbonate rock based on key properties that consist of brittleness, porosity, total organic carbon (TOC) and mineral content including clay, quartz and dolomite. For this purpose, a cross-property elastic material equation was developed in terms of the Poisson's ratio extracted from the seismic-determined ratio V_P/V_S (Ostrander, 1984) and the acoustic impedance contrast (Fatti et al., 1994; Gidlow et al., 1993; Wallace

and Young, 1996). For a homogeneous isotropic linear elastic material, the compressional wave velocity V_P [m/s] is

$$V_P = \sqrt{\frac{\lambda + 2\mu}{\rho}} \tag{3-4}$$

and the shear wave velocity V_S [m/s] is

$$V_S = \sqrt{\frac{\mu}{\rho}} \tag{3-5}$$

while the P-wave and S-wave impedances Z_{P}, Z_{S} [g/cm^3·m/s] are

$$Z_P = \rho V_P \; ; \quad Z_S = \rho V_S \tag{3-6}$$

The quantities $\lambda\rho$ "Lambda-Rho" and $\mu\rho$ "Mu-Rho" are used here instead of simply λ and μ. The parameters $(\lambda\rho, \mu\rho)$ may be derived directly from seismic AVO inversion. The Lamé parameters (λ, μ) are multiplied by density ρ because, for incident angles <30^0, the density extracted from seismic data using a Zoeppritz approximation is subject to large uncertainties (Aki and Richards, 2002; Fatti et al., 1994). The parameters $(\lambda\rho, \mu\rho)$ are related to the acoustic impedances by the formulas:

$$\lambda\rho = Z_P^2 - 2Z_S^2 \tag{3-7}$$

and

$$\mu\rho = Z_S^2 \tag{3-8}$$

Finally, the brittleness-related elastic moduli (υ, E) are expressed in term of V_P/V_S as

$$\upsilon = \frac{V_P^2 - 2V_S^2}{2(V_P^2 - V_S^2)} \quad (3\text{-}9)$$

and

$$E = \frac{\rho V_S^2 (3V_P^2 - 4V_S^2)}{(V_P^2 - V_S^2)} \quad (3\text{-}10)$$

Herein we display the values of $\lambda\rho, \mu\rho, \upsilon$, and E from Baturaja carbonate rock on a $(\lambda\rho, \mu\rho)$ crossplot overlain by contours of (υ,E) to discriminate reservoir quality.

3.5 Results

3.5.1 Carbonate Platform Parasequence Set

The stratigraphic correlation across the available wells in Pagardewa Field is shown in **Figure 3.10**. As mentioned earlier, the gamma ray logs contain information about the lateral and vertical sediment stacking patterns in the form of aggradation, progradation and retrogradation. These stacking patterns comprise the parasequence and parasequence sets which record the geological evolution of Baturaja Formation carbonate platform. The latter is defined as a carbonate ramp at early Miocene (see Chapter II). Initially, carbonate grew atop the marine paralic of the upper part of Talang Akar Formation in a transgressive sequence. This event is represented by a deflection to the left (from higher to lower) in the gamma ray log readings. This deflection is interpreted as a lithology change from calcareous, shaly-sandstone to carbonate rock (**Figure 3.10**). A marine flooding surface is defined by the high gamma ray values at the end of the period

of carbonate growth. At this time, sea level rise drowned the carbonate platform. Subsequently, the deep-water shale of Gumai Formation was deposited on the carbonate platform.

I identified four parasequence set boundaries within the carbonate platform, labeled 4-1 from oldest to youngest. The zone located between parasequence sets 3 and 4 is dominated by a progradational stacking pattern (as indicated by the shape of the gamma ray curve), so herein it is called the "progradational zone". Similarly, the zone located between parasequence sets 2 and 3 is dominated by an aggradation stacking pattern so herein is called the "aggradational zone". The aggradation zone thickens to the northwest (seaward) and thins to the southeast (landward). The youngest zone between parasequence set 2 and the marine flooding surface is the "retrogradational zone".

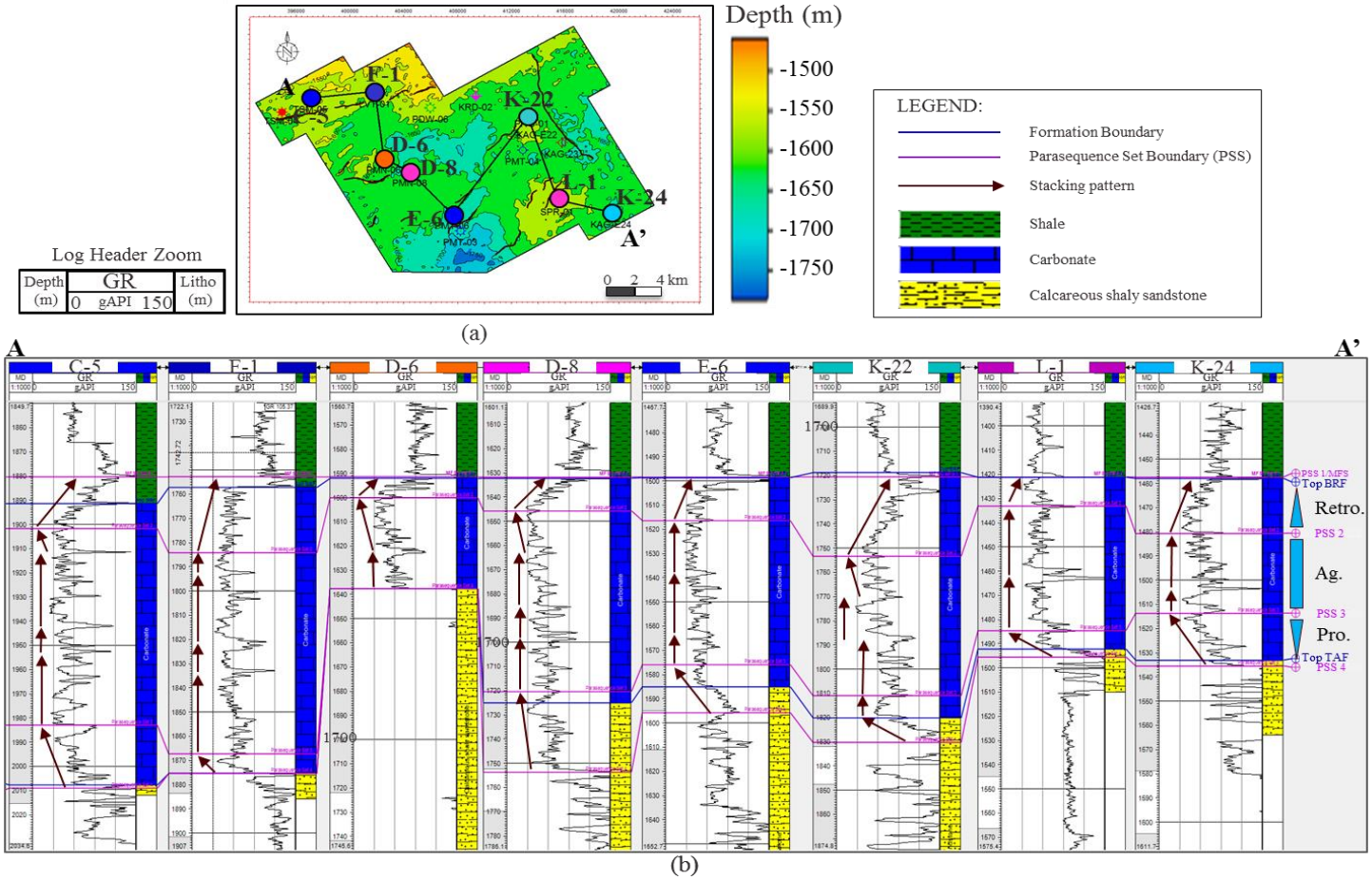

Figure 3.10. (a) Paleotopography of top Baturaja carbonate platform at early Miocene (see Chapter II). (b) Lithology correlation with stratigraphic interpretation along northwest to southeast (along line A to A' at the paleotopography map of top Baturaja Formation) showing vertical and lateral stacking patterns within the carbonate platform. (Note: Pro=Progradation, Ag=Agradation, Retro=Retrogradation).

3.5.2 Carbonate Quality Classification

A petrophysical analysis of data from one of the available wells (C-4) within the study area is shown in **Figure 3.11**. Porosity and permeability were calculated in Chapter II. A display of Lambda-Rho and Mu-Rho ($\lambda\rho, \mu\rho$), and the brittleness-related elastic moduli (Poisson's ratio and Young's modulus) are included in the figure (see Eqs (3-7) to (3-10)). However, it is difficult to discriminate the carbonate rock quality based on log-style displays such as those of **Figure 3.11**. Therefore, I transform the values into a crossplot of Lambda-Rho versus Mu-Rho (e.g. **Figure 3.12**) and overlay contours of Poisson's ratio and Young's modulus. Constant values of E and υ form linear trends on the crossplot. Similar to previous studies (Goodway et al., 2010; Knapp et al., 1995; Perez et al., 2011), such a crossplot comprises a "well-based template" that aids in classifying the carbonate rock quality of the Baturaja Formation.

In **Figure 3.12** (a**)**, the Lambda-Rho and Mu-Rho sample values extracted from the log display of 12 wells such as in **Figure 3.11** are color-coded by porosity. Porosity evidently increases toward the bottom left of the plot, i.e. toward low values of both Lambda-Rho and Mu-Rho. TOC values from three Baturaja cutting samples rock shows that the TOC are below 1 % (Geoservices, 2012c, d, f), therefore Baturaja Formation is not a source rock. However, keeping in mind the sparsity of the data, the same trend as porosity is evident (**Figure 3.12**b) for total organic carbon in the cross-plot of Lambda-Rho and Mu-Rho. I also used information from core and sidewall core laboratory analyses (Geoservices, 2012a, b, c, d, e, f, 2013a, b) to build a crossplot of V_P/V_S versus Poisson's ratio (υ) similar to that of Knapp et al. (1995). Then, I constructed a lithology classification

based on the inferred mineral content by dividing the $\lambda\rho$-$\mu\rho$ crossplot into classes separated by boundaries defined by lines of constant ν (**Figure 3.13**).

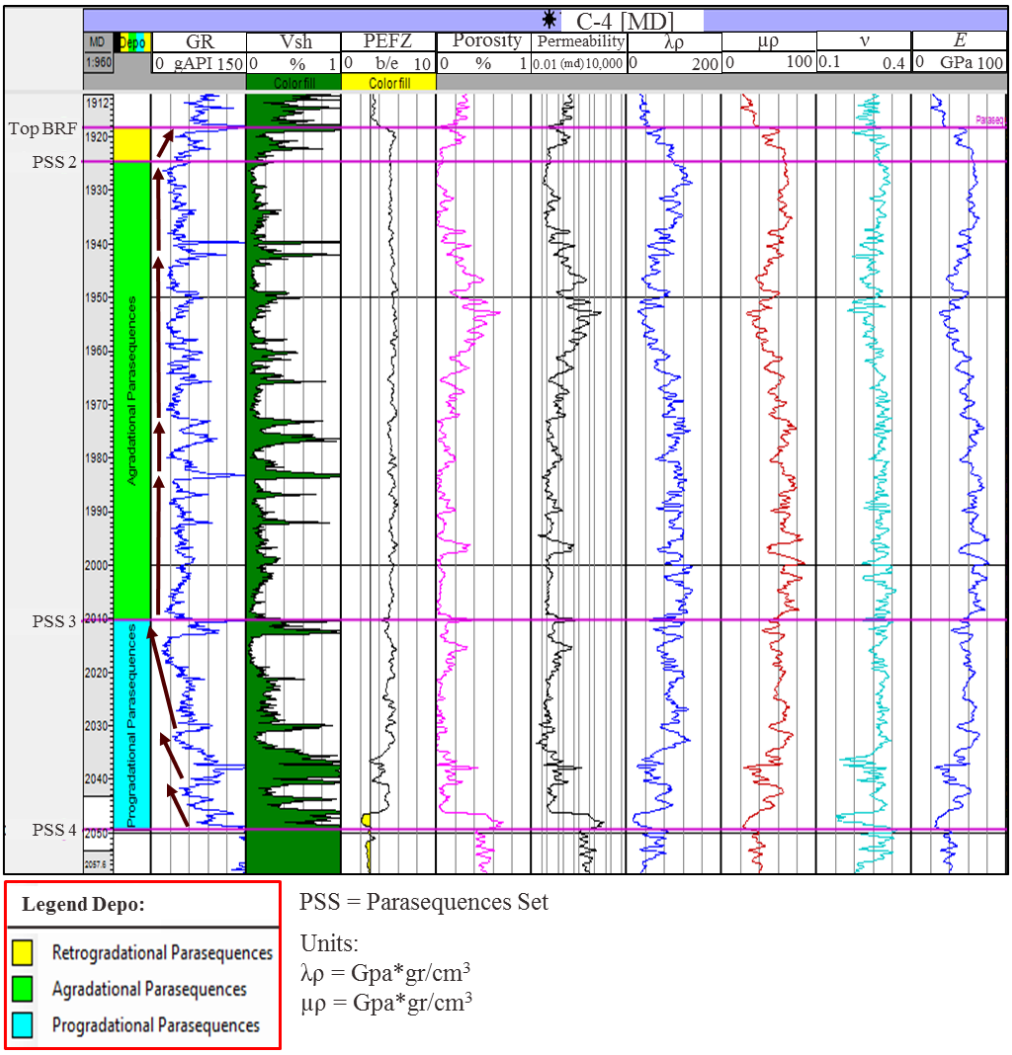

Figure 3.11. Petrophysical calculations for well C-4 (see Chapter II for porosity and permeability calculation). Lame parameters and brittleness related elastic moduli (Poisson's ratio PR and Young's Modulus E) are also included in the calculation. Note: PSS=Parasequence Set; BRF=Baturaja Formation.

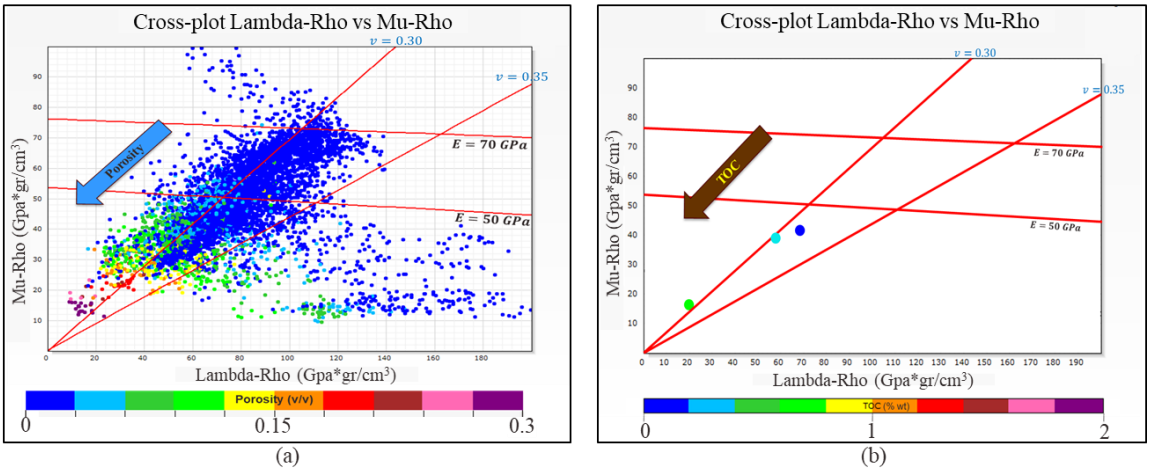

Figure 3.12. (a) Crossplot porosities of Baturaja carbonate rock on Lambda-rho versus Mu-rho. (b) Crossplot of three total organic carbon of Baturaja carbonate rock values (data from Geoservices, 2012c, d, f) on Lambda-rho versus Mu-rho.

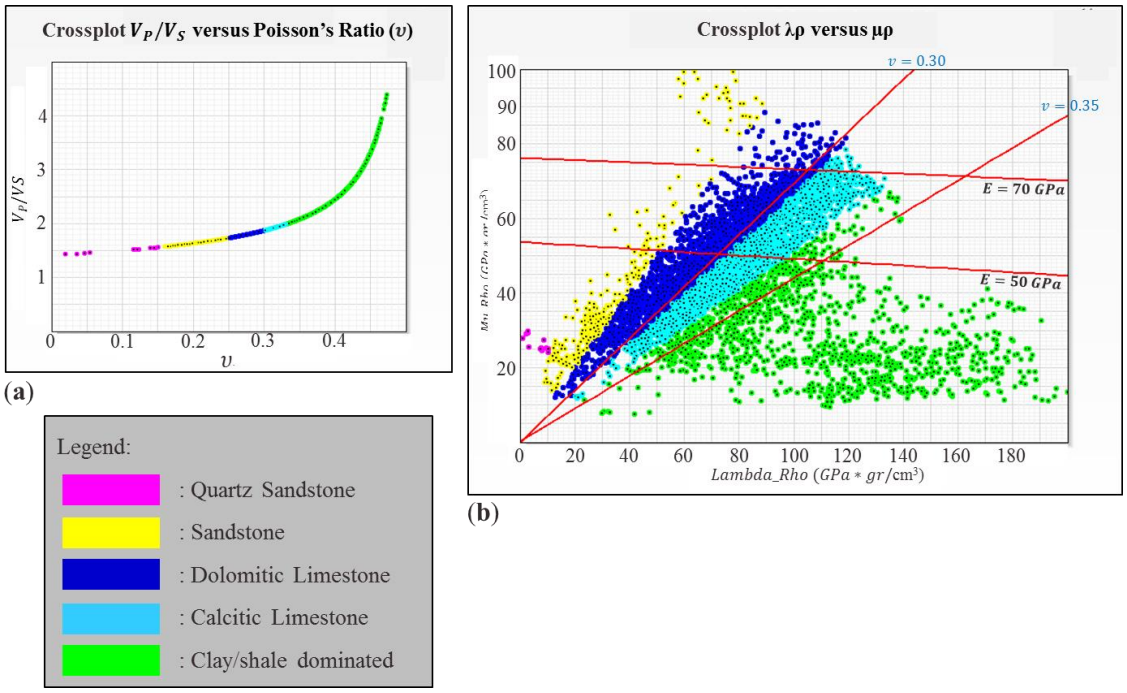

Figure 3.13. (a) Lithology classification based on minerals content resulted from crossplot of V_P/V_S versus ν. (b) The lithology classification in the frame of crossplot $\lambda\mu$ versus $\mu\rho$.

The trends for all the parameters under consideration are shown in **Figure 3.14**. These parameters are commonly used to define the quality of an unconventional reservoir. Poisson's ratio $\upsilon = 0.30$ is an important boundary in the template. As υ decreases below 0.30, the degree of brittleness, and dolomite and quartz content increases. Similarly, the degree of ductility and clay content increases as υ increases beyond 0.30. Stiffness increases in the direction of increasing Young's modulus, i.e. away from the origin of the crossplot.

Some unconventional reservoirs in North American basins have high TOC unlike the Baturaja Formation (Jarvie, 2012). With its small TOC values, Baturaja Formation is not considered as a potential source rock. Therefore, TOC is only a minor factor in determining the reservoir quality of Baturaja Formation. Instead, porosity, brittleness and mineral content are the main factors that determine the reservoir quality. The higher the porosity, the more pore space to be filled by hydrocarbon. The mineral content determines the brittleness of the rock. Quartz-rich and calcite-rich and/or dolomite-rich rock are readily fractured, compared to clay-rich rocks. Therefore, the quartz, calcite and dolomite contents of carbonate rock tend to enhance brittleness whereas clay-rich carbonate rock tends to be more ductile. A good-quality unconventional reservoir should be brittle with high porosity, TOC, quartz, calcite and/or dolomite content. In contrast, a ductile low-porosity carbonate with high clay content is likely to be a low-quality unconventional reservoir.

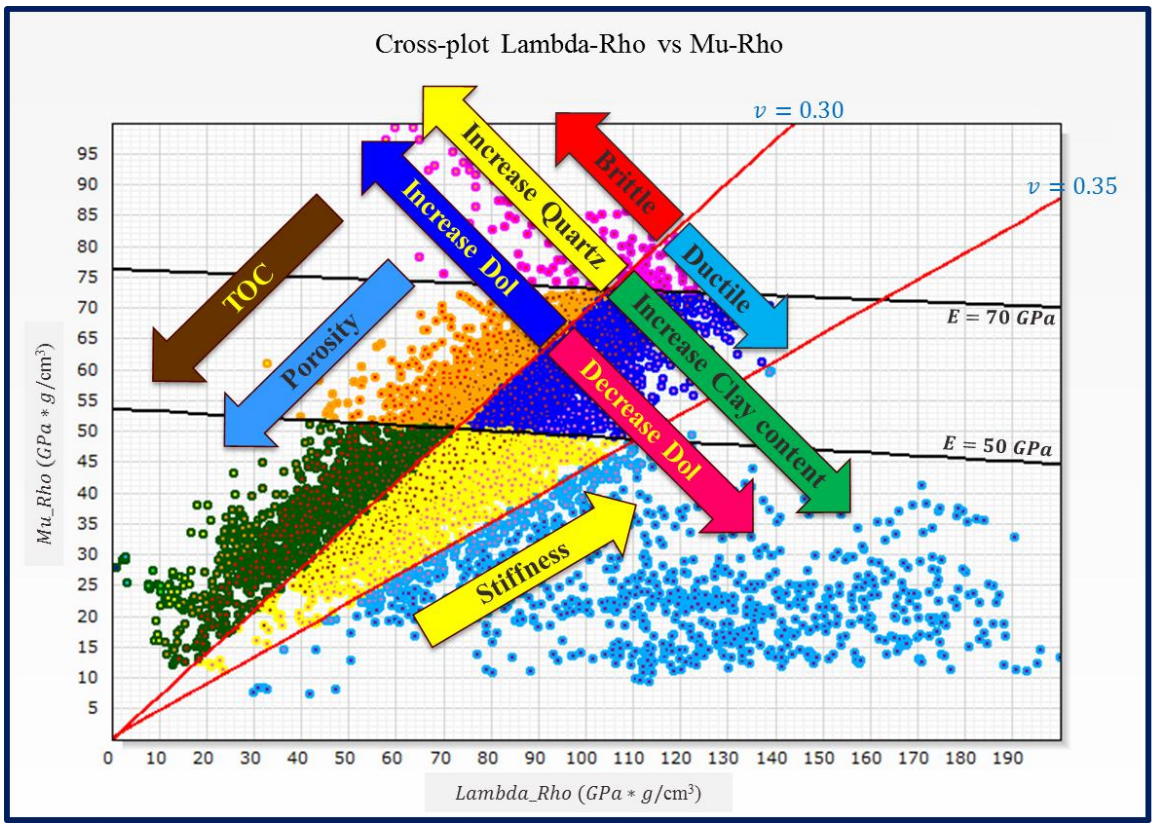

Figure 3.14. Well-based template of Baturaja carbonate rock classification. The template is built from crossplot of Lambda-rho and Mu-rho associated with Young's modulus and Poisson's ratio.

Herein I define six classes of carbonate reservoir quality as indicated by the class boundaries that are drawn on the template in **Figure 3.15**, and their attributes are listed below:

Class 1: **very good quality**; brittle, high porosity, low dolomite, low quartz, high TOC

Class 2: **good quality**; brittle, moderate porosity, high dolomite, low quartz, moderate TOC

Class 3: **moderate quality**; ductile, high porosity, very low dolomite, very low quartz, high TOC

Class 4: **less moderate quality**; ductile, moderate porosity, very low dolomite, very low quartz, moderate TOC

Class 5: **fair quality**; very low porosity, low to very low dolomite, fair TOC

Class 6: **poor quality**; very ductile, very high clay content, very low porosity, high TOC

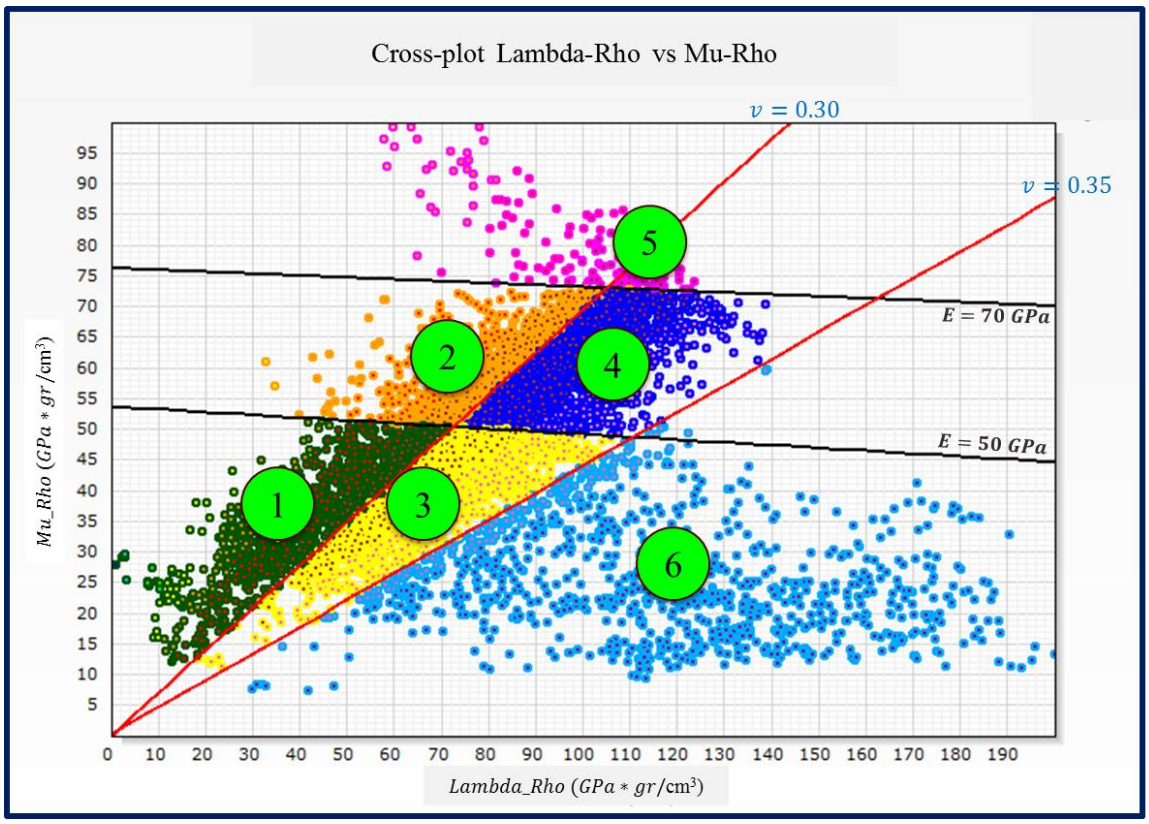

Figure 3.15. Six carbonate rock classes discriminated in Baturaja Formation from the well-based template.

3.6 Discussion

Stratigraphically, I have identified three zones in the Baturaja Formation based on the sediment stacking pattern within parasequence sets. The three zones are, respectively, propagradational, aggradational, and retrogradational. Together, they capture the geological evolution of the Baturaja carbonate ramp discussed in Chapter II. The evolution of the ramp is illustrated by reconstructed stratigraphic charts of the Baturaja Formation. For example, the reconstructed chart at well C-4 is shown in **Figure 3.16**. Here, the stacking pattern is influenced by carbonate production and accommodation space, with the latter depending on the eustatic sea-level curve. Initiation of carbonate production at Baturaja Formation was diachronous at late Burdigalian time, in a transgressive setting. While the eustatic curve was increasing at a slow rate, the carbonate production was greater than the accommodation space. This effect caused the carbonate production to prograde seaward. The carbonate growth changed to aggradation once the carbonate production rate became roughly equal to the eustatic variation. At that time, carbonate was produced mainly to keep pace with sea level rise. At end of late Burdigalian time, the sea level dropped, leading to a declining of the eustatic curve, then it gradually increased to a fast rate of rise. In this time interval, the carbonate growth started to become retrograde. The carbonate was being produced at a rate less than the increase of accommodation space, such that the growth was unable to keep pace with the fast-rising sea level. The diachronism of a drowning event on the Baturaja Formation occurred at that time (Pannetier, 1994). The carbonates were partially drowned in some places but in other

places, under relatively shallow water, carbonate continued to develop. The deep-water shale of Gumai Formation was subsequently deposited over the drowning platform.

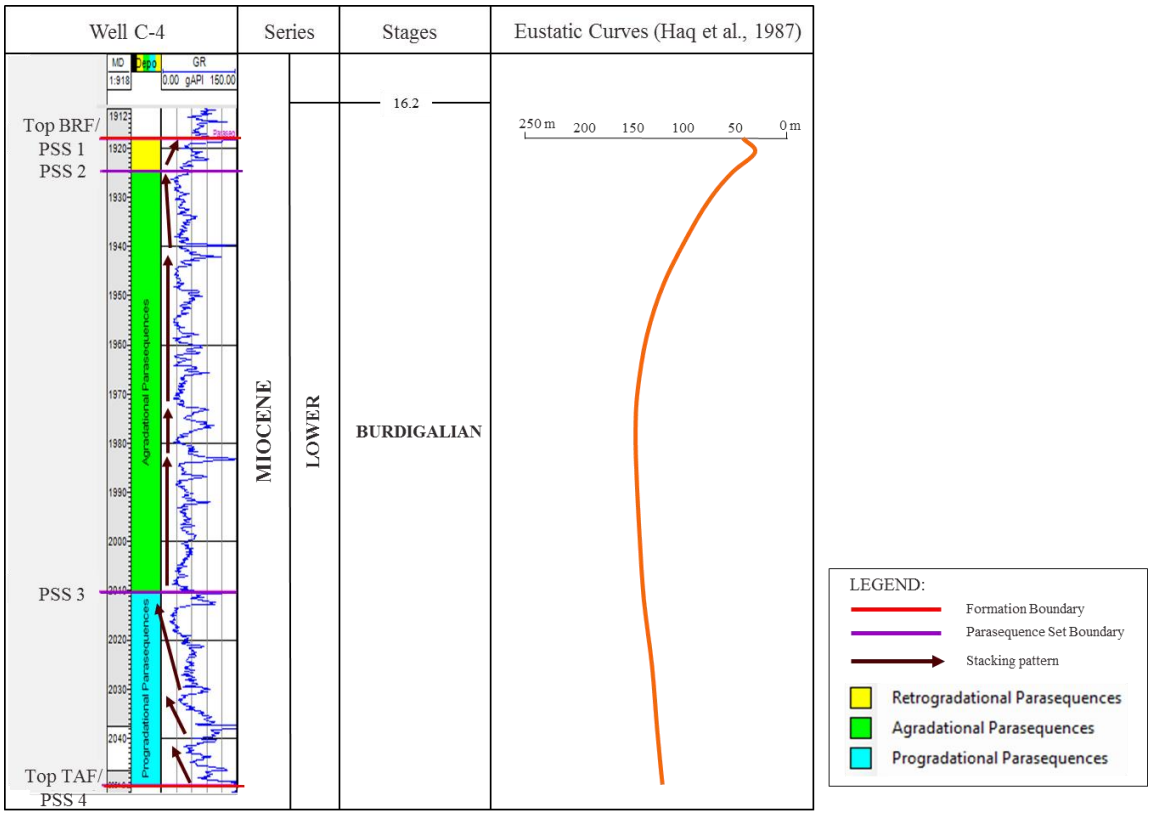

Figure 3.16. Stratigraphic chart in Baturaja Formation at well C-4

Six carbonates classes defining reservoir quality of the Baturaja Formation have been classified from the well-based template. Classes 1 and 2 denote the best reservoir quality, classes 3 and 4 are moderate quality, class 5 represents a tight reservoir of low quality and class 6 is the poorest reservoir quality. **Figure 3.17** shows the relation of the reservoir quality classification to carbonate facies descriptions from cores, side-wall cores and cuttings data (Geoservices, 2012b, c, d, f, 2013a). The well-based template relates the reservoir quality classes to specific carbonate facies in Baturaja Formation as follows:

class 1 is coral wackstone-packstone; class 2 is dolomitic wackstone-packstone; class 3 is mudstone; class 4 is wackstone-packstone; class 5 is floatstone; and class 6 is calcareous shale.

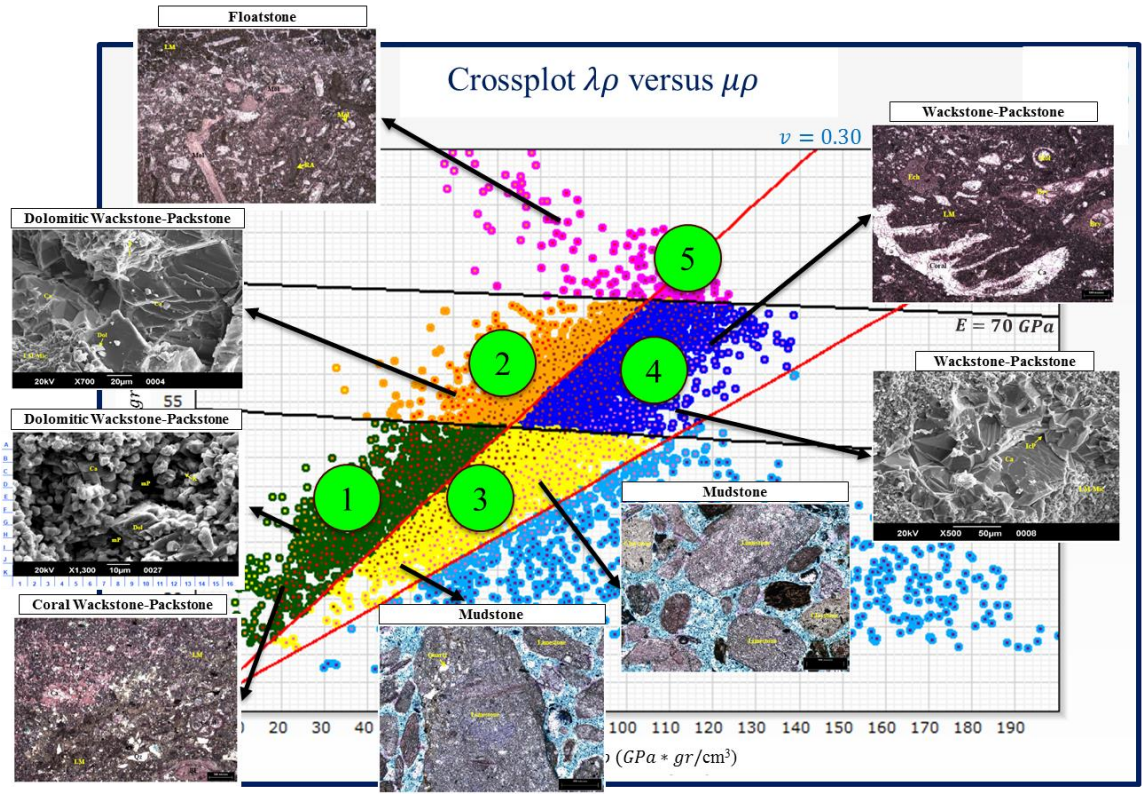

Figure 3.17. The relationship between carbonate facies information (Geoservices, 2012b, c, d, f, 2013a) and the reservoir quality classes.

It should be noted however that similar carbonate facies can have dissimilar reservoir quality. For example, wackstone-packstone can exhibit class-2 quality if the dolomite content is high (dolomitic wackstone-packstone), but will be shifted into class 4 if calcite and clay mineral dominate the facies.

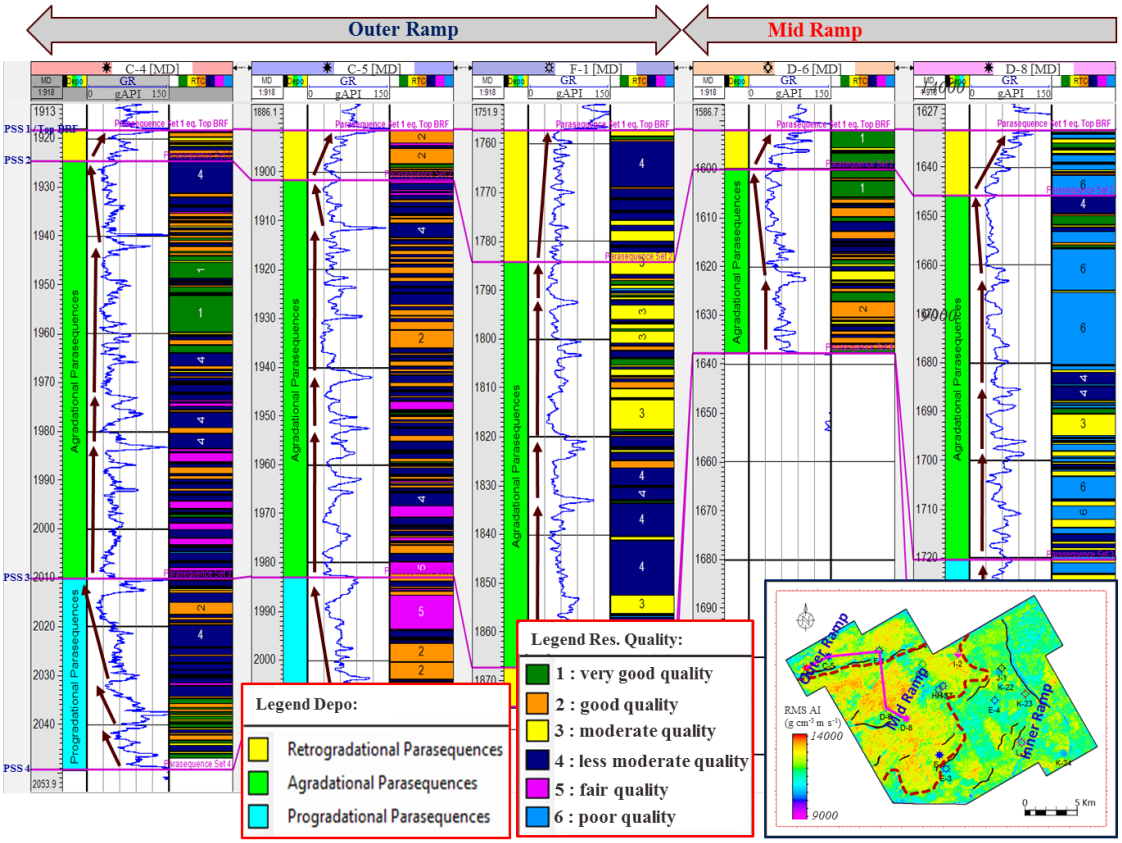

Figure 3.18. The combination of stratigraphic interpretation and carbonate rock quality classes-Part 1. Inset picture at right bottom is RMS acoustic impedance throughout Baturaja Formation interval with purple bold line represents well cross-section (see Chapter II).

The combination of stratigraphic interpretation and carbonate rock class assignment at each well location predicts both the carbonate rock quality within each parasequence set zone, and also how the depositional environment is related to the dominant class (**Figure 3.18**-**3.20**). For example, wells C-4 and C-5 are both located in the outer ramp of the Baturaja carbonate platform (Chapter II). Classes 4 and 5 dominate this environment (**Figure 3.18**). Similarly, the carbonate rocks at wells located in the middle ramp (such as wells D-6, D-8, E-6 and E-3) are dominated by classes 1 and 3 with

minor amounts of classes 2, 4 and 6 (**Figure 3.19**). Finally, the carbonate rocks at two wells located in the inner ramp, L-1 and K-24, are dominated by classes 1 and 3 with minor amounts of classes 2 ,4 and 6 (**Figure 3.20**).

Carbonate classes 1 and 3, with low Lambda-rho and Mu-rho values, are characterized by high porosity, clay and quartz content. In Chapter II, the degree of siliciclastic influences in the Baturaja carbonate platform, as inferred from a seismic RMS amplitude map, is discussed. The carbonate platform divides into two facies: a first with higher and a second with lower siliciclastic input. Carbonate classes 1 and 3 dominate the inner ramp, in which the siliciclastic input is high, and occurs in the form of detrital quartz and enhanced clay content. The siliciclastic porosities contribute to an increasing of the carbonate rock porosities in the inner ramp. Carbonate classes 4 and 5 dominate the upper part of outer ramp where wells C-4 and C-5 are located. A high degree of cementation, inferred from higher acoustic impedance and lower porosity in Chapter II, is probably the main factor for the lower reservoir quality found in the outer ramp.

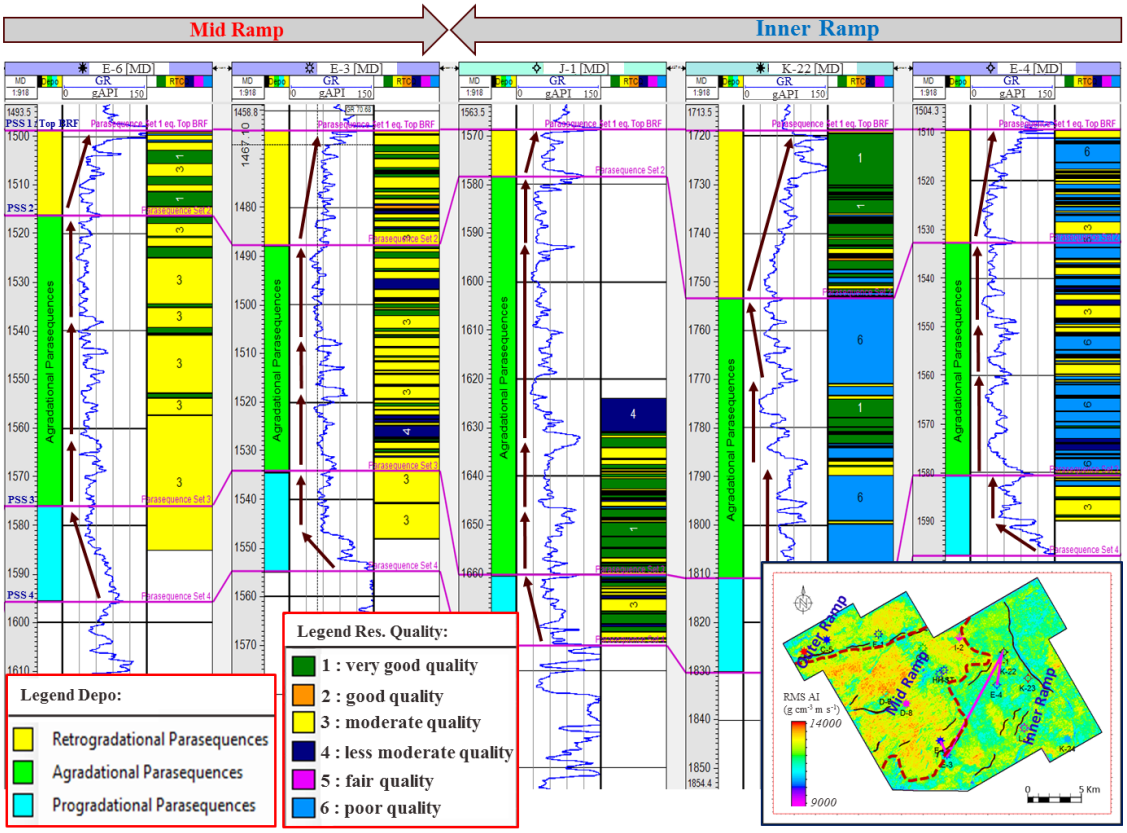

Figure 3.19. The combination of stratigraphic interpretation and carbonate rock quality classes-Part 2. Inset picture at right bottom is RMS acoustic impedance throughout Baturaja Formation interval with purple bold line represents well cross-section.

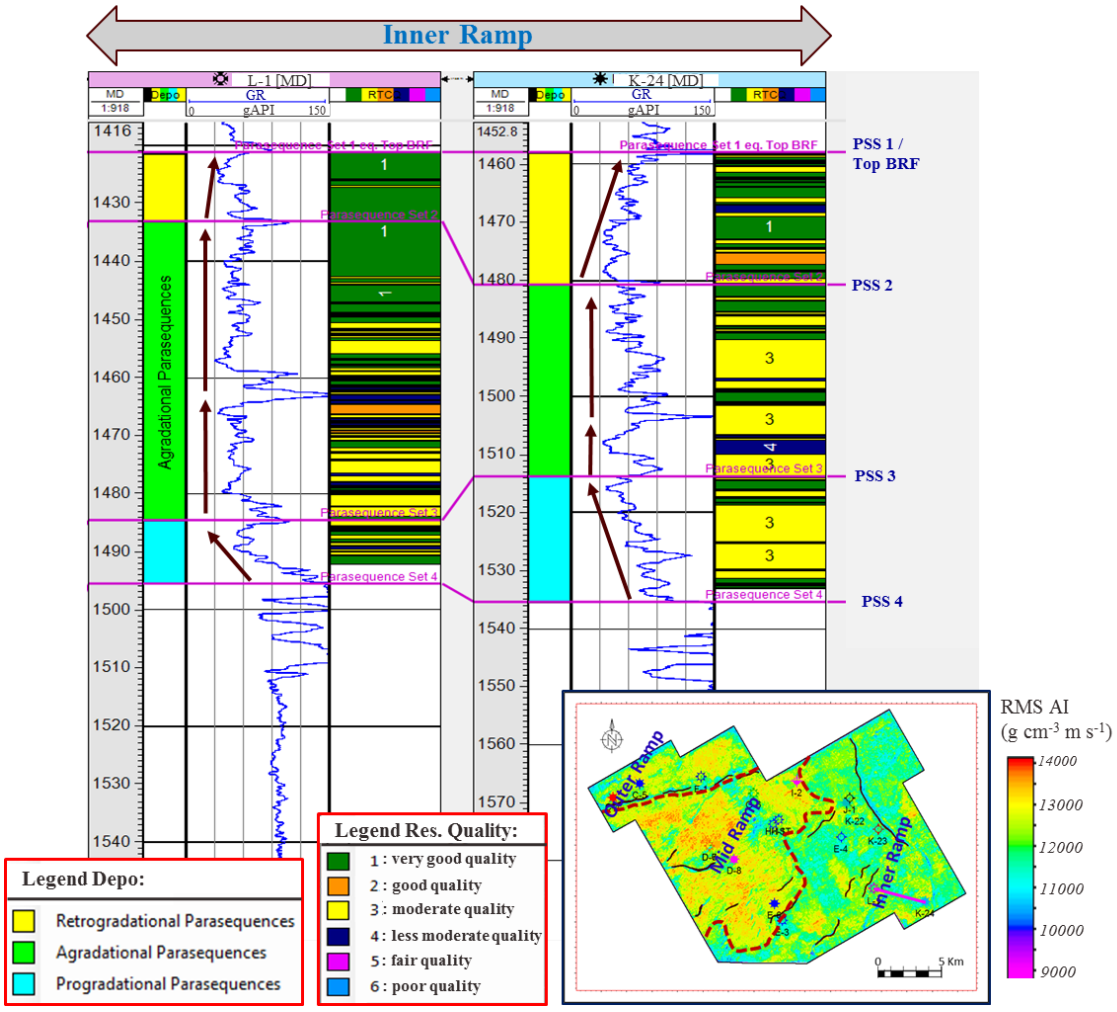

Figure 3.20. The combination of stratigraphic interpretation and carbonate rock quality classes-Part 3. Inset picture at right bottom is RMS acoustic impedance throughout Baturaja Formation interval with purple bold line represents well cross-section. The carbonate rock are influenced by higher siliciclastic material that is reflected in the domination of higher reservoir quality and lower acoustic impedance value at the two wells in inner ramps.

The histograms in **Figure 3.21** show the distribution of carbonate rock classes within each parasequence set zone. These histograms are found by calculating the percentage of the Baturaja interval that is occupied by rocks of the various quality classes and noting which parasequence set zone to which rocks within each class belong. This

analysis indicates that the lower rock class numbers, i.e. higher reservoir quality, dominate the retrogradational zone. According to the carbonate reservoir quality classification, higher reservoir quality consist of class 1 and class 2. The percentage of the reservoir that could be economically exploited from retrogradational parasequence set zone is 38.8% (from class 1) and 7.8% (from class 2). I find a lower amount, 17.3% (from class 1) and 10.3% (from class 2), that could be exploited from the aggradational parasequence set zone. I also predict that 14.1% (from class 1) and 14.8% (from class 2) of the reservoir could potentially be exploited from the progradational parasequence set zone.

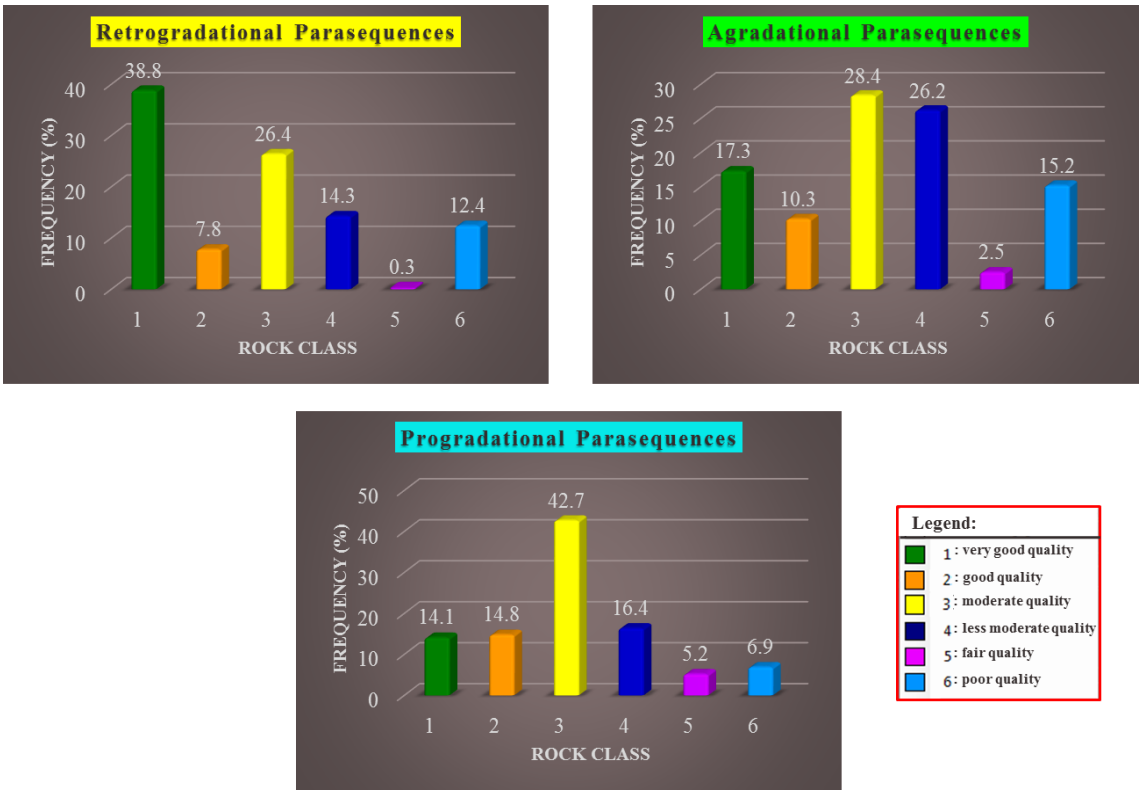

Figure 3.21. The distribution of carbonate rock classes in parasequences set zones

The retrogradational parasequence set zone has the highest fraction of high and moderate quality (classes 1 and 3) due to its favorable porosity, TOC and clay content.

Based on the eustatic curve of Haq et al. (1987), there is a large sea level drop at late Burdigalian time. This event would have exposed the carbonate rock to meteoric water. The meteoric water influenced the cementation in this area, as evidenced by the blocky calcite cement found in samples from well C-4 (**Figure 2.31**). The consequent carbonate dissolution by the meteoric water would also have increased the porosity of the carbonate rock. As sea level began to rise, clays and pelagic sediment were deposited in the retrogradational parasequence set zone. Accordingly, glauconite and carbonaceous organic matter are common in this zone, indicating that this environment experienced low-oxygen conditions. Therefore, we find that TOC and clay content are also high in the retrogradational zone.

The progradational parasequence set zone has a high fraction of moderate-quality class 3 (42.7%). No core data are available from this zone, however the oscillations of the gamma ray (GR) logs (**Figure 3.18**) suggests that multiple 4^{th} or 5^{th}-order cycles of sea level rise occurred in this zone. These cycles are indicated by multiple sharp breaks of a deepening environment (high GR values), between shallowing upward sequences (lower GR values). The deepening layer most likely is characterized by enhanced clay content and pelagic sediments that were deposited as carbonate production was temporarily terminated. Carbonate production resumed when the water depth was sufficient. The relatively high GR values in the progradational zone, compared to the values in the other two zones, indicates abundant clay minerals were deposited into the carbonate platform, especially during sea level rise at the beginning of Baturaja carbonate production. In general, high porosity and TOC also characterize the progradational zone.

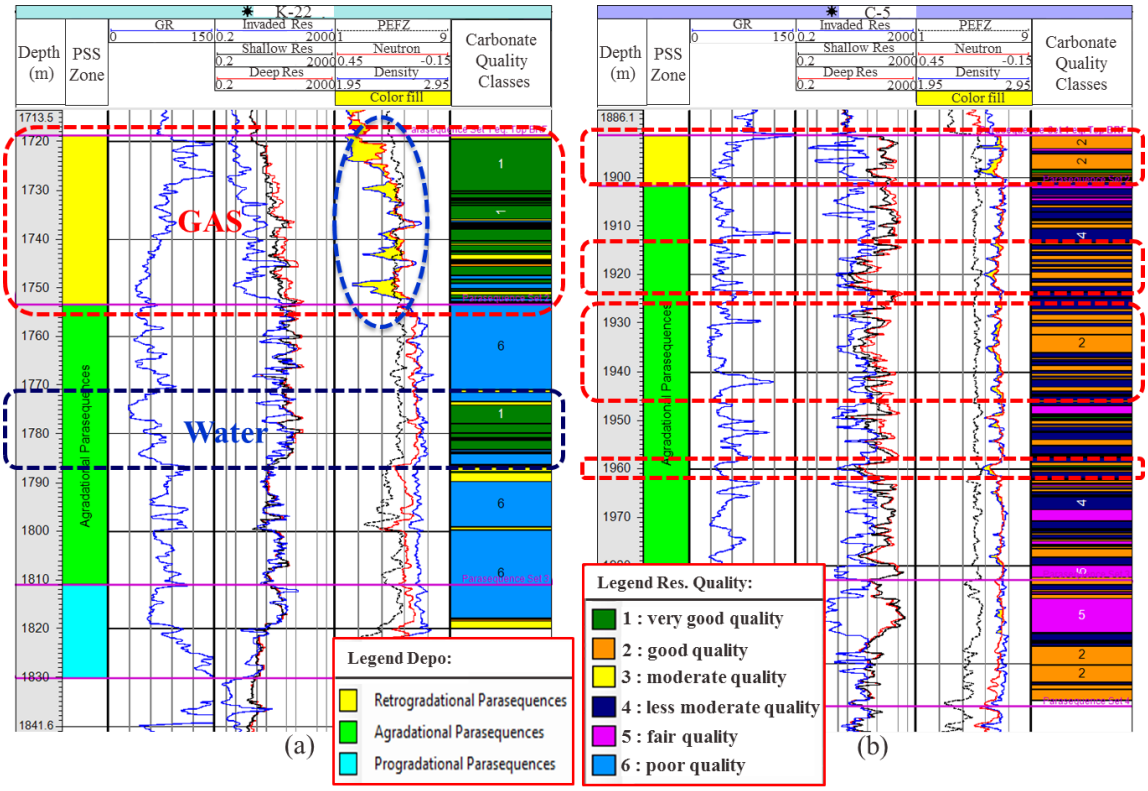

Figure 3.22. The prospective interval (inside red dashed line) consist of very good-good reservoir quality located between moderate to poor reservoir quality, neutron-density crossover values (yellow filled-zone), and gap between invaded formation and deep resistivity values. (a) At well K-22, upper prospective interval potentially contains gas, but lower interval probably only contains water. (b) Four prospective interval were identified at well C-5.

The well-based rock-quality template presented above enables explorationists to recognize, at each well location, unexploited prospective intervals in the Baturaja Formation. The prospective intervals are characterized by a number of distinctive indicators. First, the interval should be assigned to a very good or good reservoir quality class (1 or 2) and be positioned between intervals of moderate to poor quality (classes 3-6). The intervals of moderate to poor quality likely function as sealing layers. The other

indicators are based on fundamental log analysis principles. For example, the interval should also exhibit a "cross-over" of neutron and density log readings. The presence of gas makes neutron log give too low neutron porosity value and decrease the density log reading, thus it make cross-over between the logs in the log display (Rider, 2002). Finally, the interval should include a gap between invaded formation resistivity (low value) and deep resistivity (high value). At hydrocarbon rock interval, the invaded formation gives low resistivity log reading due to invasion of mud-filtrate move out the hydrocarbon, but the deeper formation give high resistivity log reading due to unaffected by the mud-filtrate invasion (Rider, 2002). **Figure 3.22** shows the prospective intervals I have identified at wells K-22 and C-5 enclosed by red dashed lines. At well K-22, a single prospective interval is identified at the upper part of Baturaja Formation at interval depth 1720–1754 m. The prospective interval consist of rocks belonging to reservoir quality class 1 located beneath the shale of the Gumai Formation and above rocks belonging to the poorest reservoir quality class 6. The prospective intervals are supported by neutron-density crossover and a large gap between invaded and deep resistivity values. Based on all indicators, the prospective interval potentially contains gas. The lower prospective interval (inside the blue dashed lines in **Figure 3.22**) at the middle part of Baturaja Formation looks promising at first glance, but it is not supported by a crossover of neutron-density values, and there is no gap between invaded and deep resistivity. This leads to a lack of prospectivity for this interval, which likely contains only water. Using this technique, four prospective intervals were identified at well C-5. These prospective intervals consist of rocks from class 2 that are located between rocks from lower-quality class 4.

The prospective zones selected from the well-based carbonate quality classification method are largely consistent with previous three drill stem tests (DST) conducted by Pertamina. These tests monitor hydrocarbon flow from the prospect intervals at well D-6 (**Figure 3.23**). Gas and condensate flows were monitored by the tests conducted in 2010. The DST-4 test reported a flow of 6.184 million standard cubic feet gas per day (MMSCFD) and 169.3 barrel condensate per day (BCPD) from interval 1600–1607 m in the upper part of the aggradational zone. DST-3 reported 6.078 MMSCFD (gas) + 172.7 BCPD (condensate) from interval 1612–1620 m in the middle part of the aggradational zone. Finally, DST-2 reported 3.094 MMSCFD (gas) + 147.7 BCPD (condensate) from interval 1624–1628 m in the lower part of the aggradational zone. The highest gas flow rate at the DST-4 interval came from a thick layer designated as class 1 (very good quality carbonate class) located in between two layers of class 4 (less moderate quality carbonate class) that act as a seal. Multiple intervals of very good and good layers of classes 1 and 2 also gave high gas flow rate at the DST-3 interval. The lower gas flow rate at the DST-2 interval is due to a narrow DST interval that penetrates only a thin layer of class 1.

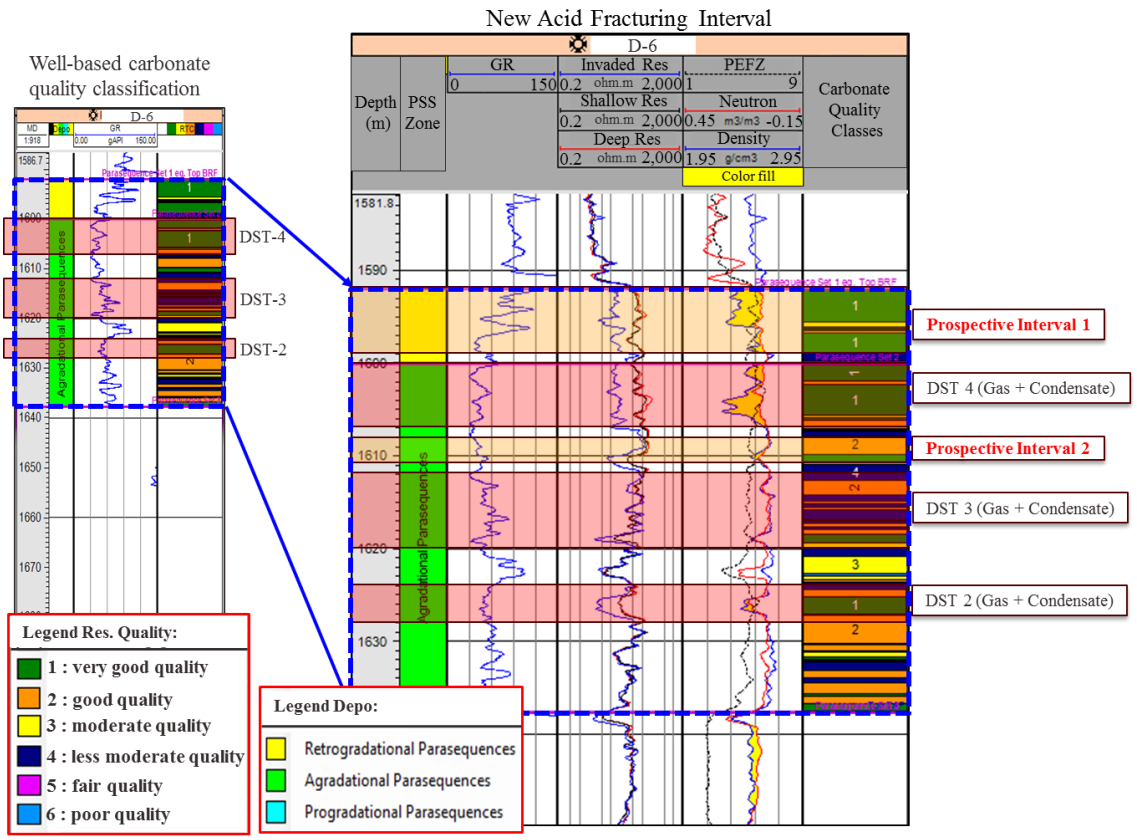

Figure 3.23. Right figure is the zoom of the left figure. Two new acid fracturing interval are suggested in Baturaja Formation in well D-6 using the technique presented in this research

To increase the hydrocarbon production from well D-6, two new acid fracturing intervals are suggested in the Baturaja Formation interval using the technique presented above (**Figure 3.23**). Prospective interval 1 consists of very good reservoir quality (class 1), whereas prospective interval 2 consists of good reservoir quality (class 2). Both of them are located between rocks of low reservoir quality (class 4). The suggested acid fracturing intervals are supported by crossover of neutron-density values, and a gap between invaded and deep resistivity log readings. The large neutron-density crossover indicates that the prospective interval 1 likely contains gas, whereas the small crossover

of neutron-density value indicates that prospective interval 2 likely contains more condensate or possibly oil.

3.7 Conclusions

Progradational, aggradational and retrogradational parasequence sets track the geological evolution of the Baturaja carbonate platform. The carbonate growth was initiated under a progradational depositional environment, which was followed by aggradational deposition, and ended with retrogradational deposition as sea-level rise drowned the carbonate platform. A combined analysis of Lamé parameters (namely, Lambda-Rho and Mu-Rho) and brittleness-related elastic moduli (notably Poisson's ratio and Young's modulus) determines the reservoir quality of the carbonate rock. The determined quality is based on well-derived petrophysical attributes such as brittleness and porosity; along with other well parameters such as TOC, clay, quartz, calcite and dolomite content. Six carbonate rock-quality classes were identified on this basis. The lowest carbonate class numbers, designating the highest reservoir quality, dominate the inner ramp due to high siliciclastic input into the environment. Higher carbonate rock class numbers, or lower reservoir quality, dominate the outer ramp due to abundant cementation in this environment. The retrogradational parasequence set zone has the highest fraction of high and moderate quality (classes 1 and 3) due to its favorable porosity, TOC and clay content. TOC and clay content increased due to the drowning of the Baturaja carbonate platform. The relatively higher gamma ray values in the progadational parasequence set zones indicate an abundance of siliciclastic material, especially as sea level rose during the early stages of Baturaja carbonate production.

With the unconventional reservoir quality determination described herein, we can recognize unexploited potential of the suggested prospective zones. The prospective intervals are supported by three factors: 1) the interval consists of very good to good quality rock located between moderate to poor quality intervals; 2) the neutron-density crossover value, and; 3) the gap between invaded formation resistivity and deeper resistivity log readings. The new acid fracturing intervals suggested here are based on those supporting factors for selecting potential prospective intervals in the existing wells. The hydrocarbon production from Baturaja Formation is expected to increase by use of the technique described herein; in such case the economic value of Pagardewa Field would be increased.

CHAPTER IV

GENERATED 3D CARBONATE QUALITY DISTRIBUTION OF BATURAJA FORMATION USING SEISMIC AVO INVERSION

4.1 Summary

Baturaja Formation is a tight carbonate gas reservoir located in Pagardewa Field, Indonesia. A seismic-based classification template is herein developed to discriminate the reservoir quality of the carbonate rock based on petrophysical parameters such as brittleness, porosity, TOC and mineral content including clay, quartz and dolomite. Similar to our previous development of a well-based template, the seismic-based template is built from a cross-plot of diagnostic parameters Lambda-Rho ($\lambda\rho$) and Mu-Rho ($\mu\rho$) overlain by contours of brittleness-related elastic moduli (Young's modulus and Poisson's ratio). The Lambda-Rho ($\lambda\rho$) and Mu-Rho ($\mu\rho$) parameters are derived from seismic AVO inversion after pre-conditioning the available migrated gathers comprising an industry 3-D dataset. A data processing workflow is developed that improves the resolution and reflector continuity of the seismic data. An AVO inversion of the improved dataset results in a contiguous 3D distribution of carbonate reservoir quality classes across the Baturaja Formation. Prospective intervals interpreted from the classification results are validated against drill stem tests involving gas and condensate flow from the middle and lower parts of the carbonate interval. The classification methodology can be used here and in similar carbonate reservoirs worldwide to guide the location of infilling wells for the purpose of

increasing hydrocarbon production from the reservoir. We envision its application to Baturaja Formation to become part of the future development plans for Pagardewa Field.

4.2 Introduction

Worldwide fossil fuel consumption is continuously increasing despite the fact that hydrocarbon production from most conventional geological reservoirs continues to decrease. The recent global demand for fuel energy has not been accompanied by significant discoveries of hydrocarbons in conventional reservoirs. To add to their diminishing hydrocarbon reserves, oil companies must either bring new concepts to existing fields or apply existing concepts to the few remaining frontier areas. Alternatively many companies are investigating unconventional reservoirs, which are those that require use of stimulation technology to alter the rock permeability or the fluid viscosity in order to produce hydrocarbon at commercially competitive rates (Cander, 2012). These reservoirs normally require multi-fractured horizontal wells to enable hydrocarbons to flow sufficiently easily that acceptable production rates can be achieved. Exploration and drilling of unconventional reservoirs including tight gas sand and shales has increased since 2005 especially in North America with the successful development of fields including the Barnett, Bakken, and Marcellus shales, in addition to the Haynesville and Eagle Ford formations.

Baturaja Formation in Indonesia is a gas-filled tight carbonate rock at Pagardewa Field in the Palembang sub-basin of Sumatra island (Doust and Noble, 2008). Previously regarded as a conventional reservoir, in this paper the Baturaja carbonate formation is treated as an unconventional reservoir based on its physical properties and the

accumulated experience from past exploitation techniques. Promising reservoir characterization strategies that can lead to increased estimated ultimate reserves often arise by formulating and working through new concepts and workflows. For example, I estimated the Baturaja Formation reservoir quality using a well-based classification technique that integrated Lamé constants and brittleness-related elastic moduli in Chapter III of this dissertation. In this chapter, we present an analogous seismic-based classification scheme in which these elastic parameters are derived from AVO inversions of an industry-supplied 3-D seismic dataset.

While compressional V_P and shear V_S seismic wave velocities are relatively insensitive to lithology and fluid-content variations in tight carbonate rocks such as those of the Baturaja Formation (see Chapter III), amplitude versus offset (AVO) inversion for the Lamé parameters ($\lambda\rho, \mu\rho$) promises to improve lithology discrimination and/or fluid detection in carbonate formations (Goodway et al. (1997). An efficient seismic data processing workflow is needed to produce optimal AVO inversions of seismic data. An AVO inversion requires that the input seismic data is broadband (i.e. rich in frequency content, both high and low), relatively noise free (high signal to noise ratio, SNR), of consistent amplitudes from trace to trace, and that recognizable signal events are temporally aligned at far source-receiver offsets. The latter is important since AVO analysis uses data gathered at far offset. Often, seismic processing workflows mute (remove) the far-offset data due to an inability to "flatten" those data to a common time datum. Thus, implementation of a technique that can align an event observed on mutiple

adjacent traces to a common time datum, from near to far offset, is important in preparing seismic data for AVO inversion.

In this study, the reservoir quality of the tight carbonate rock of Baturaja Formation is analyzed using a combination of Lamé parameters and brittleness-related elastic moduli (Young's modulus and Poisson's ratio) extracted from an industry seismic dataset. Information from petrophysical indicators is also used, such as brittleness behavior, porosity, TOC and mineral content including clay, quartz and dolomite. The main result of this research is the production of a contiguous spatial distribution of carbonate reservoir-quality classes for Baturaja Formation throughout Pagardewa Field. The seismic-based carbonate quality classes are compared at selected well locations with our previously developed well-based carbonate classification scheme. The 3D carbonate quality class distribution herein developed serves as a useful guide for selecting new infilling wells as part of future field development strategies. The methodology can be applied to similar tight-gas carbonate reservoirs worldwide.

4.3 **Geology Background**

Pagardewa Field is an oil and gas field located in Prabumulih Regency, ~80 km SW of Palembang City, the capital of South Sumatra Province, Indonesia (**Figure 4.1**). The field is located within Palembang basin in the southeastern part of the larger, prolific South Sumatra basin. Palembang basin covers an area of roughly 125 by 150 km^2 (Pulunggono, 1986). Sumatra Island comprises the southwestern margin of the stable cratonic area of Asia/Sundaland (Wilson, 2002). The basin is bounded on the southwest by faults and Mesozoic ridges that are associated with the Barisan Mountain range. On the

northeast, the basin is bounded by the stable cratonic area of Asia/Sundaland and on the eastern and southeastern sides it is bounded by the Lampung High ridge (Pulunggono, 1986).

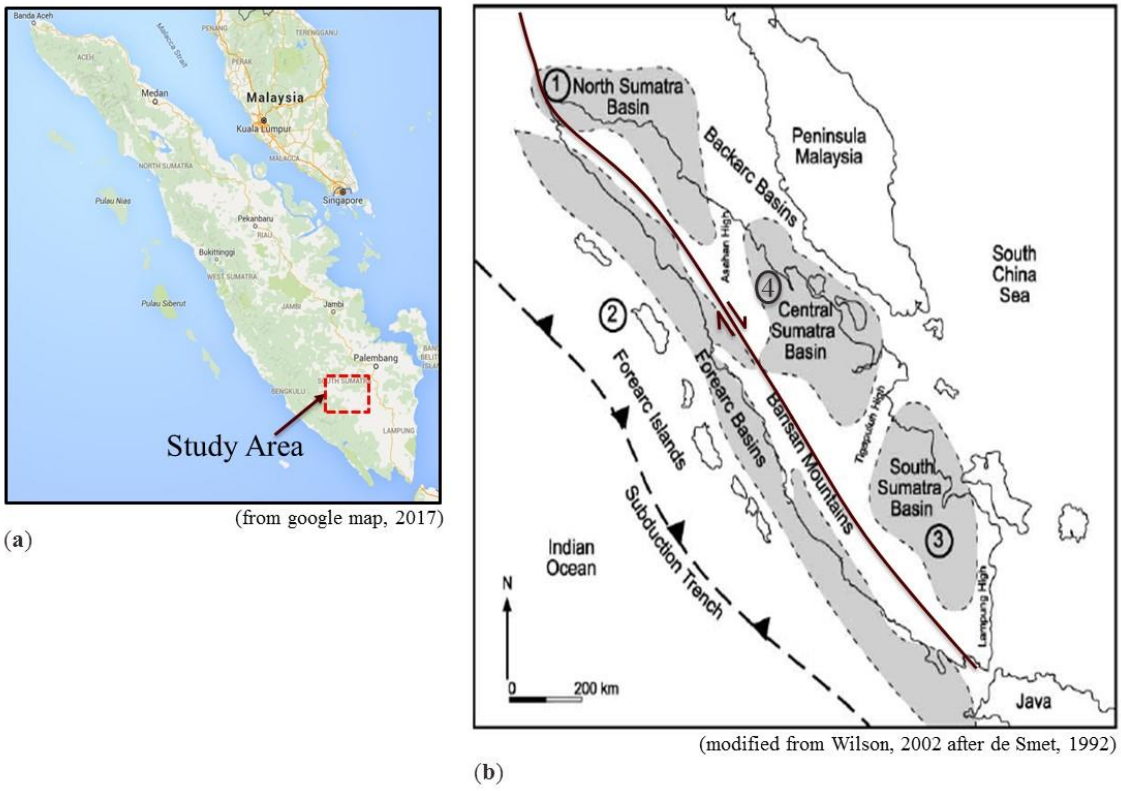

Figure 4.1. (a) Location of Pagardewa Field, South Sumatra, Indonesia. (b) Major tectono-stratigraphy features of Sumatra during the Tertiary: (1) North Sumatra Basin, (2) Forearc Basin, (3) South Sumatra Basin and (4) Central Sumatra Basin (modified from Wilson, 2002 after de Smet, 1992)

Tectonically, north-directed subduction of Indian oceanic crust has exerted a major influence on island arc and basin evolution, and contributed to an active major strike-slip system. The formation of the Barisan Mountains resulted from Paleogene-Neogene volcanism associated with the oblique subduction. The dominant tectonic forces led to the formation of three basins in the backarc and one basin in the forearc island during the

Paleogene (**Figure 4.1**). Horst and graben development during the late Eocene and Oligocene in backarc areas has been mostly infilled by lacustrine and fluvial sediment (Wilson, 2002). Consequent Oligo-Miocene subsidence resulted in thick terrestrial deposits that are overlain by marine lithologies. During the early to middle Miocene, carbonate was extensively deposited in the South Sumatra Basin. During the middle Miocene, uplift and erosion of the Barisan Mountains increased clastic sedimentation into the surrounding areas and led to a gradual expansion of the terrestrial environment (Wilson, 2002 after de Smet, 1992).

The formation of the Palembang sub-basin was controlled by geological processes that occurred over four tectonic periods (Pertamina, 2012g) (**Figure 4.2**). Basin development started in the middle Mesozoic when older rocks were folded and fractured in association with a granitic batholith intrusion. From the late Cretaceous until the late Paleogene, dextral strike slip motion along the Semangko fault created half grabens, controlling the sedimentation of Lahat Formation and Talang Akar Formation. Cenozoic rocks of the Palembang basin were deposited during two large-scale cycles, a lower transgressive sequence and an upper regressive sequence (**Figure 4.2**). In the Miocene, transgressive sedimentation of the lower Miocene Talang Akar Formation was followed by the deposition of Baturaja Formation. Initiation of Baturaja carbonate production was diachronous and coincided with rising sea level in the early Miocene. The carbonates were partially drowned in some places, but at the same time in other places, under relatively shallow water, carbonates continued to accumulate. The deep-water shales of the Gumai Formation were subsequently deposited over the drowning platform, and this was

followed by uplift of basement rocks during the Middle Miocene. The Air Benakat Formation and Muara Enim Formation were deposited during regressive stages. In a final stage during the Plio–Pleistocene, compressional tectonic processes inverted the existing structure within the basin and led to the formation of several anticlines.

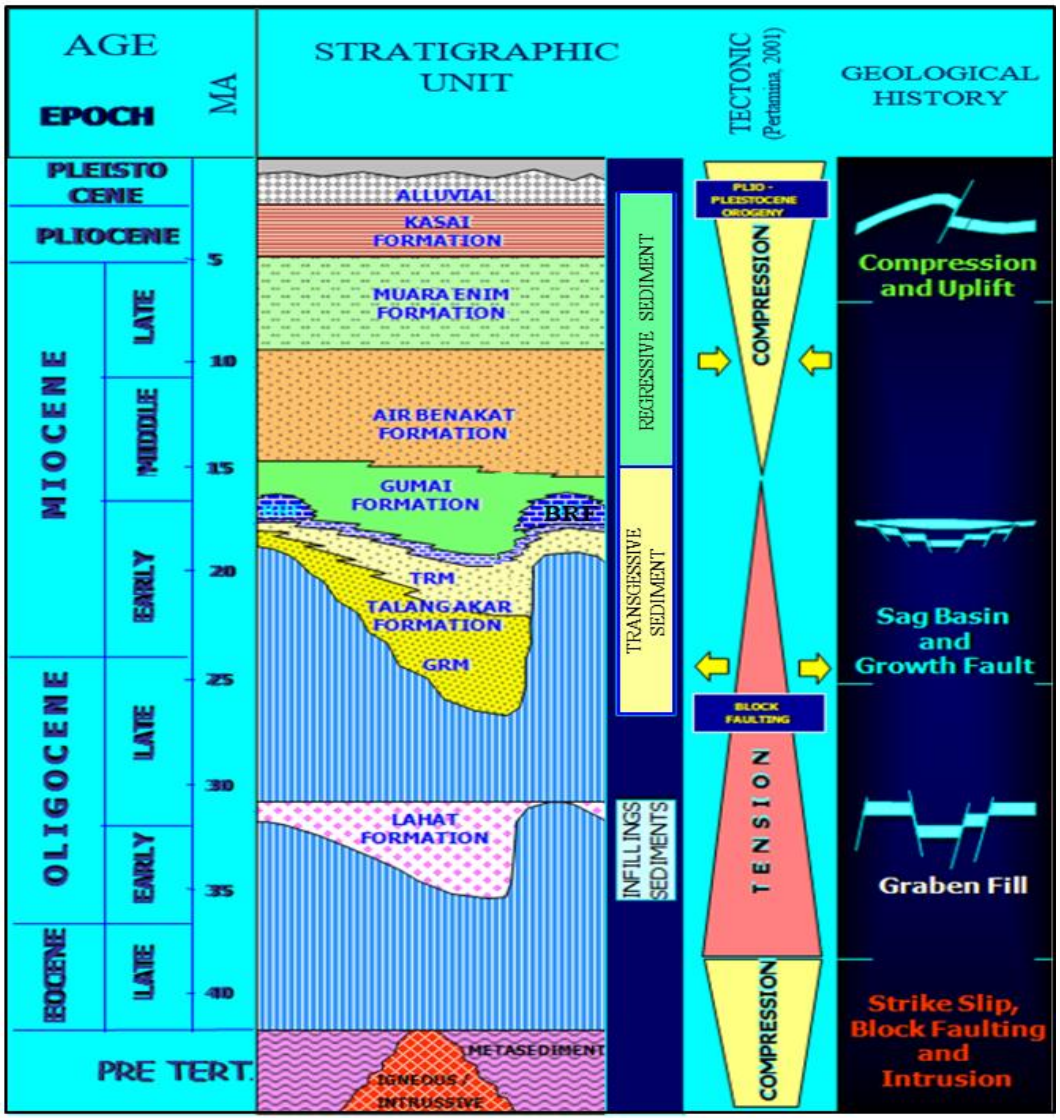

Figure 4.2. Regional stratigraphy of South Sumatra Basin (modified from Pertamina, 2012g). Noted BRF=Baturaja Formation.

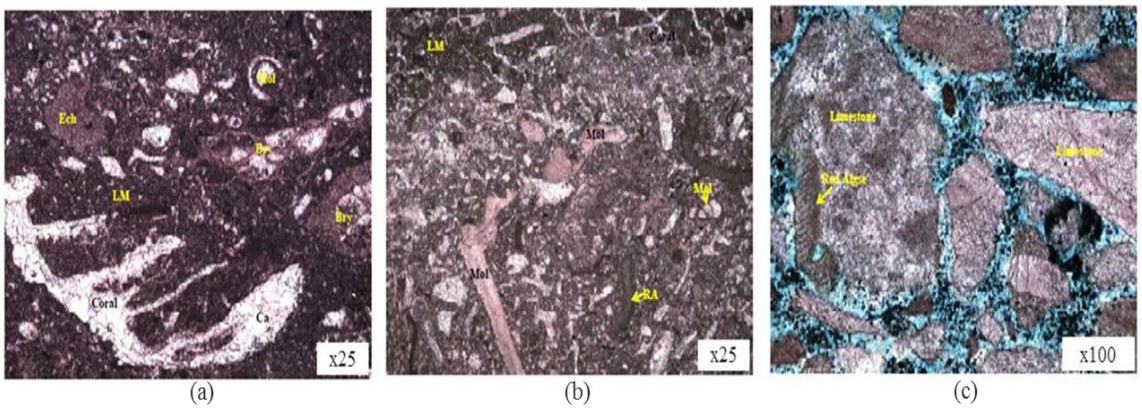

(a) (b) (c)

Figure 4.3. Petrographical descriptions from cores, sidewall cores and cutting samples. (a) Wackstone-Packstone from core sample of well C-4 at depth 1921.8 m, (b) Floatstone-Wackstone from sidewall cores sample of well C-5 at depth 1978 m and (c) Wackstone-Mudstone from cutting sample of well E-03 at depth 1480 m.

The Baturaja Fm. was deposited in the intermediate and shelfal portions of the South Sumatra Basin on or nearby platform highs (De Coster, 1974). Basuki and Pane (1976) reported that Air Kemiling Besar, an outcrop of the Baturaja Formation located 238 km SE of Pagardewa Field, consists of two massive units (upper and lower parts) that are separated by a finely-bedded unit of lime mudstones and lime wackstones intercalated with marls. In the finely-bedded unit, recrystallization and the presence of carbonaceous matter and glauconitic minerals are common. The massive units consist of mudstones, wackstones/packstones and boundstones with abundant large foraminifers in the upper part. Three dominant facies are interpreted from available cores, sidewall cores and cutting data (Pertamina, 2012d, g) in Pagardewa Field, respectively they are: wackstone-packstone; (ii) coral floatstone-wackstone; and (iii) wackstone-mudstone (**Figure 4.3**). However, the core intervals sampled only the top 10 m of the carbonate rock, and the sidewall cores sampled only at every 5-10 m spacing while the average thickness of

Baturaja Formation is 90 m. Thus, a description of the facies comprising the carbonate rock intervals at the wells is incomplete. However, a simplified two-facies interpretation based on grain sizes from cutting descriptions was made at the beginning of this research. This analysis shows that the carbonate rock interval is composed of ~75% mudstone and ~25% wackstone-packstone facies.

With reference to the Choquette and Pray (1970) classification scheme, the porosity of the Baturaja carbonates are dominated by open microfractures and micro-vugs with minor intraparticle, intracrystalline, intercrystalline, interparticle and mouldic void spaces (Geoservices, 2012a, b, c, d, e, f, 2013a, b). At Merbau Field, a gas field located 10 km west of Pagardewa Field, fractures are well developed in the Baturaja Formation (Wibowo et al., 2008). Yuliandri et al. (2011) stated fractures enhanced porosity in highly faulted area of Baturaja Formation at Pagardewa Field. However, the fractures are filled by calcite cement in many places at this field (Geoservices, 2012d, e, 2013a). Petrophysical analysis performed in this research show a strong relationship between porosity and permeability in the core data of several wells (e.g well E-3 and K-24). This is unusual in carbonate rock although it is common in siliciclastic rock (see Chapter II). The available petrographic reports show higher amount of siliciclastic input in the form of detrital quartz and clay minerals (mainly kaolinite) in those wells that exhibit the unusual porosity–permeability core relationship.

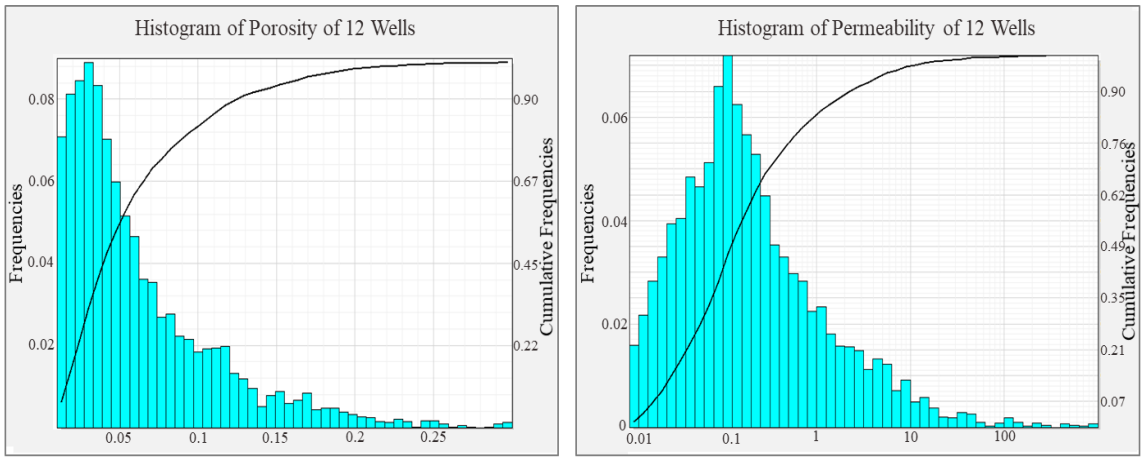

Figure 4.4. (a) Histogram of porosity from 12 wells. (b) Histogram of permeability from 12 wells. Based on the cumulative distributions (solid lines overlying the Histograms), more than 50 % of the porosity in Baturaja Formation are below 5% and permeability are below 0.1 mD. Noted solid black line is cumulative frequencies.

Figure 4.4 shows histograms of porosity and permeability in Baturaja Formation from 12 wells. The porosity and permeability estimates were discussed in Chapter II. Based on the cumulative probability distributions, as shown by the solid lines in the figure, more than 50% of the porosity estimates are below 5% and a similar number of the permeability estimates are below 0.1 mD. The Baturaja carbonates are therefore relatively tight with low porosity and permeability. Since hydrocarbons in the prospective intervals of these types of formations do not naturally flow at economic rates, the intervals have been acid-fractured to raise the permeability. Cander (2012) discriminated between unconventional and conventional reservoirs based on a crossplot of viscosity versus permeability. Pressure volume temperature (PVT) analysis of four gas samples from four wells (e.g C-4, E-6, K-22 and L-1) are plotted in Cander's graph. Their location on the crossplot suggests that Baturaja Formation is a tight gas carbonate rock and classified as an unconventional reservoir (**Figure 4.5**). Overall, the reservoir properties, such as

permeability and viscosity, and the treatment history involving acid fracturing suggest that the Baturaja Formation should be regarded as an "unconventional reservoir".

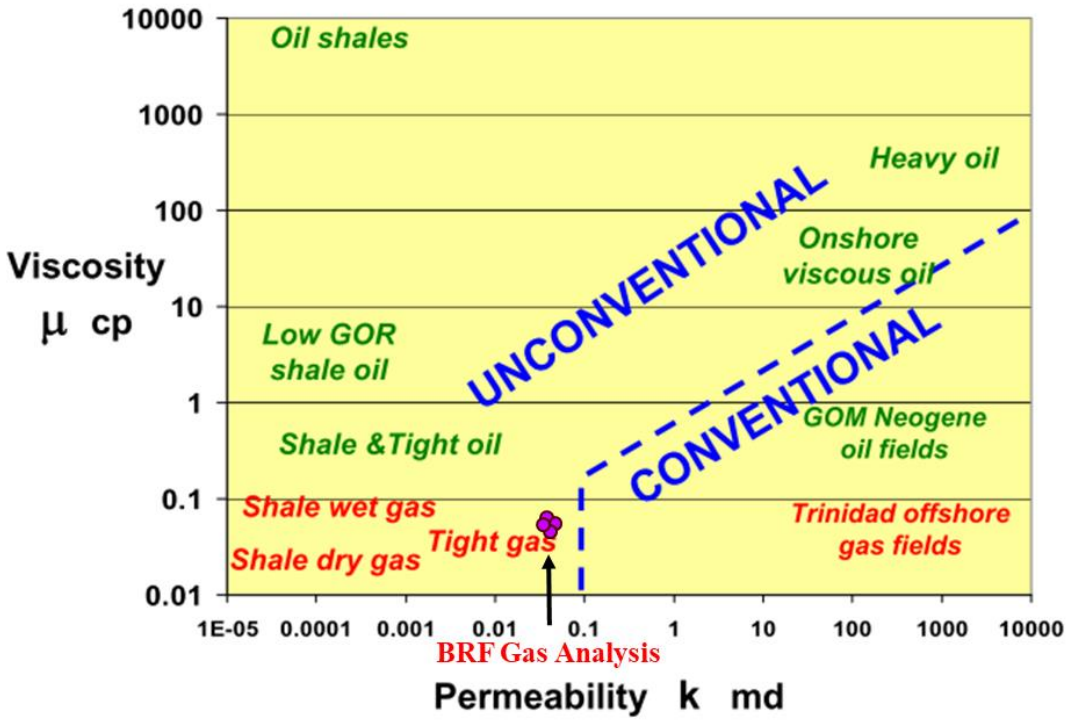

Figure 4.5. Classification of hydrocarbon-bearing reservoirs as "conventional" or "unconventional" based on a cross-plot of viscosity μ vs permeability k, as defined by Cander (2012). The Baturaja Formation (BRF) samples (purple dots) indicate that they are associated with tight gas unconventional reservoirs.

4.4 Methodology

4.4.1 Amplitude Variation with Offset (AVO)

A seismic P-wave incident at an angle $\theta_1 > 0$ is converted into reflected and transmitted P- and S-waves at the boundary between two elastic layers (**Figure 4.6**). Zoeppritz (1919) derived an equation to compute the reflected R and transmitted T amplitudes of the mode-converted waves based on conservation of stress and displacement

across the layer boundary. The Zoeppritz equation is complicated and difficult to use in practice, therefore a number of authors have made linearized approximations to the equation (see Appendix).

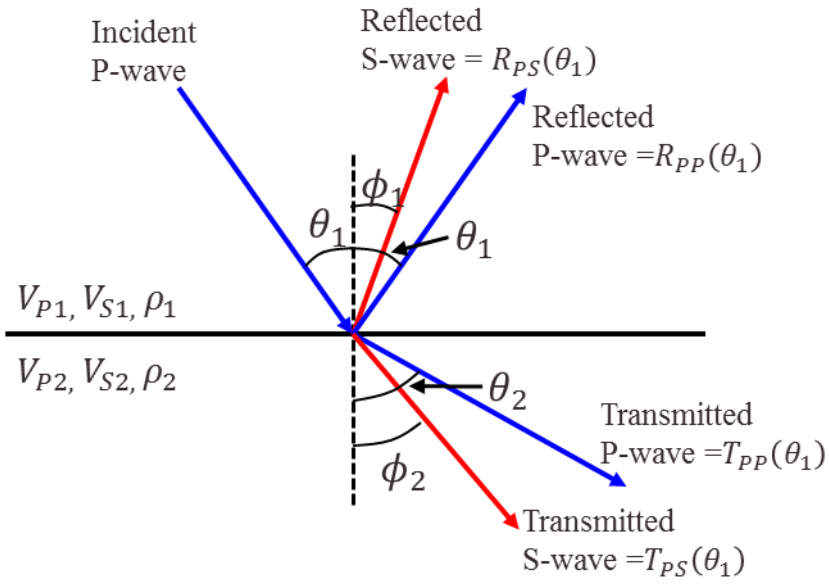

Figure 4.6. An incident seismic P-wave converted into reflected and transmitted P- and S-waves at the interface between two elastic layers (reprinted from Russell, 2014).

This research utilizes the Zoeppritz approximation developed by Fatti et al. (1994), following Smith and Gidlow (1987) and Gidlow et al. (1993). The approximation for the P-P reflection coefficient $R_{PP}(\theta_1)$ consists of a linearized combination of three terms (Aki and Richards, 2002; Bortfeld, 1961; Richards and Frasier, 1976):

$$R_{PP}(\theta_1) = aR_{AI} + bR_{SI} + c'R_D \qquad (4\text{-}1)$$

where the a and b cofficients are those used in the Aki-Richard approximation, but $c' = 4\bar{k}_{\text{sat}}\sin^2\theta - \tan^2\theta$. As explained in the Appendix, the angle θ is the average of the

incident and refracted angles at the layer boundary. The reflectivities associated with the P-impedance and S-impedance are given respectively by:

$$R_{AI} = \frac{1}{2}\left(\frac{\Delta V_P}{\bar{V}_P} + \frac{\Delta \rho}{\bar{\rho}}\right) \equiv R_{VP} + R_D \tag{4-2}$$

$$R_{SI} = \frac{1}{2}\left(\frac{\Delta V_S}{\bar{V}_S} + \frac{\Delta \rho}{\bar{\rho}}\right) \equiv R_{VS} + R_D \tag{4-3}$$

where all terms in these equations are defined in the Appendix.

For incident angles $\theta_1 < 30^0$, the intercept-gradient-curvature (Wiggins et al., 1983) and the Fatti et al. (1994) equations both provide good approximations to solutions of the Zoeppritz equation. However, the Fatti et al. (1994) approximation does better for $\theta_1 > 30^0$ (Russell, 2014). This research utilizes the Fatti et al. (1994) approximation to perform AVO inversion because we consider our CDP gathers over a wide range of incident angles $0 < \theta_1 < 42^0$.

4.4.2 Seismic Data Pre-Conditioning

The input seismic dataset is a pre-stack migrated CDP gather provided by industry. Since the seismic gather is not NMO-corrected, an NMO process is required to flatten reflection events using an appropriate velocity. Optimal results from AVO inversion are produced using wideband seismic data that are rich in frequencies (both high and low), relatively noise free (with high SNR), of consistent amplitudes, and whose reflections events are temporally aligned at far offsets. The industry-provided seismic data do not meet those requirements, so a pre-conditioning workflow is required. The goal of the pre-conditioning is to improve the quality of the pre-stack gather; especially, to maintain the

information contained at large offsets. Careful attention to seismic data pre-conditioning has been shown in many studies to improve reservoir characterization and interpretation (Schmidt et al., 2013; Veeken and Da Silva, 2004). Such improvement can be achieved even if the original seismic dataset lacks high frequency content (Saeed et al., 2014). Three specific aspects of the dataset are improved by our seismic data pre-conditioning workflow: 1) SNR; 2) offset-dependent frequency loss; 3) gather alignment at far offsets. Details of the workflow are given in the Appendix.

4.4.3 AVO Inversion

The seismic-based carbonate quality classification scheme utilizes the integrated Lamé parameters that are derived by AVO seismic inversion. The workflow of the seismic AVO inversion is shown in **Figure 4.7**. The main inputs are the 3D pre-conditioned pre-stack seismic gather and the available well data that includes density (RHOB), sonic P-wave (DT) and sonic S-wave (DTS) logs. The first step of the AVO inversion process is to convert the offset gather into an angle gather. This is done using the RMS velocity provided with the original seismic dataset. Seismic data are always bandlimited, since they can be regarded to first order as a convolution of a bandlimited wavelet with a reflectivity profile. The migrated gather provided by industry has frequency content in the range defined by FWHM of the amplitude spectrum, 10-25 Hz, or in the range defined by FWQM of the amplitude spectrum, 8-35 Hz. The dominant frequency is 20 Hz. Bandlimited zero-offset P and S reflectivities (R_{AI} and R_{SI}) are extracted from the angle gather using the Fatti equation. Once the reflectivities are extracted, the Lamé parameters

can be obtained, as will be described below. The Lame parameters are then used in the reservoir quality classification scheme.

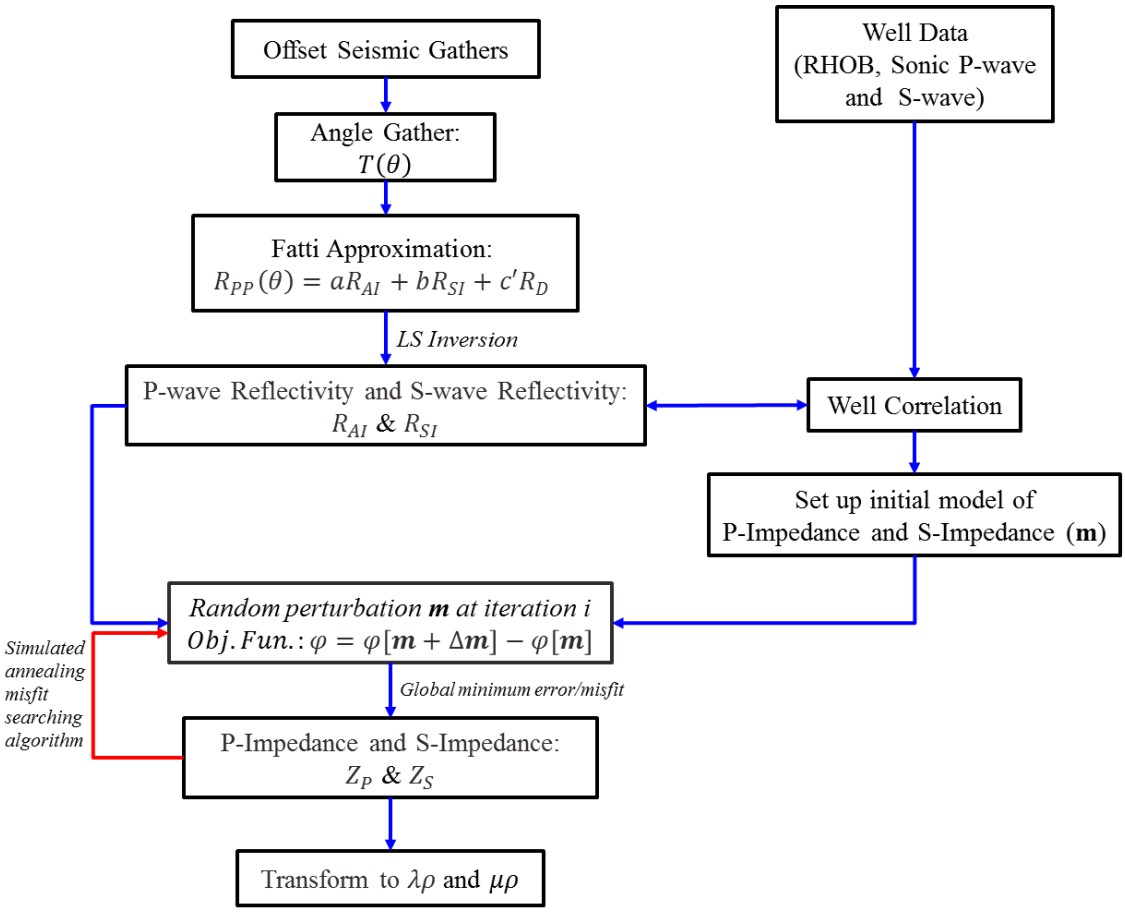

Figure 4.7. The AVO inversion workflow for the seismic-based carbonate quality classification.

The forward problem for extracting the reflectivities R_{AI}, R_{SI} and R_D from a seismic-trace angle gather can be written as the matrix equation (Russell, 2014):

$$\begin{bmatrix} R_{PP}(t,\theta_1) \\ R_{PP}(t,\theta_2) \\ \vdots \\ R_{PP}(t,\theta_N) \end{bmatrix} = \begin{bmatrix} a_1 & b_1 & c_1 \\ a_2 & b_2 & c_2 \\ \vdots & \vdots & \vdots \\ a_N & b_N & c_N \end{bmatrix} \begin{bmatrix} R_{AI} \\ R_{SI} \\ R_D \end{bmatrix} \tag{4-4}$$

where $R_{PP}(t,\theta_i)$ is the atomatically picked seismic amplitude at time t and incident angle θ_i, for $i = 1,2,\ldots,N$. The seismic amplitudes are automatically picked in every seismic sampling rate 2 ms. The corresponding quantities (a_i, b_i, c_i) are the coefficients of the Fatti equation. The unknown reflectivity terms R_{AI}, R_{SI} and R_D at the right side can be found using a standard least-square inversion approach. Rewriting matrix equation (4-4) in the general form $\mathbf{d} = \mathrm{G}\mathbf{m}$, the damped least-squares solution is

$$\mathbf{m} = (\mathrm{G}^T\mathrm{G} + \sigma\mathbf{I})^{-1}\mathrm{G}^{\mathrm{T}}\mathbf{d} \tag{4-5}$$

where

$$\mathbf{d} = \begin{bmatrix} R_{PP}(t,\theta_1) \\ R_{PP}(t,\theta_2) \\ \vdots \\ R_{PP}(t,\theta_N) \end{bmatrix};\ \mathrm{G} = \begin{bmatrix} a_1 & b_1 & c_1 \\ a_2 & b_2 & c_2 \\ \vdots & \vdots & \vdots \\ a_N & b_N & c_N \end{bmatrix};\ \mathbf{m} = \begin{bmatrix} R_{AI} \\ R_{SI} \\ R_D \end{bmatrix} \tag{4-6}$$

with I the $N \times N$ identity matrix, while σ is a pre-whitening or damping factor which is introduced to stabilize the matrix inversion in equation (4-5).

Since seismic traces are generally bandlimited, only impedances within the seismic bandwith can be faithfully recovered. The low frequency can be provided by well logs, which record signals of higher bandwidth than seismic. The low-frequency initial models of P-impedance AI and S-impedance SI were created from the available well logs by point-wise multiplication of the readings of the density and velocity logs. The well-log data are converted into the time-domain using a depth-time-conversion derived from the sonic log. A low-pass filter is applied to smooth the initial well-derived models for consistency with the bandlimited seismic data.

The initial model **m** is iteratively perturbed until the objective function, which measures the difference between synthetic and observed seismic traces, reaches a small user-defined threshold (Veeken and Da Silva, 2004). At each iterative step, the reflectivity P-Impedance R_{AI} is generated from the current P-Impedance AI contrast, likewise while the reflectivity S-Impedance R_{SI}. The synthetic seismic traces, in turn, are generated by convolution of the current reflectivity with the seismic wavelet. The latter is presumed to be a Ricker wavelet with dominant frequency 20 Hz and phase rotation 270^0 that was used for performing well-to-seismic correlations in Chapter II.

The minimum misfit between synthetic and observed traces is sought using a simulated annealing algorithm. As explained in Everett (2013), in each iteration, the search algorithm is started with a random perturbation $\Delta\boldsymbol{m}$ to the current model $\boldsymbol{m}$, then the objective function $\Delta\varphi = \varphi[\boldsymbol{m} + \Delta\boldsymbol{m}] - \varphi[\boldsymbol{m}]$ is evaluated. If $\Delta\varphi \leq 0$, the current model is accepted as a new model. If $\Delta\varphi > 0$ the current model may still be accepted with a small probability:

$$P(\Delta\varphi[\boldsymbol{m}]) \sim exp\left(-\frac{\Delta\varphi[\boldsymbol{m}]}{T}\right) \tag{4-7}$$

where T is an adjustable parameter termed the annealing temperature. T is initially set to a high value (infinity), and then it is decreased at each step following some annealing schedule, which may be specified by the user, but must end with T=0. This step is repeated a large number times until a global optimum in where small difference between synthetic and observed seismic traces is obtained, in which case the best estimate, or "final model"

is obtained. The P-impedance and S-impedance are then derived from the reflectivity R_P of the final model:

$$R_{Pj} = \frac{P_{j+1} - P_j}{P_{j+1} + P_j} \tag{4-8}$$

where R_{Pj} is final reflectivity at *j*-th layer, P_j is either acoustic (Z_P) or shear impedance (Z_S) at the *j*-th layer, P_{j+1} is the impedance at the *j*+1-st layer. Previous work has shown that this type of inversion scheme gives acceptable results even for limited well control and relatively poor-quality seismic data (Veeken and Da Silva, 2004).

Goodway et al. (1997) introduced the Lamé parameters (λ, μ) for improving fluid detection and lithology discrimination. The Lamé parameters are derived from the P- and S-impedances using the formulas:

$$\lambda\rho = Z_P^2 - 2Z_S^2 \tag{4-9}$$

$$\mu\rho = Z_s^2 \tag{4-10}$$

The first Lame parameter λ, termed the incompressibility, is sensitive to the elastic properties of the pore fluid while the second Lame parameter μ is sensitive to those of the rock matrix. It proves difficult (e.g. Goodway et al., 1997) to extract separately λ and μ from seismic data, especially from incident angles $<45^0$. A more robust parameterization is in the form of the products $\lambda\rho$, or "Lambda-Rho" and $\mu\rho$, or "Mu-Rho", both of which have SI units of [Pa·kg/m^3].

4.5 Results

4.5.1 Pre-Conditioned Seismic Data

An arbitrary 2-D slice from the 3-D seismic gather that passes through all well locations is selected to be the pilot dataset for testing the pre-conditioning workflow. This is done to find suitable parameters to use in the data processing workflow, after which these parameters are applied to the full seismic dataset. **Figure 4.8** shows the improvement of the stacked seismic gather before and after pre-conditioning. Note that improved spatial resolution and reflector continuity are achieved after the pre-conditioning workflow is applied. The pre-conditioned data reveal, for example, that onlap characteristics of reflector events (i.e. sedimentary layering) terminate into the horizon interpreted as the upper carbonate platform of Baturaja Formation (red arrows, **Figure 4.8**a). The pre-conditioned data are able to resolve the onlapping layer that was barely evident in the original data. In **Figure 4.8**b (green arrow), the pre-conditioned data better resolve the reflector continuity that can be barely recognized in the original data. The improved continuity of the reflectors in the pre-conditioned data improves the ability and confidence of the interpreter to map the lithology throughout the study area.

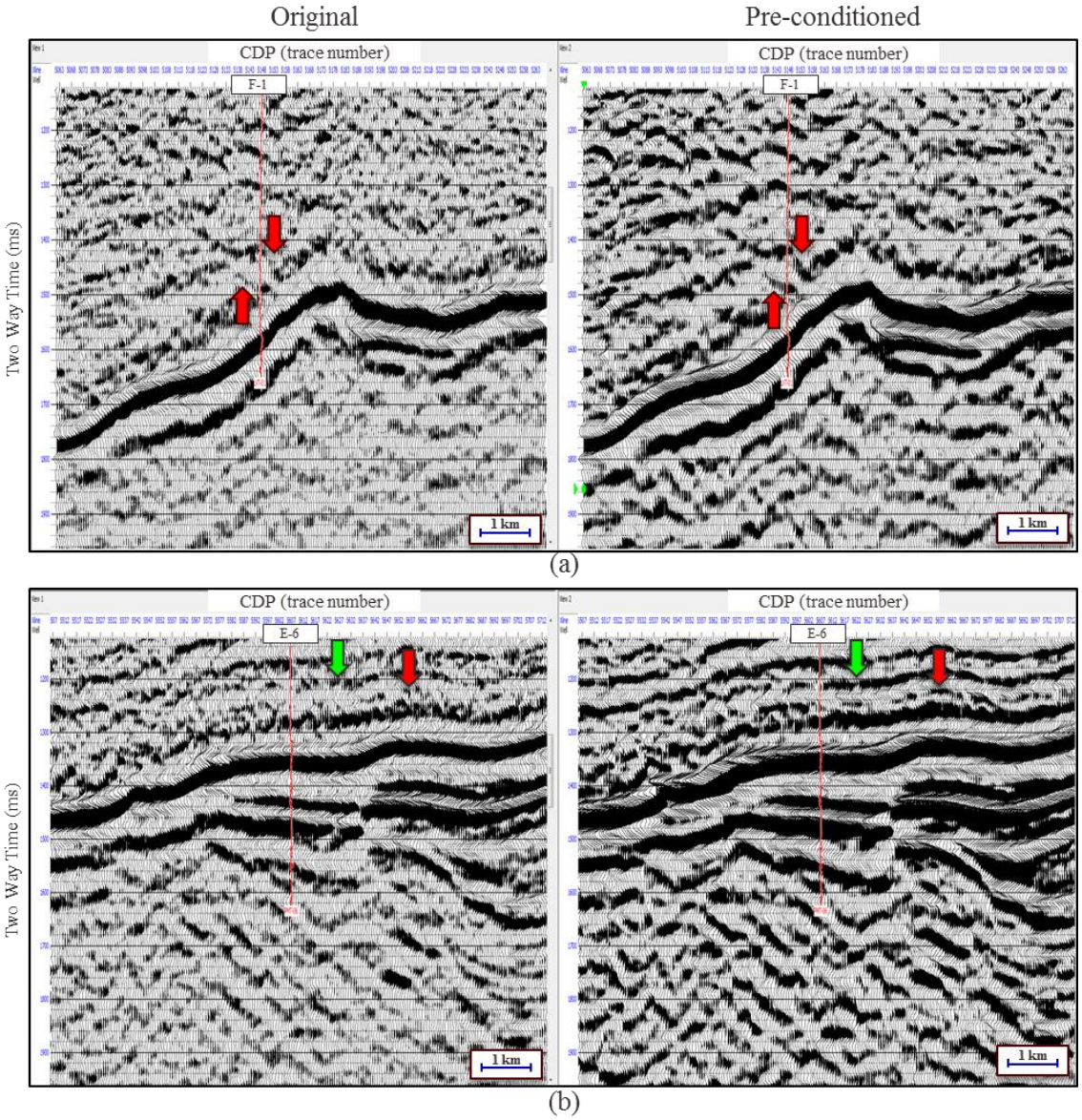

Figure 4.8. Displays of (left panel) original seismic data and (right panel) pre-conditioned seismic data for vertical section passing through the location of: (a) well F-1; (b) well E-6. Note the improvement in resolution (red arrows) and continuity of reflection events (green arrows).

Seismic amplitudes are enhanced in the preconditioned data because signals from far offsets are kept throughout the processing flow. A parabolic radon transform (Yilmaz, 2001) was used to remove multiples and random noise, after which the far offset data were

"flattened" by a trim static procedure (Hampson-Russell, 2011). During the stacking process, the flattened primary reflector event is reinforced, due to its high coherence, while multiples and noise are attenuated due to their low coherence. Eventually, the result is a higher SNR dataset, compared to the original data, characterized by spatially continuous reflectors. Unfortunately, within the carbonate interval, the spectral content of the pre-conditioned data remains similar to that of the original data. The processing flow does not enhance the frequency content of the original data. Both datasets have the same dominant frequency, namely 20 Hz. To extract higher frequencies that are embedded in the original data, a frequency enhancement technique should be inserted into the pre-conditioning processing workflow. Examples of such a technique include Gabor deconvolution (Margrave et al., 2011), spectral balancing (Nagarajappa and Downton, 2009), or an automatic non-hyperbolic velocity analysis and matching pursuit NMO algorithm (Zhang et al. (2014).

4.5.2 AVO Inversion of Lambda-Mu-Rho Analysis

An initial model that consist of low frequency model of P-wave impedance for Baturaja Formation was generated by multiplying the borehole-recorded P-wave velocity and density log readings at the well locations, applying a low-pass filter, and then interpolating and extrapolating the impedance into regions where wells are not present. The initial model serves as the starting point of the iterative optimization search for the best-fitting model. The low-pass filter I used has an amplitude spectrum that is flat below 10 Hz and ramps off on the interval 10-15 Hz. To reduce the computation time, the framework of our initial model is built from "macro-layers" that consist of horizons such

as the upper boundary (200 ms above Top Baturaja), the top of the Baturaja Formation, the bottom of the Baturaja Formation (coincident with the top of the Talang Akar Fm.) and the lower boundary (200 ms beneath the bottom of Batuaraja Formation). "Micro-layers" are automatically introduced into the macro-layers to provide the grid cells that store constant acoustic impedance (AI) values. The same technique is applied in the generation of low frequency model of S-wave impedance. **Figure 4.9** shows the initial models of P- and S-impedances. The Baturaja Formation has higher impedances of both types than does the overlying deep-water shale of Gumai Formation or the underlying fluvio-deltaic to paralic-marine sediments of Talang Akar Formation.

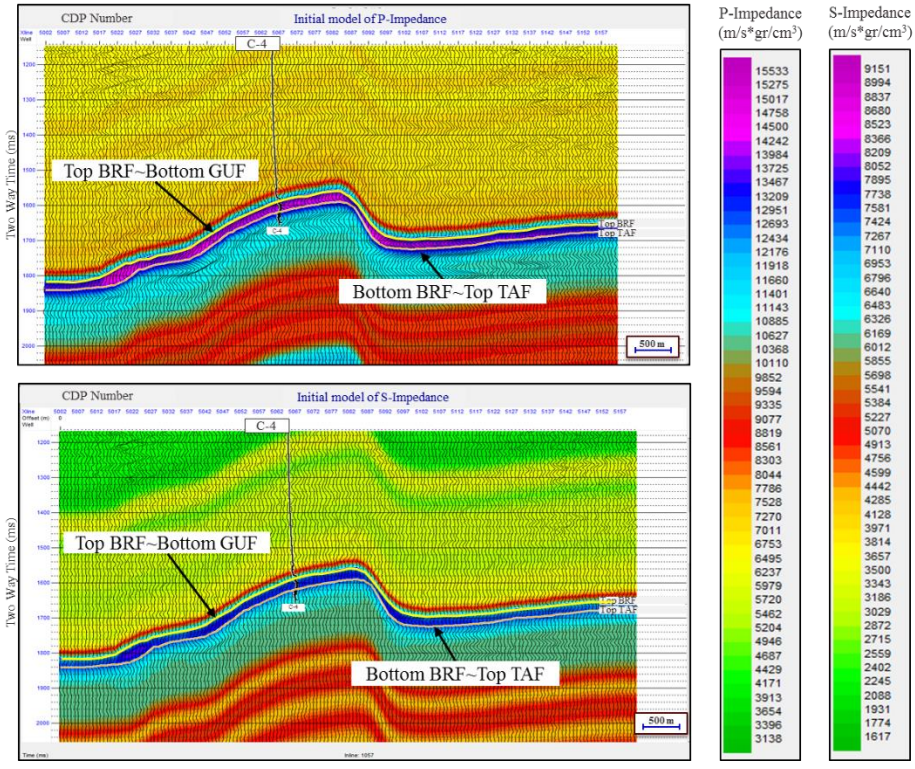

Figure 4.9. Vertical sections showing the initial model of (upper) P-Impedance and (lower) S-Impedance within a plane passing through well C-4. The Baturaja Formation has the highest P-Impedance (purple color) and S-Impedance (blue color). Note: GUF=Gumai Formation; BRF=Baturaja Formation; TAF=Talang Akar Formation.

The AVO inversion analysis was conducted by monitoring the cross-correlation between synthetic and observed seismic traces at the well locations. The analysis is conducted only at the well locations. The synthetic traces were generated by convolving the borehole-derived acoustic impedance profile with the selected seismic Ricker wavelet. In each iteration, the correlation error is measured, then each of the microlayers (at the well) is modified in thickness and amplitude in order to reduce the error. The observed seismic trace, which is either the one coincident with a well trajectory (for vertical wells), or the one closest to the well trajectory (for deviated wells), is cross-correlated against the generated synthetic trace. After a number of such iterations, the inversion result is the impedance profile that has the highest cross-correlation and the smallest error (**Figure 4.10** and **Figure 4.11**). As an example, the cross-correlation coefficient between the synthetic and observed seismic traces at well D-8 for P-wave impedance is 0.97 and the error is 0.25 (**Figure 4.10**). The cross-correlation coefficient and error at well C-5 for S-wave impedance is 0.98 and 0.19, respectively. **Figure 4.11** shows the cross-correlation coefficients at each of the wells for the P and S impedance analyses. The total cross-correlation between synthetic and observed seismic traces is 0.98 for P impedance and 0.95 for S impedance analysis. These values are considered to be good since they are close to the maximum value, 1. Note that the lowest cross-correlation value for the S impedance analysis is at well L-1. There is inaccurate trace sampling at this location due to the high inclination ($\sim 3^0$ to the vertical axis) of the well at the depth of the carbonate interval.

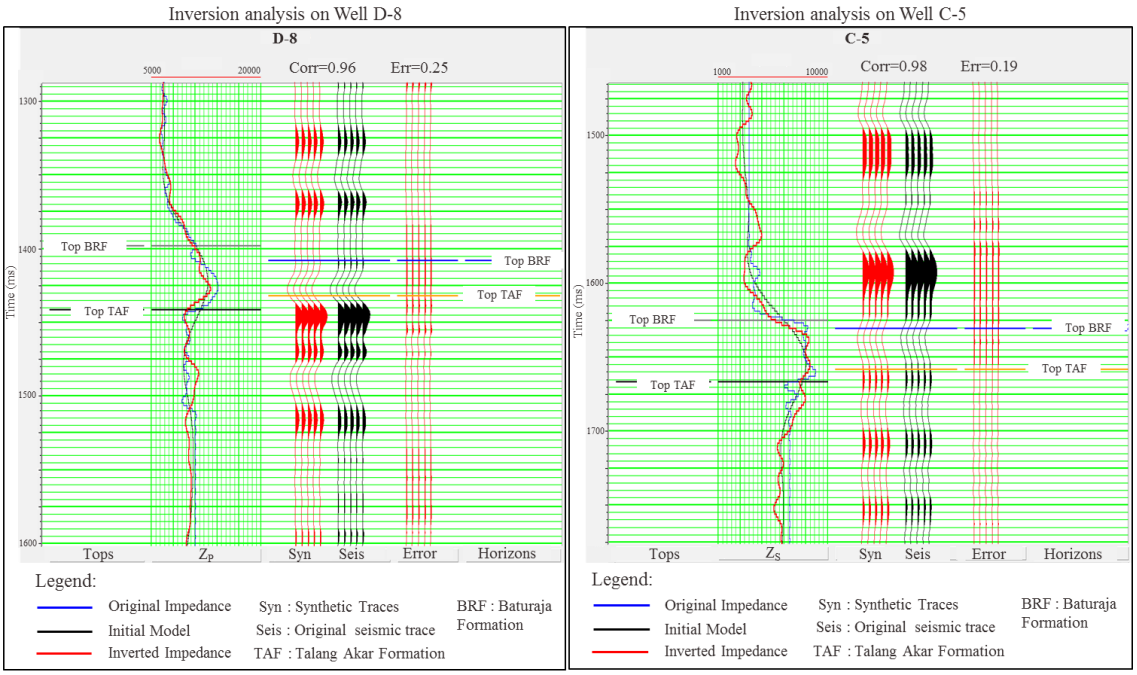

Figure 4.10. (Left) The inversion analysis for inverted P-impedance at well D-8. (Right) The inversion analysis for inverted S-impedance at well C-5. The final synthetic traces shows cross-correlation 0.96 and error 0.25 against the observed seismic trace at well D-8 and corresponding cross-correlation 0.97 and error 0.19 at well C-5.

The parameters that are used to produce the inverted impedance result at the well locations include the selected thickness of the micro-layers in the model, the amount of impedance change be allowed in the process, pre-whitening, and the maximum of iterations to get the optimum result. These parameters are applied over the entire 3D seismic volume. Applying the parameters and following the workflow in **Figure 4.7** results in inverted P-Impedance (Z_P) and inverted S-Impedance (Z_S) (**Figure 4.12**) distributed throughout the seismic volume. The carbonate platform shows lower gamma readings relative to the adjacent lithologies. This may be seen in both panels of **Figure 4.12** by the deflection to the left of the gamma ray curve at the top and its deflection to the right at the bottom of Baturaja Formation. The vertical section of inverted P-Impedance

value that passes through well D-6 shows that the carbonate rock has higher P-Impedance values than either the overlying deep-water shale of Gumai Fm. or the underlying fluvial to marine deposition of Talang Akar Fm. The inverted P-Impedance of the carbonate rock of Baturaja Fm. is ~11,200-15,000 (m/s*g/cm^3), as represented by the light blue to purple color in **Figure 4.12** (left panel). However, the inverted S-Impedance values of the Baturaja Fm. are intermediate between those of the Gumai Fm. (lower values) and Talang Akar Fm. (higher values). The inverted S-Impedance of the carbonate rock is ~5,500–7,900 (m/s*g/cm^3) as represented by light blue to purple color in **Figure 4.12** (right panel).

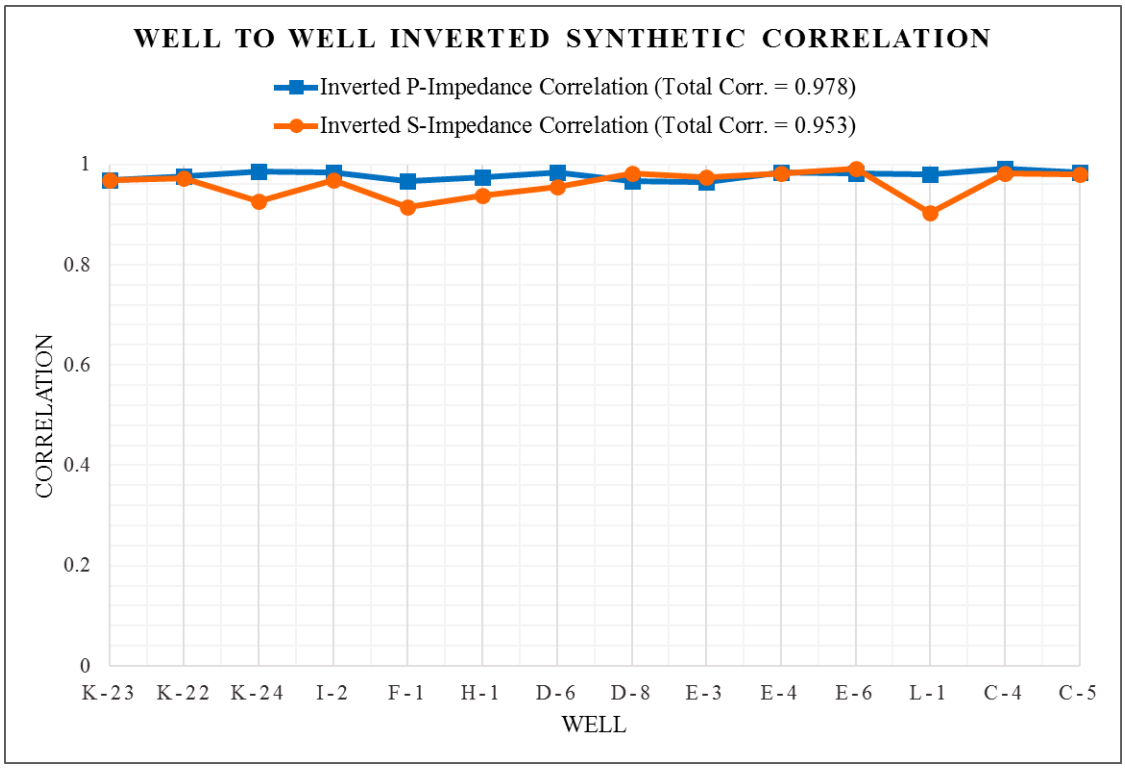

Figure 4.11. The well by well correlation of inverted synthetic and observed (original) seismic traces in P-Impedance inversion analysis and S-Impedance inversion analysis shows total correlation 0.98 and 0.95 respectively.

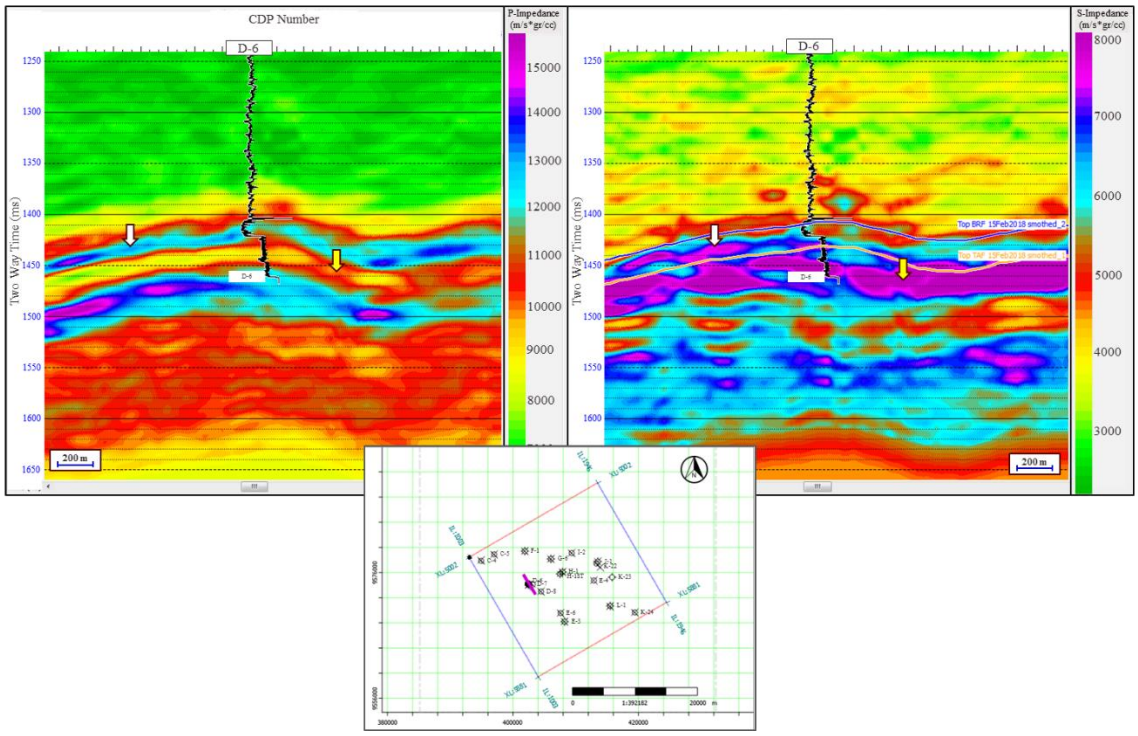

Figure 4.12. Vertical slices of (left panel) inverted P-Impedance and (right panel) inverted S-Impedance passing through the location of well D-6. The insert shows the locations of the vertical slices line on the basemap. Note the different values between inverted P-Impedance and inverted S-Impedance at same location represented by white arrow is caused by variations in fluid content, but at location represented by yellow arrow is caused by variation in lithology (yellow arrow).

4.6 Discussion

4.6.1 3D Carbonate Quality Class Distribution

Compressional P-wave velocity contains information on lithology and fluid content, while S-wave velocity only contains information on lithology (Veeken and Da Silva, 2004). Notice that the low P-Impedance value at Baturaja Fm. that is evident in the inverted P-Impedance vertical slice in **Figure 4.12** (shown by the white arrow) does not correspond to a low value in the S-Impedance vertical slice. This is because fluid content affects P-impedance but not S-impedance. It may be conjectured, on this basis, that this

location possibly contains hydrocarbon. The Talang Akar Fm. shows lower P-Impedance value than does the Baturaja Fm. (as shown by the yellow arrow). On the contrary, the Talang Akar Fm. exhibits higher S-Impedance value than the Baturaja Formation. This may be explained by the difference in lithological composition that compose the two formations. Talang Akar Formation consists of fluvial to marine siliciclastic rock (sandstone, shale, coal), while Baturaja Formation consists mainly of carbonate rock. Porous and saturated sandstones lower the P-Impedance value in Talang Akar Formation; for example, just 5% saturation of gas in the rock can significantly lower the P-compressional velocity.

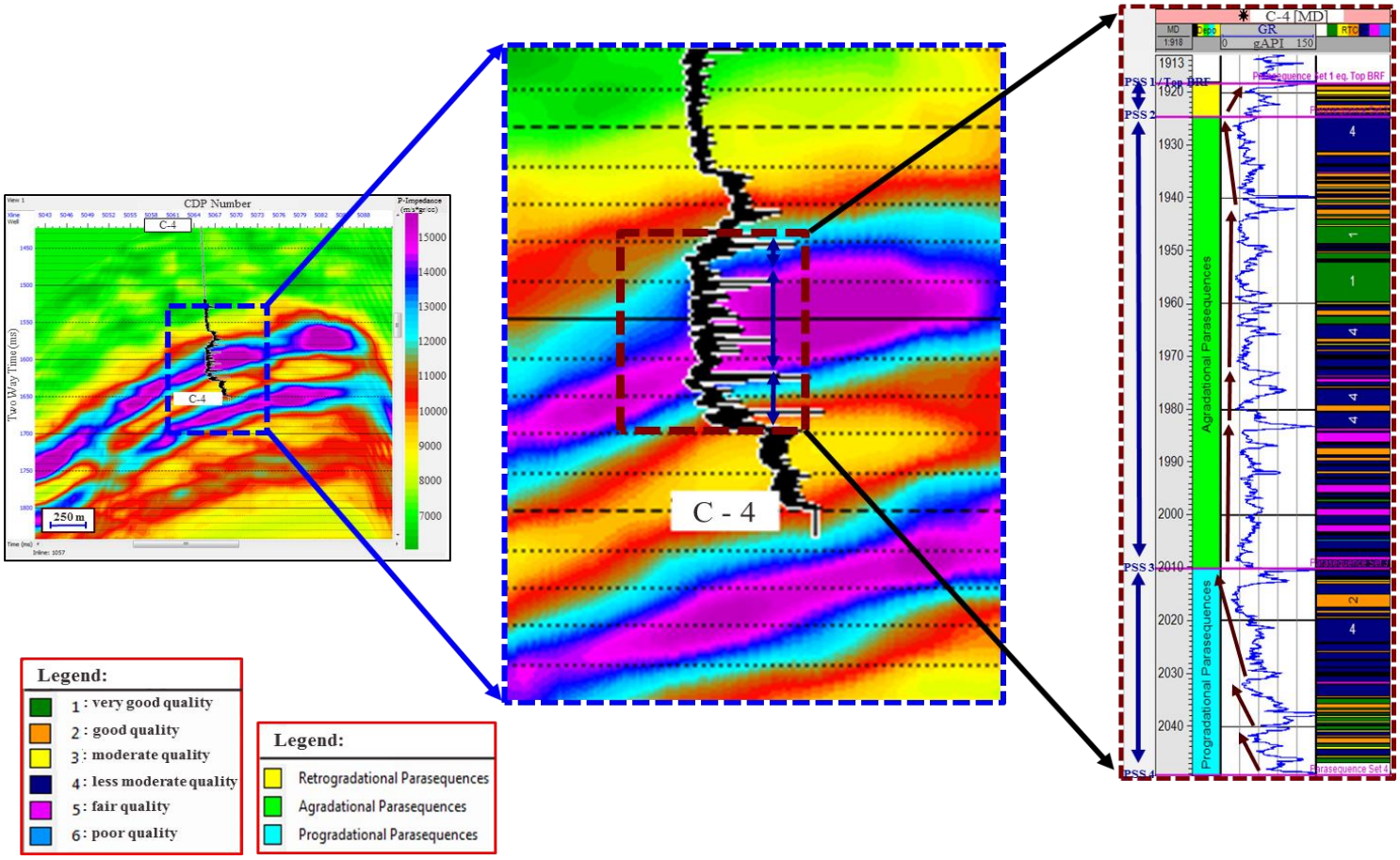

Figure 4.13. The relation of (left) inverted P-Impedance to (right) the Parasequences set zones of carbonate Baturaja Formation which were constructed in Chapter III. Lower P-Impedance value at progradational parasequences set zone, higher P-Impedance value at agradational parasequences set zones and lower P-Impedance value at retrogradational parasequences set zones.

The inverted P-Impedance profile is consistent with the evolution of Baturaja Formation as a carbonate ramp, as suggested earlier in this dissertation. Progradational zones are represented by low to moderate P-Impedance values 10,000–13,000 m/s*g/cm^3, aggradational zone by moderate to high values 13,000–15,400 m/s*g/cm^3, and retrogradational zone by moderate values 12,000–13,000 m/s*g/cm^3 (**Figure 4.13**). Higher P-Impedance values are associated with the aggradational zones because of the relatively low siliciclastic influence on the platform. Rather, in these zones the carbonate grew consistently vertical such that the aggradational zones become dominated by marine cementation that later evolve to meteoric and burial cement (see in Chapter II for the explanation and the evidence in **Figure 2.31**). At the initiation of carbonate growth in the progradational zones, siliciclastic frequently entered the carbonate platform. The total porosities in the progradational zones are therefore higher than those of the aggradational zones, lowering the P-Impedance of the former. At the time when drowning of the platform started, specifically within the retrogradational zone, shale and pelagic sediment are deposited onto the carbonate platform. This also contributes to increasing the porosities, lowering the P-Impedance in these areas.

It is difficult to characterize carbonate rock quality based only on P-Impedance and S-Impedance values. Since Baturaja Fm. is most appropriately classified as an unconventional reservoir, I suggest that the formations therein should be analyzed using unconventional geophysical procedures, for example based on Lamé parameters (Lambda and Mu) and brittleness related elastic moduli (Poisson's ratio and Young's modulus). **Figure 4.14** shows the Lambda-Rho and Mu-Rho profiles derived from the seismic AVO

inversion result. These are more easily analyzed if they are transformed into a cross-plot of integrated Lamé parameters and elastic moduli values. Taking this approach, in the previously chapter I developed a well-based template to discriminate the carbonate quality of Baturaja Fm. into six classes. That template was based on a cross-plot of Lame parameters overlain by contours of elastic moduli. A similar type of template is used here but the cross-plot is based on the seismic AVO inversion result, rather than on the well information. Similar to the well-based template classification, the seismic-based carbonate quality classes are determined from an interpretation of the trends on the cross-plots shown by parameters such as brittleness, porosity, TOC and mineral contents such as clay, quartz and dolomite. These parameters are commonly used to define the quality of an unconventional reservoir (Chopra et al., 2013; Jarvie, 2012; Rickman et al., 2008). These trends may be summarized as follows. As Poisson ratio $\upsilon \leq 0.30$, the degree of brittleness, and dolomite and quartz content increases, whereas the ductility and clay content increases as $\upsilon > 0.30$. Stiffness increases in the direction of increasing Young's modulus values, i.e. away from the origin of the crossplot. The seismic-based carbonate quality classification that results by consideration of these trends is shown in **Figure 4.15**.

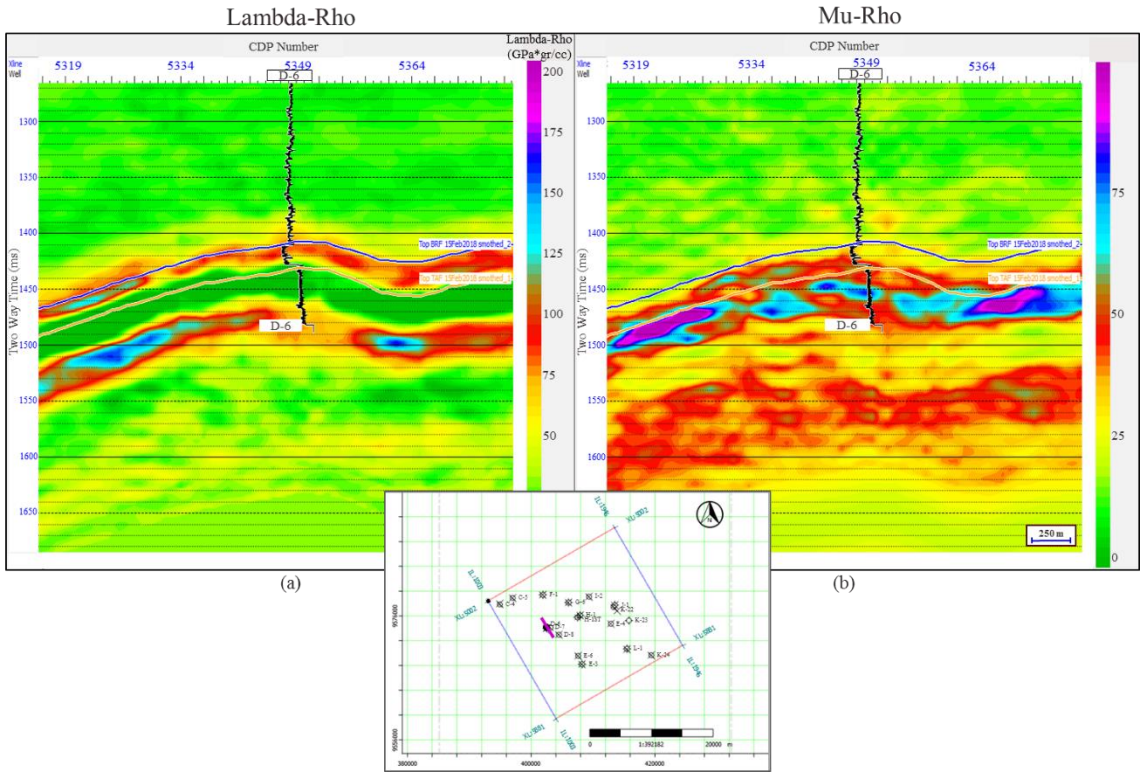

Figure 4.14. The generated (a) Lambda-Rho ($\lambda\rho$) and (b) Mu-Rho ($\mu\rho$) section pass through well D-6. The insert shows the locations of the vertical slices line on the basemap.

4.6.2 Validation of Well-based and Seismic-based Carbonate Quality Classification

The seismic-based carbonate quality template is designed to classify the carbonate reservoir quality of Baturaja Formation. However, the seismic-based template has lower discrimination power compared to the well-based template. For example, the well-based scheme distinguished four carbonate quality classes in Baturaja Formation at well D-6 along with characteristic of thin-layer sequences belonging to each class (**Figure 4.16**). However, at well D-6, the seismic-based scheme can resolve only three classes: 1, 3 and 6 (**Figure 4.15**). This result is expected due to the low spatial resolution of the input seismic data compared to that of the well logs. The pre-conditioning processing workflow

did not include a technique to increase the dominant frequency of the seismic data. Since the dominant seismic frequency is only 20 Hz, it is recommended that a seismic enhancement technique, e.g. Gabor deconvolution (Margrave et al., 2011), spectral balancing (Nagarajappa and Downton, 2009), or an automatic non-hyperbolic velocity analysis and matching pursuit NMO algorithm (Zhang et al., 2014), should be inserted into the pre-conditioning processing flow. This additional step would improve the spatial resolution of the seismic data within the carbonate interval and possibly allow more carbonate quality classes to be distinguished.

The seismic-based carbonate quality classification scheme subdivides the Baturaja carbonate interval into: (1) a poor quality class comprising the upper part; (2) a moderate quality class comprising the middle part; (3) a very good quality class comprising the lower part. At well D-6, the retrogradational parasequence set zone consists of very good quality carbonate. This zone hosts a promising reservoir, of highest porosity. However, without a good seal, this zone would not become a good hydrocarbon trap (**Figure 4.16**) since hydrocarbons can migrate or leak elsewhere. Prospective intervals in the aggradational parasequence set zone consist of very good to good quality carbonate. These intervals are located between moderate quality carbonates which, taken together, can form a good hydrocarbon trap. In this scenario, the good-quality carbonate comprises the reservoir whereas the moderate-quality carbonate provides the seal.

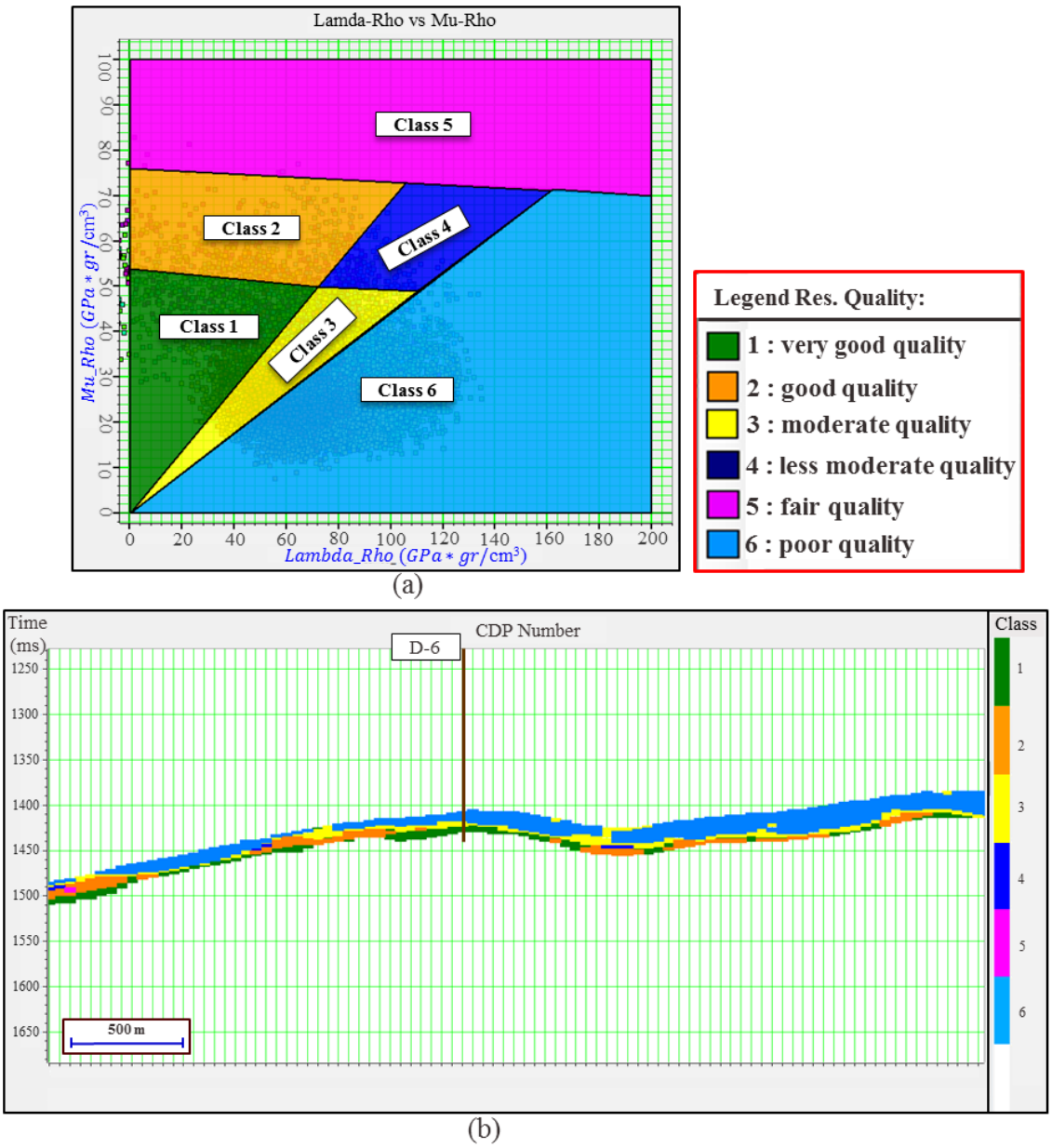

Figure 4.15. Seismic-based template for carbonate quality classification in Baturaja Formation. (a) The carbonate quality classification based on cross-plot of Lambda-Rho and Mu-Rho bounded by Poisson's ratio and Modulus Young isovalue. (b) The vertical slices of 3D carbonate rock quality derived from the cross-plot pass through well D-6. The cross-section line is plotted in the basemap on **Figure 4.12**.

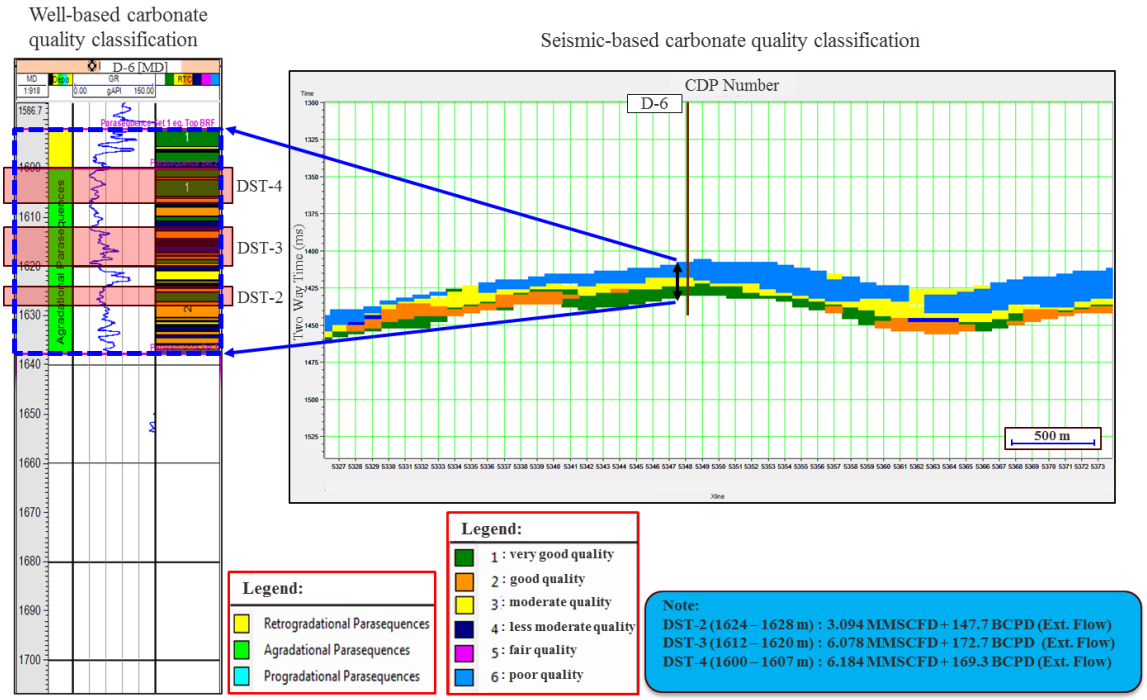

Figure 4.16. Well- versus seismic-based carbonate quality classification. Fewer carbonate quality classes are discriminated from seismic-based carbonate quality classification rather than well-based carbonate quality classification due to resolution of the seismic data. Note the DST tests results validated the interpreted prospective interval from the well-based and seismic-based carbonate quality classification.

Results from three drill stem tests (DST), which monitors hydrocarbon flow from the prospect interval after acidized fracturing, validated the interpretations from both the well-based and seismic-based classification. The DST results of gas and condensate flow from the prospect interval are consistent with the interpretation of a good hydrocarbon trap. The DST-4 test reported a flow of 6.184 Million Standard Cubic Feet Gas Per Day (MMSCFD) and 169.3 Barrel Condensate Per Day (BCPD) from interval 1600–1607 m in the upper part of the aggradational zone. DST-3 reported 6.078 MMSCFD (gas) + 172.7 BCPD (condensate) from interval 1612–1620 m in the middle part of the aggradational

zone. Finally, DST-2 reported 3.094 MMSCFD (gas) + 147.7 BCPD (condensate) from interval 1624–1628 m in the lower part of the aggradational zone. The highest gas flow rate at DST-4 interval came from a thick layer designated as class 1 (very good quality carbonate classes) located in between two layers of class 4 (less moderate quality carbonate class) that act as a seal. Multiple interval of very good and good layer of class 1 and 2 also gives high gas flow rate at DST-3 interval. Lower gas flow rate at DST-2 interval due to narrow DST interval that only penetrate thin layer of class 1.

Notwithstanding that fewer classes are discriminated by the seismic-based carbonate quality classification scheme, the results are consistent with the hydrocarbon flow test results. The interpreted prospective zone based on the vertical slices of the seismic-based carbonate quality classes in **Figure 4.16** are the middle part (moderate carbonate quality) and the lower part (very good carbonate quality) of Baturaja Formation. The 3D seismic-based carbonate quality distribution can thus be used as a guide to develop the Pagardewa Field by suggesting suitable locations of infilling wells.

4.7 Conclusions

The pre-conditioned seismic data workflow improved the spatial resolution and reflector continuity of the original dataset that was provided by industry. The workflow did not improve the frequency content of the original data so that the spectra of pre-conditioned and original data are similar, with dominant frequency at ~20 Hz. To recover higher frequencies from the original data, a frequency enhancement technique such as Gabor deconvolution, or spectral balancing, or an automatic non-hyperbolic velocity analysis and matching pursuit NMO algorithm is recommended to be included into the

pre-conditioning workflow; however, this is beyond the scope of the present work. The total cross-correlation between synthetic and observed seismic traces at the available well locations is 0.98 for P-Impedance and 0.95 for S-Impedance. The high value of the correlation coefficients in the inversion analysis provides confidence in the inversion results across the entire seismic volume.

The geologic evolution of the carbonate platform of Baturaja Formation proposed earlier in this dissertation is consistent with the P-Impedance inversion results. The higher P-Impedance at the aggradational zones is due to extensive cementation. At the progradational zones, higher porosities are caused by abundant siliciclastic input into the platform, lowering the P-Impedance. At retrogradational zones, considerable amounts of shale and pelagic sediment are deposited onto the carbonate platform when drowning of the platform occurs. This contributes to an increase in porosity concomitantly lowering the P-Impedance.

Fewer carbonate classes are discriminated in Baturaja Formation by the seismic-based carbonate quality template as opposed to the well-based template developed in the previous chapter. This is due to the inherently low dominant frequency of the input seismic data provided by industry. A frequency enhancement technique should be inserted into the pre-conditioning data processing flow to enhance the frequency and spatial resolution of the input seismic data within the carbonate interval. An example analysis at well D-6 shows the seismic-based carbonate quality classification partitioned the carbonate interval into a zone of poor reservoir quality at the upper part, one of moderate quality at the middle part and one of very good quality at the lower part. The hydrocarbon prospective zones

are thus suggested to be the middle and lower parts of the carbonate interval. This suggestion is validated by three successful gas and condensate drill stem flow tests from the interval. Despite our recommendation to enhance the quality of the input seismic data, the 3D seismic-based carbonate quality distribution developed herein remains a useful guide to determine suitable locations of infilling wells as part of the development strategy to increase the hydrocarbon production in Pagardewa Field. Ultimately, the methodology should increase the commercial production rates of the Baturaja Formation as unconventional reservoir.

CHAPTER V

CONCLUSIONS

Carbonate production at upper Baturaja carbonate platform is dominated by oligophotic gravel-producing biota such as larger foraminifers and red algae with subordinate contributions from aphotic biota such as mollusks, bryozoans and echinoids. Based on the dominant light-dependent biota distribution and the paleotopography of the carbonate platform at early Miocene, the suitable depositional environment of upper Baturaja Formation at Pagardewa Field is herein suggested to be a carbonate ramp. The carbonate ramp consists of two carbonate facies that are distinguished by their siliciclastic influence and have been identified based on seismic amplitude response and petrography information. Facies A consists mainly of carbonate constituents, whereas facies B contains higher amounts of non-carbonate constituents in the form of detrital quartz and clay minerals (kaolinite) in addition to its carbonate constituents. The siliciclastic influence is higher in the inner ramp rather than in the mid- and outer-ramps. This is indicated by higher gamma-ray and volumetric concentration of clay/shales in the inner ramp. The outer and mid ramp zones have moderate to high acoustic impedance values due to extensive cementation. To the contrary, the higher siliciclastic input in the inner ramp contributes to its lower acoustic impedance.

The spatial distribution of porosity throughout the field was predicted from the acoustic impedance distribution inverted from the industry-provided seismic dataset. The analysis shows that the inner ramp has the highest porosities (10–12%). These higher

values are due to the enhanced contribution of siliciclastic input. Lower porosities (6–10%) were found in the middle and outer ramp due to the higher degree of cementation. These areas are relatively unaffected by sea level variations. A new stratigraphic hydrocarbon trap was suggested from the carbonate platform analysis in the study area. It is suggested herein that stratigraphic plays are located near the lateral boundaries between the two carbonate facies A and B. The traps are proposed to have formed as a result of lateral contrasts in acoustic impedance and porosity.

The combination of Lamé parameters (more specifically, Lambda-Rho and Mu-Rho) and brittleness-related elastic moduli (Poisson's ratio and Young's modulus) explains the quality of Baturaja Formation in terms of parameters such as brittleness, porosity, TOC and mineral content including clay, quartz, calcite and dolomite content. Six carbonate reservoir quality classes have been discriminated from the well-based carbonate rock quality classification scheme. Higher carbonate reservoir quality dominates the inner ramp due the high siliciclastic input into the environment. Lower carbonate reservoir quality dominates the outer ramp due extensive cementation in this environment. Carbonate quality classes 1 and 3 are distributed predominantly in the retrogradational zone rather than in the aggradational and progradational zones due to its favorable porosity, TOC and clay content. The unconventional reservoir approach applied to the Baturaja Formation enables the recognition of unexploited potential prospective zones. The reservoir quality classes can be used to identify prospective intervals for acid fracturing treatment to maximize the hydrocarbon production in the existing wells. The prospective intervals suggested herein are characterized by three factors: 1) the interval

consists of very good to good quality rock (classes 1-2) located in between moderate to poor quality intervals (classes 3-6); 2) a crossover of the neutron-density log value indicative of the presence of gas, and; 3) the existence of a gap between invaded formation resistivity (low log reading value) and deeper resistivity (high log readings value).

The pre-conditioned seismic data processing workflow improved the resolution and reflector continuity of the original migrated seismic dataset that was provided by industry. The evolution of the Baturaja carbonate platform was well-described by the P-impedance inversion results. Higher P-impedance values within the aggradational zones are due to the abundance of cementation. Within the progradational zones, high porosities are due to the dominant influence of siliciclastic input into the platform, which serves to lower the P-impedance. Within retrogradational zones, at the time when drowning of the platform occurs, abundant shale and pelagic sediment were deposited onto the carbonate platform. This fine-grained deposition contributes to an increase in porosity and concomitant lowering of the P-impedance.

Fewer carbonate quality classes were discriminated within the Baturaja Formation using the seismic-based carbonate-quality template, as opposed to the well-based template. This is due to the inherently low dominant frequency, and hence lower vertical resolution, of the input seismic dataset. It is suggested to incorporate a frequency enhancement technique into the pre-conditioning seismic data processing workflow. This would increase the high-frequency content and concomitantly increase the resolution of the seismic data within the carbonate interval. At well D-6, the seismic-based carbonate quality classification is able to identify prospective intervals in the middle and lower parts

of the Baturaja carbonate reservoir. The identified intervals are consistent with results from three successful drill-stem gas and condensate flow tests conducted in 2010. Despite the recommendation that the frequency content of the input seismic data should be enhanced, the resulting 3D seismic-based carbonate quality distribution developed herein can still be used as a guide to decide upon appropriate locations of infilling wells for the purpose of further developing the Pagardewa Field.

By changing the approach to the Baturaja Formation from that appropriate for a "conventional reservoir" to that appropriate for an "unconventional reservoir", the resulting modified technique leads to suggestions, with improved confidence, of prospective zones within Baturaja Formation. These suggestions hopefully can be used in strategies to increase the hydrocarbon production from the Baturaja Formation, which eventually will impact the economic value of Pagardewa Field.

The methods described in this research can be used on carbonate reservoirs worldwide that fall into the unconventional category to find unexploited prospective intervals zone within existing oil fields, that were previously studied as conventional reservoirs. The work is important to the overall field of petroleum geology and reservoir characterization given the lack of new discoveries of conventional hydrocarbon resources along with ever-increasing global demand for energy. The analysis is sufficiently general that it could be applied to similar unconventional carbonate reservoirs worldwide.

REFERENCES

Ahr, W. M., 2008, Geology of carbonate reservoirs: the identification, description, and characterization of hydrocarbon reservoirs in carbonate rocks, John Wiley & Sons, 277 p.

Aki, K., and P. G. Richards, 2002, Quantitative Seismology, University Science Books, 704 p.

Al-Rahim, A. M., and A. A. Abdulateef, 2017, 3D Seismic Genetic Inversion for Reservoir Characterization and Prospects Identification: International Journal of Science and Research (IJSR) v. 6.

Alamsyah, M. N., B. W. Handono, and A. Syafriya, 2015, 3D Seismic Reservoir Characterization and Delineation in Carbonate Reservoir: International Conference & Exhibition.

Anselmetti, F. S., and G. P. Eberli, 1997, Sonic velocity in carbonate sediments and rocks: Carbonate seismology, v. 6, p. 53.

Avseth, P., T. Mukerji, and G. Mavko, 2010, Quantitative seismic interpretation: Applying rock physics tools to reduce interpretation risk, Cambridge University Press.

Basuki, P., and S. Z. Pane, 1976, The hydrocarbon prospects of the Baturaja Formation in South Sumatra: Indonesian Petroleum Association, 5th Annual Convention, June, p. 109-131.

Bortfeld, R., 1961, Approximations to the reflection and transmission coefficients of plane longitudinal and transverse waves: Geophysical Prospecting, v. 9, p. 485-502.

Cander, H., 2012, PS What Are Unconventional Resources? A Simple Definition Using Viscosity and Permeability, AAPG Annual Convention and Exhibition, Long Beach, California.

Chopra, S., R. K. Sharma, and K. J. Marfurt, 2013, Some current workflows in shale gas reservoir characterization: CSEG Recorder, v. 38, p. 42-52.

Choquette, P. W., and L. C. Pray, 1970, Geologic nomenclature and classification of porosity in sedimentary carbonates: AAPG bulletin, v. 54, p. 207-250.

De Coster, G., 1974, The geology of the central and south Sumatra basins: Indonesian Petroleum Association, 3rd Annual Convention, p. 77-110.

Dolberg, D. M., J. Helgesen, T. H. Hanssen, I. Magnus, G. Saigal, and B. K. Pedersen, 2000, Porosity prediction from seismic inversion, Lavrans Field, Halten Terrace, Norway: The Leading Edge, v. 19, p. 392-399.

Doust, H., and R. A. Noble, 2008, Petroleum systems of Indonesia: Marine and Petroleum Geology, v. 25, p. 103-129.

Dunham, R. J., 1962, Classification of carbonate rocks according to depositional textures, Classification of Carbonate Rocks - A Symposium, p. 108-121.

Emery, D., and K. Myers, 1996, Sequence Stratigraphy, Blackwell Sci., Oxford, UK, 297 p.

Everett, M. E., 2013, Near-surface applied geophysics, Cambridge University Press, 402 p.

Fatti, J. L., G. C. Smith, P. J. Vail, P. J. Strauss, and P. R. Levitt, 1994, Detection of gas in sandstone reservoirs using AVO analysis: A 3-D seismic case history using the Geostack technique: Geophysics, v. 59, p. 1362-1376.

Flügel, E., 2013, Microfacies of carbonate rocks: analysis, interpretation and application, Springer Science & Business Media.

Gallagher, K., M. Sambridge, and G. Drijkoningen, 1991, Genetic algorithms: An evolution from Monte Carlo Methods for strongly non-linear geophysical optimization problems: Geophysical Research Letters, v. 18, p. 2177-2180.

Geoservices, P., 2012a, Rock Description & Biostratigraphy of Ditch Cuttings Samples from Well KAG-E24, Pagardewa Field, South Sumatra Province, Indonesia, Jakarta.

Geoservices, P., 2012b, Rock Description for Conventional Core Samples from Well KAG-E22, Pagardewa Field, South Sumatra Province, Indonesia, Jakarta.

Geoservices, P., 2012c, Rock Description for Conventional Core Samples from Well SPR-01, Pagardewa Field, South Sumatra Province, Indonesia, Jakarta.

Geoservices, P., 2012d, Rock Description for Conventional Core Samples Well Tasim-04, Pagardewa Field, South Sumatra, Indonesia, Jakarta.

Geoservices, P., 2012e, Routine Core Analysis, Rock Description & Biostratigraphy for Rotary Sidewall Core & Ditch Cutting samples from Well Lavatera-01, Pagardewa Field, South Sumatra Province, Indonesia, Jakarta.

Geoservices, P., 2012f, Routine Core Analysis, Rock Description & Biostratigraphy for Rotary Sidewall Core & Ditch Cutting samples from Well PMT-03, Pagardewa Field, South Sumatra Province, Indonesia, Jakarta.

Geoservices, P., 2013a, Provisional Petrographic Description of Sidewall Core Samples from Well Tasim-05, Pagardewa Field, South Sumatra Province, Indonesia, Jakarta.

Geoservices, P., 2013b, Rock Description & Biostratigraphy of Ditch Cuttings Samples from Well PMN-8, Pagardewa Field, South Sumatra Province, Indonesia, Jakarta.

Gidlow, P., G. Smith, and P. Vail, 1993, Hydrocarbon detection using fluid factor traces: A case study: 3rd SAGA Biennial Conference and Exhibition.

Goodway, B., T. Chen, and J. Downton, 1997, Improved AVO fluid detection and lithology discrimination using Lamé petrophysical parameters;"λρ","μρ", & "λ/μ fluid stack", from P and S inversions, SEG Technical Program Expanded Abstracts 1997, Society of Exploration Geophysicists, p. 183-186.

Goodway, B., M. Perez, J. Varsek, and C. Abaco, 2010, Seismic petrophysics and isotropic-anisotropic AVO methods for unconventional gas exploration: The Leading Edge, v. 29, p. 1500-1508.

Haecker, M., 1992, Convergent gridding: a new approach to surface reconstruction: Geobyte, v. 7, p. 48-53.

Hampson-Russell, 2011, Seismic Lithology & AVO Workshop, Singapore.

Hampson, D., 1986, Inverse velocity stacking for multiple elimination, SEG Technical Program Expanded Abstracts 1986, Society of Exploration Geophysicists, p. 422-424.

Han, D.-H., 1987, Effects of porosity and clay content on acoustic properties of sandstones and unconsolidated sediments, Stanford Univ., CA (USA).

Haq, B. U., J. Hardenbol, and P. R. Vail, 1987, Chronology of fluctuating sea levels since the Triassic: Science, v. 235, p. 1156-1167.

Holditch, S. A., 2013, Unconventional oil and gas resource development – Let's do it right: Journal of Unconventional Oil and Gas Resources, v. 1-2, p. 2-8.

Holland, J. H., 1992, Adaptation in natural and artificial systems: an introductory analysis with applications to biology, control, and artificial intelligence: MIT press, 439-444 p.

Huuse, M., and D. Feary, 2005, Seismic inversion for acoustic impedance and porosity of Cenozoic cool-water carbonates on the upper continental slope of the Great Australian Bight: Marine Geology, v. 215, p. 123-134.

Ikelle, L. T., and L. Amundsen, 2005, Introduction to petroleum seismology, Society of Exploration Geophysicists, 679 p.

Jalalalhosseini, S., S. Eskandari, and E. Mortezazadeh, 2015, The technique of seismic inversion and use of the relation between inversion results and porosity log for predicting porosity of a carbonate reservoir in a south Iranian oil field: Energy Sources, Part A: Recovery, Utilization, and Environmental Effects, v. 37, p. 265-272.

Jarvie, D. M., 2012, Shale Resource Systems for Oil and Gas: Part 1—Shale-gas Resource Systems, Shale Reservoirs-Giant Resources for the 21st century: AAPG Memoir v. 97, p. 69-87.

Knapp, R. W., D. E. Hedke, and N. L. Anderson, 1995, Amplitude Variation with Offset: Bulletin Kansas Geological Survey, p. 34-38.

Kumar, V., C. H. Sondergeld, and C. S. Rai, 2012, Nano to macro mechanical characterization of shale: SPE Annual Technical Conference and Exhibition.

Loucks, R., R. Moody, J. Bellis, and A. Brown, 1998, Regional depositional setting and pore network systems of the El Garia Formation (Metlaoui Group, Lower Eocene), offshore Tunisia: Geological Society, London, Special Publications, v. 132, p. 355-374.

Ma, Y. Z., S. Holditch, and J.-J. Royer, 2015, Unconventional Oil and Gas Resources Handbook : Evaluation and Development, Elsevier Science & Technology, 526 p.

Maliva, R. G., and J. Dickson, 1992, Microfacies and diagenetic controls of porosity in Cretaceous/Tertiary chalks, Eldfisk field, Norwegian North Sea (1): AAPG Bulletin, v. 76, p. 1825-1838.

Margrave, G. F., M. P. Lamoureux, and D. C. Henley, 2011, Gabor deconvolution: Estimating reflectivity by nonstationary deconvolution of seismic data: Geophysics, v. 76, p. W15-W30.

Mavko, G., T. Mukerji, and J. Dvorkin, 2009, The rock physics handbook: Tools for seismic analysis of porous media, Cambridge university press, 511 p.

Nagarajappa, N., and J. Downton, 2009, AVO compliant spectral balancing: Expanded Abstracts of the 2009 Joint CSPG/CSEG/CWLS Conference.

Nichols, G., 2009, Sedimentology and stratigraphy, John Wiley & Sons, 419 p.

Ostrander, W., 1984, Plane-wave reflection coefficients for gas sands at nonnormal angles of incidence: Geophysics, v. 49, p. 1637-1648.

Pannetier, W., 1994, Diachronism of drowning event on Baturaja limestone in the Tertiary Palembang sub-basin, South Sumatra, Indonesia: Journal of Southeast Asian Earth Sciences, v. 10, p. 143-157.

Pavlova, M. A., and I. Reid, 2010, Geophysical inversion of 3d seismic data in panax's limestone coast geothermal project to determine reservoir porosity: Proceedings of the World Geothermal Congress, p. 25-29.

Perez, M., D. Close, B. Goodway, and G. Purdue, 2011, Developing templates for integrating quantitative geophysics and hydraulic fracture completions data: Part I-Principles and theory, SEG Technical Program Expanded Abstracts 2011, Society of Exploration Geophysicists, p. 1794-1798.

Pertamina, 2010a, Internal Company Report: Final Well Report of Well Tasim Pagardewa (PDW) - 06, Jakarta, Pertamina, p. 75.

Pertamina, 2010b, Internal Company Report: Final Well Report of Well Tasim Prabumenang (PMN) - 6, Jakarta, Pertamina.

Pertamina, 2011, Pertamina Internal Report, Jakarta, Pertamina.

Pertamina, 2012a, Internal Company Report: Final Well Report of Well Kuang (KAG) - E22, Jakarta, Pertamina, p. 44.

Pertamina, 2012b, Internal Company Report: Final Well Report of Well Kuang (KAG) - E24, Jakarta, Pertamina, p. 49.

Pertamina, 2012c, Internal Company Report: Final Well Report of Well Lavatera (LVT) - 1, Jakarta, Pertamina, p. 42.

Pertamina, 2012d, Internal Company Report: Final Well Report of Well Pemaat (PMT) - 4, Jakarta, Pertamina, p. 19.

Pertamina, 2012e, Internal Company Report: Final Well Report of Well Semparuti (SPR) - 1, Jakarta, Pertamina, p. 43.

Pertamina, 2012f, Internal Company Report: Final Well Report of Well Tasim (TSM)-4, Jakarta, Pertamina, p. 38.

Pertamina, 2012g, Internal Company Report: Final Well Report of Well Tasim (TSM)-5, Jakarta, Pertamina, p. 38.

Pertamina, 2012h, Internal Company Report: Final Well Report of Well Tasim Prabumenang (PMN) - 8, Jakarta, Pertamina.

Pertamina, 2013a, Internal Company Report: Final Well Report of Well Pemaat (PMT) - 6, Jakarta, Pertamina.

Pertamina, 2013b, Internal Company Report: Final Well Report of Well Puring (PRG) - 1, p. 52.

Pomar, L., 2001, Types of carbonate platforms: a genetic approach: Basin Research, v. 13, p. 313-334.

Pomar, L., P. Bassant, M. Brandano, C. Ruchonnet, and X. Janson, 2012, Impact of carbonate producing biota on platform architecture: insights from Miocene examples of the Mediterranean region: Earth-Science Reviews, v. 113, p. 186-211.

Pulunggono, A., 1986, Tertiary Structural Features Related to Extensional And Compressive Tectonic in The Palembang Basin, South Sumatra: Indonesian Petroleum Association-15th Annual Convention, p. 187-212.

Raymer, L., E. Hunt, and J. S. Gardner, 1980, An improved sonic transit time-to-porosity transform, SPWLA 21st Annual Logging Symposium, Lafayette, Louisiana, Society of Petrophysicists and Well-Log Analysts.

Richards, P. G., and C. W. Frasier, 1976, Scattering of elastic waves from depth-dependent inhomogeneities: Geophysics, v. 41, p. 441-458.

Rickman, R., M. J. Mullen, J. E. Petre, W. V. Grieser, and D. Kundert, 2008, A practical use of shale petrophysics for stimulation design optimization: All shale plays are not clones of the Barnett Shale: SPE Annual Technical Conference and Exhibition.

Rider, M. H., 2002, The geological interpretation of well logs: Caithness, Whittles Publishing, 280 p.

Rumelhart, D. E., G. E. Hinton, and R. J. Williams, 1986, Learning representations by back-propagating errors: nature, v. 323, p. 533.

Russel, H., 2011, Workshop AVO-Part 2, Singapore.

Russell, B. H., 2014, Prestack seismic amplitude analysis: An integrated overview: Interpretation, v. 2, p. SC19-SC36.

Saeed, A. N., G. F. Margrave, and L. R. Lines, 2014, Pre-stack (AVO) and post-stack inversion of the Hussar low frequency seismic data.

Sam Boggs, J., 2006, Principles of Sedimentology and Stratigraphy, Pearson Education, 662 p.

Sambridge, M., and G. Drijkoningen, 1992, Genetic algorithms in seismic waveform inversion: Geophysical Journal International, v. 109, p. 323-342.

Schmidt, D., A. Veronesi, F. Delbecq, and J. Durand, 2013, Seismic data preconditioning for improved reservoir characterization (Inversion and fracture analysis): Integration Geo Convention (2013), Canada.

Shuey, R., 1985, A simplification of the Zoeppritz equations: Geophysics, v. 50, p. 609-614.

Smith, G., and P. Gidlow, 1987, Weighted stacking for rock property estimation and detection of gas: Geophysical Prospecting, v. 35, p. 993-1014.

Takahashi, T., and S. Tanaka, 2010, Rock physics model for interpreting dynamic and static Young's moduli of soft sedimentary rocks: ISRM International Symposium-6th Asian Rock Mechanics Symposium.

Tucker, M. E., and V. P. Wright, 2009, Carbonate sedimentology, John Wiley & Sons, 482 p.

Van Wagoner, J., 1985, Reservoir facies distribution as controlled by sea-level change: SEPM Mid-Year meeting, Golden, CO., p. 91-92.

Van Wagoner, J., H. Posamentier, R. Mitchum, P. Vail, J. Sarg, T. Loutit, and J. Hardenbol, 1988, An overview of the fundamentals of sequence stratigraphy and

key definitions, The Society of Economic Paleontologists and Mineralogists (SEPM).

Veeken, P., and M. Da Silva, 2004, Seismic inversion methods and some of their constraints: First break, v. 22, p. 47-70.

Vernik, L., and A. Nur, 1992, Petrophysical classification of siliciclastics for lithology and porosity prediction from seismic velocities (1): AAPG Bulletin, v. 76, p. 1295-1309.

Wallace, R., and R. Young, 1996, Pre-stack inversion: Evolving the science of inversion: CSEG Recorder, v. 21, p. 3-3.

Wangen, M., 2000, Generation of overpressure by cementation of pore space in sedimentary rocks: Geophysical Journal International, v. 143, p. 608-620.

Wibowo, R. A., W. Hindadari, S. Alam, P. D. Silitonga, and R. Raguwanti, 2008, Fractures identification and reservoir characterization of gas carbonate reservoir at Merbau Field, South Palembang Basin, Sumatra, Indonesia: Adapted from oral presentation at AAPG Annual Convention, San Antonio, TX, April, p. 20-23.

Wiggins, R., G. Kenny, and C. McClure, 1983, A method for determining and displaying the shear-velocity reflectivities of a geologic formation: European patent application, v. 113944.

Wilson, M. E., 2002, Cenozoic carbonates in Southeast Asia: implications for equatorial carbonate development: Sedimentary Geology, v. 147, p. 295-428.

Wyllie, M. R. J., A. R. Gregory, and L. W. Gardner, 1956, Elastic wave velocities in heterogeneous and porous media: Geophysics, v. 21, p. 41-70.

Yilmaz, Ö., 2001, Seismic data analysis, v. 1, Society of Exploration Geophysicists Tulsa, OK, 2027 p.

Yuliandri, I., T. Usman, and M. Panguriseng, 2011, Seismic Based Characterization of Baturaja Carbonate at 3D Topaz Area, AAPG International Convention and Exhibition, Milan, Italy, AAPG, p. 24.

Zhang, B., D. Chang, T. Lin, and K. J. Marfurt, 2014, Improving the quality of prestack inversion by prestack data conditioning: Interpretation, v. 3, p. T5-T12.

Zoeppritz, K., 1919, Uber reflexion und durchgang seismischer wellen durch unstetigkeitsflächen. Nachr. Ges. Wiss. Gottingen, Math: Phys. Kl, v. 1919, p. 25.

APPENDIX

Zoeppritz Approximations

A seismic P-wave incident at an angle $\theta_1 > 0$ is converted into reflected and transmitted P- and S-waves at the boundary between two elastic layers (**Figure 4.6**). Zoeppritz (1919) derived equation (A-1), below, to compute the reflected R and transmitted T amplitudes of the mode-converted waves based on conservation of stress and displacement across the layer boundary. In this equation, θ_2 is the angle of refraction of the P-wave, whereas ϕ_1, ϕ_2 are respectively the angles of reflection and refraction of the converted S-waves.

$$\begin{bmatrix} R_{PP} \\ R_{PS} \\ T_{PP} \\ T_{PS} \end{bmatrix} = \begin{bmatrix} -\sin\theta_1 & -\cos\phi_1 & \sin\theta_2 & \cos\phi_2 \\ \cos\theta_1 & -\sin\phi_1 & \cos\theta_2 & -\sin\phi_2 \\ \sin 2\theta_1 & \frac{V_{P1}}{V_{S1}}\cos 2\phi_1 & \frac{\rho_2 V_{S2}^2 V_{P1}}{\rho_1 V_{S1}^2 V_{P2}}\cos\phi_1 & \frac{\rho_2 V_{S2} V_{P1}}{\rho_1 V_{S1}^2}\cos 2\phi_2 \\ -\cos 2\phi_1 & \frac{V_{S1}}{V_{P1}}\sin 2\phi_1 & \frac{\rho_2 V_{P2}}{\rho_1 V_{P1}}\cos 2\phi_2 & -\frac{\rho_2 V_{S2}}{\rho_1 V_{P1}}\sin 2\phi_2 \end{bmatrix}^{-1} \begin{bmatrix} \sin\theta_1 \\ \cos\theta_1 \\ \sin 2\theta_1 \\ \cos 2\phi_1 \end{bmatrix} \quad \text{(A-1)}$$

To solve the Zoeppritz equation, the P-wave velocity V_P, S-wave velocity V_s, and density ρ must be known for each layer, and the incident P-wave angle θ_1 must also be known. The transmitted P-wave angle θ_2 is derived from the incident P-wave angle using Snell's Law, while the P-wave reflected angle obeys the law of reflection. The Zoeppritz equation (A-1) is complicated and difficult to use in practice, therefore a number of authors have made linearized approximations to Zoeppritz equation. In this appendix we explore some of these approximations.

The P-wave reflection coefficient R_{PP} as a function of incident angle θ_1, for "small contrasts" of P-wave velocity, S-wave velocity and density across the elastic boundary,

can be approximated by the linear summation of three terms (Aki and Richards, 2002; Bortfeld, 1961; Richards and Frasier, 1976):

$$R_{PP}(\theta_1) = aR_{VP} + bR_{VS} + cR_D \qquad \text{(A-2)}$$

where the cofficients are given by $a = 1 + \tan^2\theta$; $b = -8\bar{k}_{\text{sat}}\sin^2\theta$; and $c = 1 - 4\bar{k}_{\text{sat}}\sin^2\theta$. In equation (A-2),

$$R_{VP} = \frac{\Delta V_P}{2\bar{V}_P} \; ;$$

$$R_{VS} = \frac{\Delta V_S}{2\bar{V}_S} \; ;$$

$$R_D = \frac{\Delta \rho}{2\bar{\rho}} \quad ;$$

are reflectivities. The quantity $\theta = \frac{1}{2}(\theta_1 + \theta_2)$ is the average of the incident and refracted angles, while

$$\bar{V}_P = \frac{1}{2}(V_{P1} + V_{P2}) \; ;$$

$$\bar{V}_S = \frac{1}{2}(V_{S1} + V_{S2}) \; ;$$

$$\bar{\rho} = \frac{1}{2}(\rho_1 + \rho_2) \quad ;$$

are the averages of the velocity and density values across the layer interface. The quantities $\Delta V_P \; ; \Delta V_S \; ; \Delta \rho$ are the differences of the velocity and density values across the interface. The parameter $\bar{k}_{sat} = \left(\frac{\bar{V}_S}{\bar{V}_P}\right)^2_{sat}$ is the ratio of shear to compressional wave velocity for saturated rocks, with the velocities being the average values of the two layers.

Fatti et al. (1994), following Smith and Gidlow (1987) and Gidlow et al. (1993), derived an alternate version of equation (A2) as:

$$R_{PP}(\theta_1) = aR_{AI} + bR_{SI} + c'R_D \qquad \text{(A-3)}$$

where the a and b cofficients are the same ones as used in the Aki-Richard approximation (A2), but with $c' = 4\bar{k}_{\text{sat}}\sin^2\theta - \tan^2\theta$. The reflectivities associated with P-impedance and S-impedance are introduced here as:

$$R_{AI} = \frac{1}{2}\left(\frac{\Delta V_P}{\bar{V}_P} + \frac{\Delta\rho}{\bar{\rho}}\right) = R_{VP} + R_D \ ;$$

$$R_{SI} = \frac{1}{2}\left(\frac{\Delta V_S}{\bar{V}_S} + \frac{\Delta\rho}{\bar{\rho}}\right) = R_{VS} + R_D.$$

Wiggins et al. (1983) also rearranged equation (A2), into the form:

$$R_{PP}(\theta_1) = a'R_{AI} + b'R_{GI} + c''R_{VP} \qquad \text{(A-4)}$$

with the reflectivity of gradient impedance defined as:

$$R_{GI} = R_{VP} - 8\bar{k}_{\text{sat}}R_{VS} - 4\bar{k}_{\text{sat}}R_D.$$

The Wiggins coefficients a', b', c'' in equation (A4) are not dependent on $\bar{k}_{sat}$ but rather are given by $a' = 1\ ; b' = \sin^2\theta$ and $c'' = \tan^2\theta\ \sin^2\theta$. In the geophysical literature, R_{GI} is called the gradient, R_{AI} is called the intercept and R_{VP} is called the curvature. Equation (A-4) is the basis for many of the empirical AVO analyses performed in industry. For incident angles less than 30^0, the intercept-gradient-curvature equation (A-4) and the Fatti et al. (1994) equation (A-3) both approximate very well the solutions of the Zoeppritz equation. However, according to Russell (2014), the Fatti et al. (1994) approximation does better for incident angles larger than 30^0.

Shuey (1985) has modified equation (A4) from its dependence on parameters V_P, V_S and ρ to a dependence on parameters V_P, ρ and Poisson's ratio (υ):

$$R_{PP}(\theta_1) = a'R_{AI} + b'R_{GI} + c''R_D \qquad \text{(A-5)}$$

where the reflectivity of gradient impedance becomes

$$R_{GI} = R_{VP} - 2(R_{AI} + R_{VP})\left(\frac{1-2\bar{\nu}}{1-\bar{\nu}}\right) + \frac{\Delta\nu}{(1-\bar{\nu})^2}.$$

The parameter R_{GI} now depends on R_{AI}, R_{VP}, $\bar{\nu}$ and $\Delta\nu$. Poisson's ratio is given by

$$\nu = \frac{V_P^2 - V_S^2}{2(V_P^2 - V_S^2)}.$$

The parameters $\bar{\nu} = \frac{\nu_{i+1}+\nu_i}{2}$ and $\Delta\nu = \nu_{i+1} - \nu_i$ are respectively Poisson's ratio average and Poisson's ratio difference across the boundary of the two elastic media. The Shuey equation (A-5) provides a good approximation of the Zoeppritz reflectivity for incident angles up to 30–35^0 (Veeken and Da Silva, 2004).

Seismic Pre-conditioning Workflow

Our seismic dataset are processed using the seismic processing package in Humpson-Russel Suite™. The details of the seismic pre-conditioning data processing workflow are described in this section. The workflow included (in order of processing):

1. NMO Correction

The normal moveout (NMO) time correction at offset x and zero-offset time t_0 can be written as:

$$\Delta t_{NMO} = t(t_0, x) - t_0 = \sqrt{t_0^2 + \frac{x^2}{V_{NMO}^2(t_0)}} - t_0 \qquad \text{(A-6)}$$

where $V_{NMO}^2(t_0)$ is NMO Velocity, the velocity that best flattens the reflection events. For N-horizontal-layered-media, the Root-Mean-Square velocity of *i*-th layer:

$$V_{rms}^2 = \frac{\sum_{i=1}^{N} V_i^2 \Delta\tau_i}{\sum_{i=1}^{N} \Delta\tau_i} \quad \text{(A-7)}$$

where $\Delta\tau_i$ is the vertical two-way time through the *i*-th layer. With offset smaller than depth, the $V_{NMO}^2(t_0)$ approach the value of V_{rms}^2. Thus, we used the provided V_{rms}^2 dataset from migration step in previous processing flow to approximate V_{NMO}^2 in this step to flatten only the primary reflector but not the multiples. The NMO correction has the positive benefit of increasing SNR by means of the stacking process in which coherent signals on multiple adjacent traces are reinforced and incoherent noise together with bed multiple and water bottom multiple are suppressed.

2. Mute

An NMO correction can generate the "hockey stick" effect along with "NMO stretch" at far offset (Yilmaz, 2001; Zhang et al., 2014). In offset-time plot, the discrepancy at far offset is similar in appearance to a hockey stick. The discrepancy is occurs due to inability of the NMO velocities to flatten the far-offset data. One method to eliminate such discrepancies and other noise at far offset is by applying a mute. Since it is desired to retain far-offset information for the AVO inversion analysis, the mute was applied only at short times (corresponding to shallow depths) in regions outside of Baturaja Formation. The reliability of P-impedance estimation from seismic data do not depend on angles, unlike S-Impedance estimation is reliable when the incidence angle is

less than 300, whereas density is reliable when the angle is less than 45^0 (Zhang et al., 2014). Therefore, our mute was designed to remove all traces at incident angles greater than 45^0.

3. Super Gather

A super gather is the process of forming average Common Depth Point (CDP) gather to enhance the signal-to-noise ratio (Hampson-Russell, 2011). Often called a common offset stack, the averaging is done by collecting adjacent CDPs and adding them together. The technique has two important parameters to be set up: (1) the number of offsets determines how many offsets will appear in each final gather (t-x domain); (2) the lateral smoother, the moving window dimension consist of number of crosslines and inlines to be averaged to smooth the output CDP. This technique is very robust tool for reducing random noise while preserving offset-dependent amplitude variation (Hampson-Russell, 2011).

4. Parabolic Radon Transform

Another noise suppression tool that is used in our data pre-conditioning workflow is based on the Parabolic Radon Transform. A practical approach of this technique was presented by (Hampson, 1986). First, the input Common Mid Point (CMP) gather is NMO corrected using hyperbolic move-out correction

$$t_n = \sqrt{t^2 - \frac{4h^2}{v_n^2}} \tag{A-8}$$

where t_n is time after NMO correction and v_n is the velocity hyperbolic moveout correction velocity function. The move-out events resulted approximately parabolic events:

$$t_n = \tau + qh^2 \tag{A-9}$$

where h is the half-offset, τ is the two-way zero-offset time and q is the parameter that defines the curvature of the parabola.

The forward and inverse Radon transform in the coordinates of the NMO-corrected gather $d(h, t_n)$ as expressed in (Yilmaz, 2001) after (Hampson, 1986) are:

$$u(q, \tau) = \sum_h d(h, t_n = \tau + qh^2) \tag{A-6-1}$$

$$d'(h, t_n) = \sum_h u(q, \tau = t_n - qh^2) \tag{A-6-2}$$

The noises are removed in parabolic radon transform domain $u(q, \tau)$, then perform inverse to the offset domain $d'(h, t_n)$.

After NMO correction, coherent events can be modelled as having a parabolic shape in time-offset coordinates:

$$Seismic\ Gather = Modeled\ Primary + Modeled\ Multiple + Random\ Noise \tag{A-12}$$

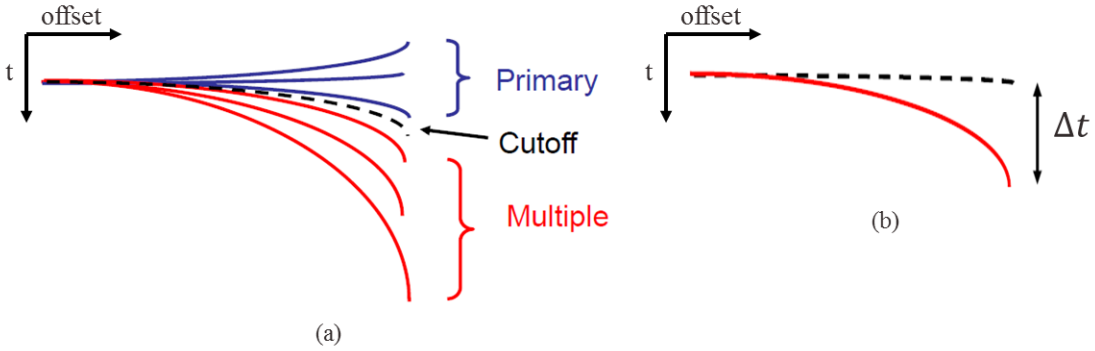

Figure A.1. (a) Parabolic-shaped models of coherent reflection events (primary and multiple) after NMO correction; (b) an individual parabola from figure (a) is defined by its move-out in the amount of Δt at far offset (reprinted from Russel, 2011)

INVEST^{TM}, Hampson-Russel software package, can create a "fan" of possible parabolas to model the events actually found in the data such as equation (A-12) (see **Figure A.1**a). An individual parabolic shape is defined by the event move-out at far offset Δt (**Figure A.1**b). All events with Δt greater than a specific cut-off value are assumed multiples and other signal energy that is not easily represented by a parabola is assumed to be random noise. The parabolic radon transform eliminates the multiple by subtracting the modeled multiple from the events contained in the original super gathers. Subtracting both modeled primary + modeled multiple from the super gather gives the random noise. Those random noise is scaled then subtracted to the original super gathers to get the events that is free of random noise. So the radon transform can remove either multiples or random noise or both.

5. Trim Static

Time variant trim static is a data processing technique that corrects for residual move-out errors. In our processing flow, the trim static is applied after the parabolic radon

transform. This is a beneficial tool for flattening the far offset. The static correction is performed over a series of overlapping windows in each CDP gather. A pilot trace is constructed by stacking a CDP gather, then each of offset trace in the CDP gather is cross-correlated with the pilot trace using a series of smaller, overlapping windows, and calculate time shift then interpolate the calculated shifts between windows (**Figure A.2**). This technique is included here because it is a good tool for flattening far offsets (Russel, 2011).

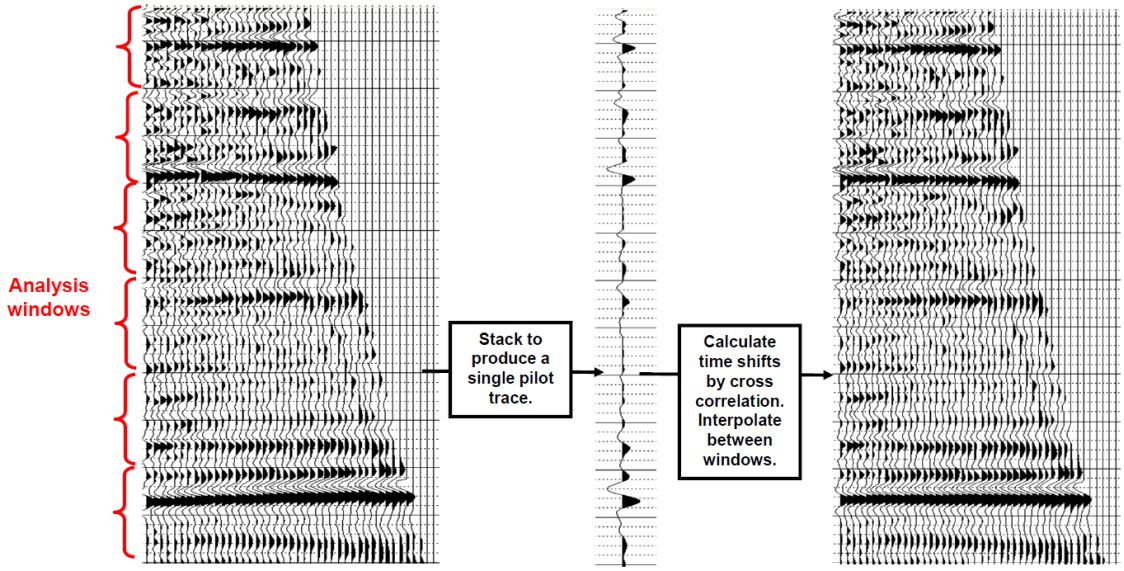

Figure A.2. Time variant trim static procedure (reprinted from Russel, 2011)

6. Stack

For this study, "stacking" is the process of averaging the individual traces that comprise a CDP gather. In the stacking process, the amplitude of a flattened primary reflector is enhanced whereas the amplitude of parabolic multiples is attenuated. This technique is the final step of the workflow and provides an enhancement of SNR. The

stacking can be generate in each processing step describe previously for quality checking of the selected parameters in each step.